CHARACTERIZATION OF THE RAT *ATG16L1* GENE AND ITS ROLE IN AUTOPHAGY AND DISEASE

A DISSERTATION PRESENTED TO THE FACULTY OF THE GRADUATE SCHOOL AT THE UNIVERSITY OF MISSOURI IN PARTIAL FULFILLMENT OF THE REQUIREMENTS FOR THE DEGREE DOCTOR OF PHILOSOPHY

BY

DR. KARI LYNN CHESNEY

DR. ELIZABETH C. BRYDA, DISSERTATION SUPERVISOR

DECEMBER 2020

The undersigned, appointed by the dean of the Graduate School, have examined the dissertation entitled

CHARACTERIZATION OF THE RAT *ATG16L1* GENE
AND ITS ROLE IN AUTOPHAGY AND DISEASE

presented by Kari Chesney, a candidate for the degree of Doctor of Philosophy, and hereby certify that, in their opinion, it is worthy of acceptance.

_____

Elizabeth C. Bryda, PhD

_____

Craig L. Franklin, DVM, PhD

_____

Jim Amos-Landgraf, PhD

_____

Aaron Ericsson, DVM, PhD

_____

Christopher Baines, PhD

DEDICATION PAGE

This work is dedicated to my parents, Robert and Cheri Chesney, whose love and support made this work possible. Also, to my husband, Brad Siegler, who has been my biggest motivator and inspiration throughout this journey.

ACKNOWLEDGEMENTS

First, I would like to extend my utmost gratitude to my advisor, Dr. Elizabeth Bryda for her guidance and mentorship these last five years. Without her encouragement and motivation, this dissertation would not be possible. She has shown me incredible support, both in and out of the lab, these last many years, and I consider her as not only just an advisor, but a friend.

I would also like to thank Drs. Craig Franklin, Aaron Ericsson, Jim Amos-Landgraf, and Chris Baines for serving as my committee members and supporting my work. I could not have asked for a more dedicated, brilliant group of scientists and mentors to inspire my research and push me to become the best scientist I can be. I have learned a great deal from each of you, and your guidance will surely lead me toward a bright future.

Furthermore, I would like to express my sincere thanks to the faculty, staff, and residents of the Comparative Medicine program. These folks have become a second family to me during my post-DVM studies, and I will miss them all dearly.

A special thanks to my family; Robert, Cheri, and Kelli Chesney. I could not have gotten through this work without your constant support.

Finally, I would like to acknowledge the love and cuddles received from many furry family members these many years; Tai, Navi, Blinkin, Luna, Vanta, and Slater. My mental health has survived because of you.

TABLE OF CONTENTS

LIST OF TABLES

LIST OF FIGURES

LIST OF ABBREVIATIONS

AF = autophagic flux

ANOVA = analysis of variance

Atg = autophagy

Atg12 = autophagy related 12

Atg16l1 = autophagy related 16-like 1

Atg5 = autophagy related 5

BCA = bicinchoninic acid

BLAST = basic local alignment search tool

bp = base pair

BSA = bovine serum albumin

Cas = cellular apoptosis susceptibility

CD = Crohn's disease

CMV = human cytomegalovirus

CON = control group

COX = cyclooxygenase

CRISPR = clustered regularly interspaced short palindromic repeats

ddH_2O = double distilled water

DEPC = diethyl pyrocarbonate

DNA = deoxyribonucleic acid

dNTP = deoxynucleotide triphosphate

dsDNA = double stranded DNA

EDTA = ethylenediaminetetraacetic acid

EGFP = enhanced green fluorescent protein

ELISA = enzyme-linked immunosorbent assay

em = embryonic mutation

F = female

F344 = Fischer 344 rat strain

FBS = fetal bovine serum

FITC = fluorescein isothiocyanate

FT = full transcript

GI = gastrointestinal

GM = gut microbiome

gRNA = guide ribonucleic acid

GWAS = genome-wide association study

H&E = hematoxylin and eosin stain

HCl = hydrochloric acid

HDR = homology directed repair

HEK293 = human embryonic kidney cells

HET = heterozygous

HM = hypomorphic

HOM = homozygous

hr = hour

HRP = horseradish peroxidase

IBD = inflammatory bowel disease

IFA = immunohistofluorescence

IFN = interferon

IgG = immunoglobulin G

IL = interleukin

LB = Luria-Bertani

LC3 = microtubule-associated protein 1A/1B-light chain 3

M = male

MEM = minimal essential media

MNV = murine norovirus

MOPS = 3-(N-morpholino)propanesulfonic acid

mRNA = messenger ribonucleic acid

NaCl = sodium chloride

NHEJ = non-homologous end joining

NSAID = nonsteroidal anti-inflammatory

NSD = nonsteroidal anti-inflammatory treated group

OTU = operational taxonomic unit

PAGE = polyacrylamide gel

PAM = protospacer adjacent motif

PAS = Period Acid Schiff stain

PBS = phosphate buffered saline

PC = Paneth cell

PCoA = principle component analysis

PCR = polymerase chain reaction

PE = phosphatidylethanolamine

PERMANOVA = permutational analysis of variance

PMSF = phenylmethylsulfonyl fluoride

P-S = penicillin-streptomycin antibiotic

PSBT = phosphate buffered saline with Triton X-100

PVDF = polyvinylidene difluoride

RFU = relative fluorescence unit

RIPA = radioimmunoprecipitation assay

RNA = ribonucleic acid

rpm = revolutions per minute

rRNA = ribosomal ribonucleic acid

RRRC = University of Missouri Rat Resource and Research Center

RT-PCR = real time polymerase chain reaction

SD = Sprague Dawley rat stock

SDS = sodium dodecyl sulfate

SNP = single nucleotide polymorphism

ssODN = single-stranded oligonucleotide

SST = serum separator tube

STE = sucrose, EDTA, Tris buffer

STET = sucrose, Triton X-100, EDTA, Tris buffer

T300A = threonine to alanine substitution at amino acid position 300

TAE = Tris base, acetic acid and EDTA

TBS = tris-buffer saline

TBST = tris-buffered saline with Triton X-100

Th1 = T helper type 1 cell

Th2 = T helper type 2 cell

TNF = tumor necrosis factor

Tris = tris (hydroxymethyl) aminomethane

UC = ulcerative colitis

ULK1 = ubiquitin-like 1

WD 40 = beta transducin repeats

WK = week

WT = wild type

ABSTRACT

Crohn's disease (CD) is a potentially life-threatening inflammatory condition of the gastrointestinal tract affecting approximately 1.6 million Americans. Previous studies confirm the important role of genetics in IBD. More than 160 genetic alleles have been linked to CD, one of which lies in the autophagy-related 16-like 1 (*ATG16L1*) gene. In humans, a threonine to alanine amino acid variant at position 300 (T300A) of the evolutionarily conserved autophagy-related 16-like 1 (ATG16L1) protein is correlated with increased predisposition to CD. Using CRISPR-Cas9 technology, our laboratory developed the first reported genetically modified rat model of CD by inserting the T300A variant into the rat genome. An additional rat model with a knock-out mutation of the *Atg16l1* gene was also developed to perform loss-of-function analyses. This dissertation research characterizes the wild type (WT) and T300A susceptibility variant *Atg16l1* genes in the rat as well as understanding the mechanistic function of rat *Atg16l1* in autophagy.

Prior to this research, the rat *Atg16l1* gene had two known and one predicted splice variants; however, no further characterization of this gene had been done in wild type animals. Through collection and amplification of DNA from select rat tissues, we confirmed four splice variants and revealed that they exist in different combinations depending on the tissue. In addition, *in vitro* work revealed all splice variants could produce protein. Additional phenotypic characterization found that, like non-diseased intestinal tissue from human CD patients, Paneth cells exhibited abnormal granulation patterns. From this study we were able to determine that the T300A rat model faithfully recapitulates pre-disease

signs seen in humans. However, in order to address the usefulness of the model, we began to explore methods to incite CD signs.

Very few studies evaluating the effect of known environmental triggers of CD on specific genetic susceptibility variants have been performed. I developed two exposure studies, one acute using high-dose nonsteroidal anti-inflammatory (NSAID) and one chronic using both low-dose NSAID or *ad libitum* Western diet formulated rodent feed. These studies confirmed that rats heterozygous (HET) for the T300A variant are more susceptible to NSAID toxicity than WT littermates, and our model does express mild histologic changes comparable to CD lesions in human CD patients as compared to WT littermates when exposed to low-dose NSAID or Western diet. These studies support the T300A rat model as a valuable tool for both acute and chronic environmental studies of IBD.

In addition to animal model studies, we also performed *in vitro* work to evaluate the effect of each WT rat splice variant on autophagy. By transfecting HEK293 cells with one of each of the four WT rat variants, we have begun to understand how each *Atg16l1* variant effects autophagic flux. This information is crucial to understanding the underlying mechanism of autophagy and how autophagy functions in different tissues of the body. This research sets the foundation for using the *Atg161* T300A rat model in CD research and will help elucidate the role of *Atg16ll1* in autophagy. A better understanding of the T300A variant and the influence *Atg16l1* on autophagy will facilitate the potential for future targets of therapeutics for CD and other autophagy-related diseases.

CHAPTER 1: BACKGROUND AND SIGNIFICANCE

Molecular Genetics & CRISPR/Cas9

Advances in molecular genetics have propelled our understanding of biological processes from early observational studies at the macroscopic level to extremely detailed information at the single nucleotide level. In the last several decades, with the modernization and expansion of computer power and programming, the development of genome sequencing technology has enabled researchers to visualize high-resolution DNA sequences and begin to understand not only differences between species, but also between individuals of a species, within a single individual, between classes of cells, and even between healthy, diseased, and malignant cells. This enormous body of data mandated the development of analytical tools that have allowed us to probe the functions of genes and target their variations. The most recent, and quite possibly the most powerful, of these tools was originally discovered in 1987 in *Escherichia coli* and later found in archaeal genomes, bacteriophages, archaeal viruses, and plasmids (Bolotin, Quinquis, Sorokin, & Ehrlich, 2005; Y Ishino, Shinagawa, Makino, Amemura, & Nakata, 1987; Francisco J. M. Mojica, Díez-Villaseñor, García-Martínez, & Soria, 2005; F. J. M. Mojica, Juez, & Rodriguez-Valera, 1993). Conservation of this system amongst multiple kingdoms highlights it as a vital process for sustaining life in these organisms (Karginov & Hannon, 2010). Today, this system is known as clustered regularly interspaced short palindromic repeats, or CRISPR.

The CRISPR endonuclease system is part of an adaptive immune system which involves a set of CRISPR-associated (Cas) genes to incorporate snippets of invading viral DNA into

the CRISPR locus, known as CRISPR arrays (Makarova, Grishin, Shabalina, Wolf, & Koonin, 2006). The structural features of bacterial CRISPRs include: repeat sequences with constant length and dyad symmetry (two areas of a DNA strand whose base pair sequences are inverted repeats of each other) that form palindromic structures and spacer regions which also have constant length but no sequence homology (Figure 1.1) (Yoshizumi Ishino, Krupovic, & Forterre, 2018).

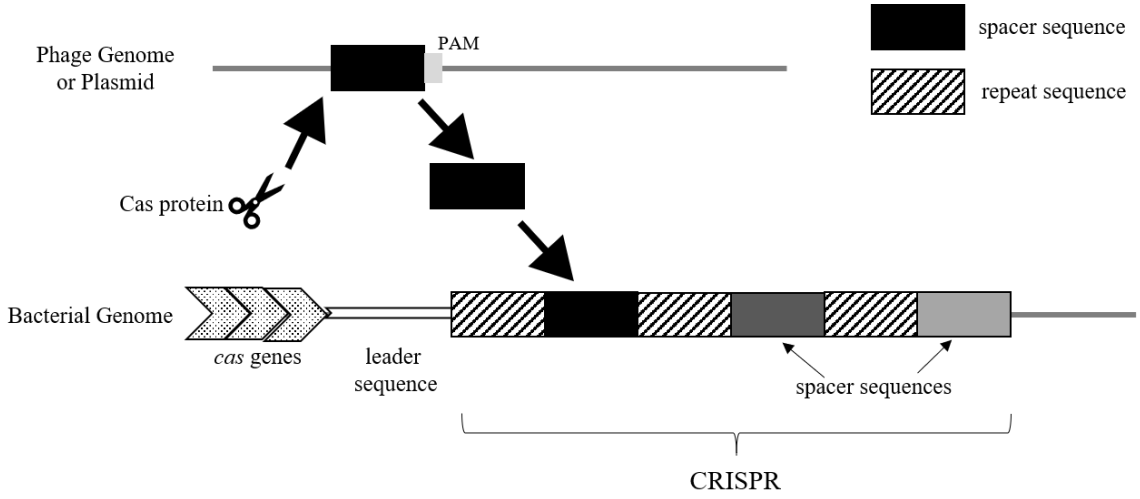

Figure 1.1: The structure of CRISPR. CRISPR consists of partially palindromic repeats (hash boxes) separated by short variable spacer sequences (solid boxes). When phage or plasmid genetic material invades a bacterium, Cas protein recognizes the proto-spacer adjacent motif (PAM) and incorporates the proto-spacer (black) into CRISPR. CRISPR is eventually processed into small mature crRNAs containing one spacer sequence to bind Cas proteins and provide immunity to subsequent phages and plasmids.

This system allows the bacterium to transcribe and express incorporated materials as RNA templates for targeted destruction of repeat viral invaders through cutting of the viral DNA by Cas endonucleases (Lino, Harper, Carney, & Timlin, 2018). Similarly, researchers have artificially created RNA targets with "guide" sequences that functionally mimic the CRISPR bacterial system. The first CRISPR system to be reconstituted in mammalian cells, and the most common CRISPR system used in model development, was derived from

Streptococcus pyogenes bacteria and uses Cas9 as the functioning endonuclease. The RNA "guides" are comprised of a 20-nucleotide sequence - the spacer - that determines the specificity of the sequence. Guides always contain a 5'-NGG (where N can be any nucleotide) protospacer adjacent motif (PAM) which can be directed toward almost any specific DNA sequence in any species genome with an appropriate PAM. Guide RNA works by binding to both the specific DNA target as well as a Cas endonuclease, in most cases Cas9, for cutting by that selected endonuclease. Cas9 contains two nuclease domains, HNH and RuvC, which are each responsible for cleaving one strand of the target DNA (Garneau et al., 2010; Gasiunas, Barrangou, Horvath, & Siksnys, 2012). Once the DNA is cut, the cell's own repair machinery is used to add or delete genetic material or to make changes to the DNA by replacing an existing segment with a customized DNA sequence. This can be completed by either non-homologous end joining (NHEJ) or homology directed repair (HDR) (Symington & Gautier, 2011). NHEJ occurs when the ends of the cut DNA are chemically ligated back together and because of the error-prone nature of this type of repair, it often results in small deletions, insertions, inversions, or duplications. HDR, on the other, is a repair mechanism that involves incorporation of a donor DNA sequence. When performing genetic engineering, it is possible to create much larger deletions, insertions, and duplications, or base mutations when HDR occurs. During HDR, a donor DNA fragment designed to have matching 5' and 3' ends to the cut 5' and 3' ends of the genomic sequence can be ligated into the original DNA strand.

Due to its ease of use and affordability, the CRISPR/Cas9 system has sparked global interest for its use as a prevention and treatment tool for human and animal diseases.

CRISPR has opened new opportunities to generate mutations in almost any genetic background and any species. This technology is particularly powerful in rodent species where assisted reproductive techniques, necessary for CRISPR modification, have already been developed (Kaneko, 2018). Both single-gene disorders and more complex diseases are currently being explored using CRISPR technology, including the disease of interest for this dissertation, inflammatory bowel disease (IBD) (Jinek et al., 2012).

Inflammatory Bowel Disease

Inflammatory bowel disease (IBD) is characterized as chronic inflammation of the gastrointestinal tract. IBD includes two major forms of chronic intestinal inflammation: ulcerative colitis (UC) and Crohn's disease (CD) which have many of the same characteristics. Both diseases traditionally manifest between 20 and 40 years of age and most affected individuals will eventually progress to relapsing and chronic disease (Xavier & Podolsky, 2007). Currently, there are no disease-specific therapies and no treatments for either UC or CD.

There are several defining factors of each IBD that distinguish them from one another. CD can affect any region of the gastrointestinal system from mouth to rectum, while UC is restricted to the colon and rectum. UC involves diffuse, focal mucosal inflammation that extends proximally from the rectum causing erosion and potential ulceration of the mucosa (Xavier & Podolsky, 2007). CD can have a multifocal, or patchy, manifestation with affected areas in multiple regions of the gastrointestinal tract simultaneously; however, the terminal ileum and proximal colon are the most common sites for presentation, particularly

over Peyer's patches. CD can also be a transmural (occurring across the entire wall of the intestinal organ) disease, while CD only affects the mucosal layer of the intestinal lumen. Histopathological features of UC include a significant increase in neutrophil infiltration within the lamina propria and crypts as well as depletion of goblet cell mucin both within cells and in the intestinal lumen. Histopathologic features of CD include aggregation of macrophages that commonly result in non-caseating granulomas.

There is no single diagnostic test for CD, and patients are diagnosed by ruling out other possible causes for signs and symptoms. Once diagnosed, CD patients should expect a lifetime of managing their disease, because there is no cure for CD and no single therapy that works for every patient. The goal of therapy is to minimize inflammation and reduce the incidence of disease flare up (acute relapse of disease signs). Anti-inflammatory drugs, antibiotics, and immunosuppressants are commonly prescribed to manage CD; however, all these treatments must be taken long term and have potentially harmful side effects. Unfortunately, therapy only works to mitigate relapse in about half of all CD patients, and those who experience constant relapse or severe complications of their disease will require surgery to resect areas of the damaged gastrointestinal tract – sometimes more than once.

In most cases, the causes of IBD remain unknown. The lack of treatments and therapies can be directly related back to the complexity of CD pathogenesis and its multifactorial etiology, both of which researchers are still exploring. Most researchers agree that a combination of genetic susceptibility and immune dysregulation causes an abnormal reaction to the intestinal microbiota (hereby referred to as the microbiota) and/or

environmental triggers that result in disease symptoms. While the remainder of this chapter will focus on the genetics of CD, it is important to recognize how these other factors contribute to disease pathogenesis.

Etiology of Crohn's Disease

As with all inflammatory diseases, immune dysregulation has a strong impact on CD manifestation. A skewed Th1 immune response plays a pivotal role in CD pathogenesis (Fuss et al., 1996; Matsuoka et al., 2004). Activation of macrophages seems to be a key highlight of CD initiation and increases in macrophage production result in increased TNF-α (tumor necrosis factor alpha), IL-1 (interleukin 1), and IL-6. Healthy macrophages lack expression of the innate immune receptor CD14, a protein responsible for detecting bacteria (Rogler et al., 1998; Smythies et al., 2005); however, an abundance of unique macrophages expressing CD14 have been found in intestinal tissues from human patients (Kamada et al., 2008), and these macrophages produce larger amount of proinflammatory cytokines (IL-23, TNF-α, IL-6) than typical resident intestinal macrophages (Kamada et al., 2008). A unique subset of macrophages displaying increased CD11b has also been found within the mesentery of CD patients and is correlated with IFN-γ (interferon gamma) production not normally seen in macrophages from healthy human tissues. The ratio of these $CD11b^{high}$ macrophages and $CD11b^{low}$ macrophages is extremely skewed in CD patients, correlated to the increase in proinflammatory cytokine production and loss of the regulatory function that $CD11b^{low}$ macrophages typically play (Bloemendaal et al., 2020). In addition to the effect of proinflammatory macrophages, there is a strong correlation between CD14 macrophages and activated T-lymphocytes producing IFN-γ. The increase

in IFN-γ secreting T-lymphocytes, as well as $CD11^{high}$ macrophages, may explain granuloma formation in CD patients, and it has been observed that lamina propria T-lymphocytes lose their physiological unresponsiveness to microbial antigens. This suggests that CD may be caused, in part, by hyperreaction of the local cellular immune system to commensal microbial and nutritional antigens in the gastrointestinal lumen (Khor, Gardet, & Xavier, 2011).

A large body of evidence suggests that the balance between the host microbiota and the host defensive immunological response to that microbiota plays an essential role in initiation of chronic IBD. Several studies have found therapeutic benefits to prescribing antimicrobial drugs and probiotics to patients with acute IBD flare-ups (Fabia et al., 1993; Gionchetti et al., 2003; Madsen, Doyle, Jewell, Tavernini, & Fedorak, 1999; Schultz et al., 2002; Sutherland et al., 1991). Other studies have revealed significant differences in the microbiota, including appearance of attaching and effacing *Escherichia coli* (Barnich et al., 2007) and increases in abundance of *Ruminococcus gnavus* (Henke et al., 2019), *Shigella*, *Fusobacterium*, *Desulfovibrio*, and *Campylobacter* (Metwaly, 2019). Perhaps more convincing still is the discovery that mouse strains which "spontaneously" develop chronic colitis seem to require the presence of luminal flora and have no signs of disease in gnotobiotic conditions (Elson et al., 2005). However, gnotobiotic mice given humanized microbiota from CD patients do present with features of CD, including proinflammatory gene expression in the gut mimicking those seen in human CD patients (Nagao-Kitamoto et al., 2016). Unfortunately, current knowledge of the microbiota is limited by the tools at our disposal, and the identity of many bacteria present in the microbiota are still unknown,

all of which limits our full understanding of the implications of microbiota on disease pathogenesis.

Perhaps even more complicated to understand regarding CD etiology is how environmental factors play a role in disease initiation and progression. Monozygotic twin studies suggest that extrinsic factors play a major role in disease etiology. These studies have found a concordance rate (the rate of probability that two people with shared genes will develop the same organic disease) for CD in monozygotic twins to be between 20-50% (Halfvarson, Bodin, Tysk, Lindberg, & Järnerot, 2003; M. Orholm, 2000; Thompson, Driscoll, Pounder, & Wakefield, 1996; Tysk, Lindberg, Järnerot, & Flodérus-Myrhed, 1988). If CD was entirely due to genes, the concordance rate should approach 100%. Smoking is one of the most-studied environmental factors related to CD etiology, with current and former smokers at an increased risk for development of CD (Vedamurthy & Ananthakrishnan, 2019). Smoking has been found to both modulate the immune responses and diversity/composition of the intestinal microbiome (Biedermann et al., 2014; Biedermann et al., 2013) as well as the composition and integrity of the epithelial membrane of the intestinal tract (Allais et al., 2016). Smokers tend to have a worse CD prognosis and an increased need for prescription drugs (corticosteroids, immunosuppressants, etc.) and surgery (Lakatos, Szamosi, & Lakatos, 2007). Interestingly, the effect of smoking on the risk of CD has been correlated to ethnic and geographical differences with findings from India, Asia, and Australia revealing minimal, if any, effect of smoking on CD incidence (Arora et al., 2018; Ng et al., 2013); however, these variations may also be due to differences in CD susceptibility genes in these populations (Croucher et al., 2003;

Silverberg et al., 2007; S.-K. Yang et al., 2014; S.-K. Yang, Ye, & Song, 2015), a linkage that has not been conducted as of yet. Other environmental factors that have been explored include stress, air pollution (Kaplan et al., 2010), use of oral contraceptives (Cornish et al., 2008), diet (Amre et al., 2007; Riordan, Ruxton, & Hunter, 1998; Wild, Drozdowski, Tartaglia, Clandinin, & Thomson, 2007), and use of nonsteroidal anti-inflammatory drugs (Long et al., 2016); though, many of the findings in these areas are much more inconsistent than the data correlating smoking to CD incidence. However, like smoke exposure, many of the differences in environmental factors may be due to differences in susceptibility genes in particular populations – an area of investigation that has yet to be explored.

Genetic Etiology of Crohn's Disease & Model Development

Understanding the genetics underlying CD has become the most common pathway for researchers to develop a better understanding of mechanistic factors affecting disease. As stated earlier, with a concordance rate of as high as 50% for CD in monozygotic twins, it is obvious that genetics plays a major role in disease pathogenesis (Halfvarson et al., 2003; M. Orholm, 2000; Thompson et al., 1996; Tysk et al., 1988). In addition, familial studies documenting family histories of CD report risk factors between 2-14% (Biancone et al., 2014; Satsangi, Rosenberg, & Jewell, 1994). The age of onset and initial disease location are also genetically linked (Bayless et al., 1996; Halme et al., 2006; Peeters et al., 1996).

Powerful tools, such as genome-wide association studies (GWAS), developed in the last two decades have propelled genetic research from familial association toward understanding specific genetic loci responsible for conferring susceptibility. GWAS

requires large cohorts of individuals with and without a disease that are relatively well matched (e.g. low population stratification; because allele frequencies can differ between subpopulations, population stratification can lead to false positive or negative associations) (Marees et al., 2018). Then, using single nucleotide polymorphisms (SNPs), consistent genetic-based differences between individuals with and without disease can be identified. If successful, it allows researchers to narrow their investigation to a specific locus involved in a phenotypic trait(s) without the need for trial and error experimentation.

The first GWAS involving loci implicated in increased IBD susceptibility was published in the mid-2000's (Yamazaki et al., 2005) (Barrett et al., 2008). Through the use of additional cohorts, increased sample sizes, and meta-analyses, over 200 genetic loci associated with IBD have been discovered – many of which overlap with other chronic immune disorders and affect specific populations more or less than others (Jairath & Feagan, 2020). Of the 200+ loci associated with IBD, 30 and 23 loci are uniquely linked to Crohn's disease (CD) and ulcerative colitis (UC), respectively (McGovern, Kugathasan, & Cho, 2015). Those 30 specific loci associated with CD have implicated cellular mechanisms such as autophagy, the IL-17/IL-23 axis, and the failure to suppress aberrant immune responses in the pathogenesis of disease (Verstockt, Smith, & Lee, 2018).

One of the most frequent loci associated with CD, particularly in Caucasian populations, is located in the *ATG16L1* gene (Hampe et al., 2007; Rioux et al., 2007). The *ATG16L1* gene, located on human Chromosome 2 (2q37.1) is an evolutionarily conserved autophagy gene required for both macroautophagy and xenophagy (Venter et al., 2001).

Macroautophagy (hereby referred to as autophagy) is the ubiquitous cellular process that delivers old or damaged organelles or intracellular bacteria (xenophagy) to the lysosome for degradation (Levine & Kroemer, 2008). This process is important for balancing sources of energy at critical periods of development, in response to stress, and minimally during periods of health (Glick, Barth, & Macleod, 2010). In addition, autophagy is a promotor of cellular senescence (irreversible cell cycle arrest) and cell surface antigen presentation, protector against genome instability, and preventer of necrosis. Thus, autophagy plays a key role in preventing autoimmune diseases, cancers, neurodegeneration, infections, and many other disorders. *ATG16L1* is known to have a vital role in the creation of the double membrane bound vesicle called the autophagosome that entraps unwanted materials and goes on to fuse with the lysosome.

ATG16L1 protein is responsible, in part, for formation of the autophagosome (Figure 1.2). During the early stages of autophagosome maturation, ATG16L1 functions as an adaptor to stabilize the ATG5-ATG12-ATG16L1 protein complex (He & Klionsky, 2009). The ATG16L1 protein complex acts to lipidate and recruit LC3B-II to the phagophore to induce curvature and elongation of the membrane (Glick et al., 2010). In mammalian species, the phagophore originates from the endoplasmic reticulum in dynamic equilibrium with other cytosolic membrane structures (Bernales, McDonald, & Walter, 2006; Ogata et al., 2006). Once the membrane has fused to create the vesicle, ATG5-ATG12-ATG16L1 dissociates from the vesicle, and the newly formed autophagosome delivers the unwanted material to the lysosome. The autophagosome binds to the lysosome, releasing its enzymatic contents, specifically acid hydrolases, into the now designated autophagolysosome (Cohn & Hirsch,

1960; Hirsch & Cohn, 1960). These hydrolases destroy bacteria and break down cellular components into their building blocks to be recycled for use in new cellular processes. Autophagy is critical during both health and disease, since basal autophagy functions during health to remove old cellular organelles and recycle their components, and accelerated autophagy occurs during periods of stress (nutritional, infectious, etc.) to protect the cell and return to baseline (Levine & Kroemer, 2008).

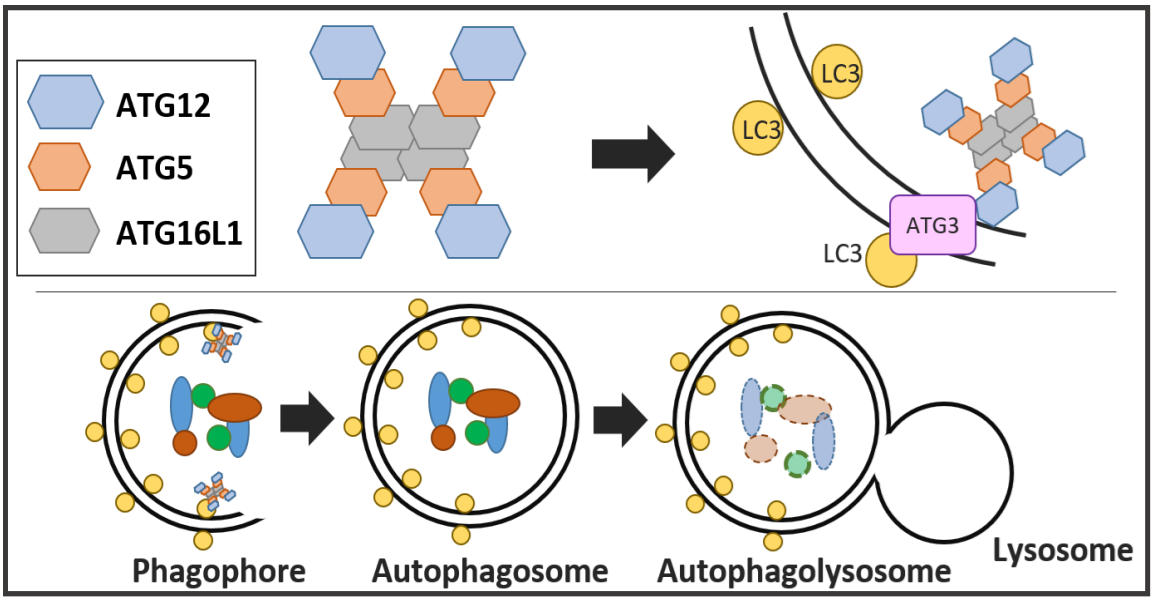

Figure 1.2: Development of the autophagolysosome. ATG16L1 protein complexes with ATG5 and ATG12, two other autophagy proteins, to lipidate LC3 located on the phagophore. Lipidation initiates elongation of the phagophore to create a double membrane bound autophagosome which encapsulates unwanted cellular debris or intracellular bacteria. Lysosomes within the cellular cytoplasm fuse with the autophagosome to deliver acidic hydrolases into the autophagosome and destroy any encapsulated material, either killing bacteria or breaking down cellular components for recycling and reutilization.

The *ATG16L1* CD susceptibility genetic variant is a single guanine-to-adenine base pair change which alters the wild type threonine amino acid at position 300 in the protein structure to an alanine (T300A) (Hampe et al., 2007). This amino acid change directly precedes a caspase cleavage site (D-x-x-D, where "D" signifies aspartic acid and "x"

signifies any amino acid) and results in increased caspase-3 mediated cleavage of the ATG16L1 protein (Murthy et al., 2014). In a healthy system, the amount of ATG16L1 is normally regulated by baseline caspase 3 activity. However, the presence of the T300A variant during stress results in enhanced ATG16L1 cleavage and diminished autophagy. The location of this amino acid change has been confirmed in human, mouse, and, by our laboratory, in the rat to directly precede this caspase cleavage site.

Multiple studies have confirmed defects in stress-induced autophagy in the presence of the T300A variant as well as in hypomorphic *Atg16l1* mouse models. Loss of functional Atg16l1 in mice blocks autophagy in Paneth cells (PCs), specialized ileal epithelial immune cells (Saitoh et al., 2008). Blockage results in increased inflammasome activation and irregular proinflammatory cytokine production in the presence of bacterial endotoxin and reduced secretion of PC immunoregulatory peptides (alpha defensins, lysozyme, etc.) into the intestinal lumen (Cadwell et al., 2008). The same study found similar PC findings in the ileal tissues of CD patients with the T300A variant. Mice hypomorphic for *Atg16l1* have also been shown to be more susceptible to inflammatory disease following intestinal injury when also infected with murine norovirus (MNV) (Cadwell et al., 2008). Interestingly, this susceptibility was associated with an increase in proinflammatory cytokine production and not changes in viral behavior or replication, suggesting that a disordered inflammatory response is responsible for disease and not high viral load (Matsuzawa & Cadwell, 2019). Nutrient starvation (glucose or amino acid) results in a 50% reduction of ATG16L1 in the presence of the T300A variant (Murthy et al., 2014). T300A has also been implicated in the invasion and survival of intracellular bacteria

(xenophagy). *In vitro* studies evaluating the role of the T300A variant in fibroblasts, epithelial cells, and macrophages have found that the variant decreases clearance of both *Salmonella typhimurium* and *Yersenia enterocolitica* compared to wild type cells (Fujita et al., 2009; Kuballa, Huett, Rioux, Daly, & Xavier, 2008; Messer et al., 2013; Murthy et al., 2014).

The potential mechanism of action and initiation of disease resulting from decreased autophagy is thought to be an amplified pro-inflammatory cytokine response in infected cells. ATG16L1 has been shown to modulate endotoxin-induced inflammasome activation and increased production of IL-1β, IL-18 and TNF-α (Matsuzawa & Cadwell, 2019; Saitoh et al., 2008). Both IL-1β and IL-18 overproduction have been found to exacerbate colitis, though additional studies need to be conducted to determine whether these cytokines are in part responsible for initiation and/or progress of other inflammatory bowel diseases, such as CD (Maeda et al., 2005) (ISHIKURA et al., 2003) (Nakahira et al., 2011) (Shi et al., 2012). Anti-TNF agents are commonly used as highly efficient, though not targeted or specific, therapies for CD patients, revealing the importance of this cytokine in the pathogenesis of CD (Adegbola, Sahnan, Warusavitarne, Hart, & Tozer, 2018). However, about 1/3 of CD patients do not respond to anti-TNF therapy, highlighting the multifactorial etiology and variable disease phenotype of CD. These deficits in treatment require further knowledge of how specific etiologic agents affect the disease process and how they may be treated by one or more therapies depending on the related phenotype.

While several mouse studies using CRISPR developed models have uncovered vital information as to how *Atg16l1* functions during CD development, disease in these models has only ever been initiated by artificial conditions, such as introduction of pathogenic bacteria like *Salmonella typhimurium* (Conway et al., 2013). Other researchers have attempted to elicit disease signs by inducing multiple susceptibility variants in combination with *Atg16l1* to simulate human pathogenesis. In one study, researchers developed a tissue specific A20-*Atg16l1* double deficit mouse model (Slowicka et al., 2019). A20 is a ubiquitin editing protein and negative regulator of inflammatory signaling that can bind to the WD region of the ATG16L1 protein (Coornaert, Carpentier, & Beyaert, 2009). This model develops spontaneous IBD; however, spontaneous disease is not found in human IBD patients nor has this combination of deficiencies been found in human IBD patients. Neither the hypomorphic *Atg16l1* mouse model nor the T300A variant mouse model has been shown to have disease signs with known or suspected environmental triggers of disease, such as nicotine, high fat/high sugar diet, or long-term non-steroidal anti-inflammatory use. In summary, there are currently no mouse models that fully mimic the genetic and phenotypic features of human CD. Thus, it is important to develop new animal models that may better recapitulate disease initiation and progression in human patients.

The ability to use CRISPR/Cas9 technology to genetically engineer any species has provided opportunities to create new animal models to study human disease. The following chapters highlight work that was conducted to generate and characterize the first reported rat models of IBD, created by taking advantage of genome editing tools. Two specific rat models will be described: a Fischer 344 (F344) rat strain carrying the same T300A

susceptibility variant found in human patients (F344-*Atg16l1*$^{em8/RRRC}$) and an *Atg16l1* knock-out Sprague Dawley (SD) rat stock (SD-*Atg16l1*$^{em2/RRRC}$). The long-term goal of the research is to further understand how *ATG16L1* functions during CD in human patients and to develop a new model of IBD/CD that can be used to test new therapies and treatments for patients with the T300A susceptibility variant.

Because wild type rat *Atg16l1* has not been characterized previously, initial studies focused on determining the mRNA and protein expression patterns of rat *Atg16l1*. This included identification of *Atg16l1* splice variants using a 15-tissue panel to evaluate tissue-specific expression patterns and demonstration that these alternative transcripts encoded protein isoforms using *in vitro* transfection of individual splice variant sequences into HEK293 cells. *In vitro* evaluation of each WT splice variant on the process of autophagy was assessed using verified methods of quantifying autophagy, including Western blot analysis of LC3B-II, ratios of autophagosomes to autophagolysosomes, and autophagosome counts. Preliminary genotypic and phenotypic characterization of the two genetically engineered rat models (F344-*Atg16l1*$^{em8/RRRC}$ and SD-*Atg16l1*$^{em2/RRRC}$) included verification of the gene alterations carried by each and assessment of basic histology, intestinal permeability and intestinal microbiome. The F344-*Atg16l1*$^{em8/RRRC}$ strain was also subjected to acute and chronic environmental exposure studies to determine whether this model can elicit signs of IBD and/or CD using known triggers of CD in human patients. Our work offers the first detailed characterization of wild type rat *Atg16l1*, describes two novel rat models that can be used for the study of autophagy and provides validation of the F344-*Atg16l1*$^{em8/RRRC}$ rat strain as a useful tool for future IBD and CD research.

CHAPTER 2: MATERIALS AND METHODS

Animals

All studies were performed in accordance with the *Guide for the Care and Use of Laboratory Animals* and were approved by the University of Missouri Institutional Animal Care and Use Committee. Rats were group-housed by sex and strain on the same ventilated rack with a maximum of four rats per 144 $in.^2$ microisolator cage (Thoren Maxi-Miser® Interchangeable System, Hazelton, PA). Environmental parameters included: 14:10 hour light-dark cycle, humidity between 50-70% and temperature between 70-74°F. All animals were provided *ab libitum* autoclaved food (Lab Diet 5008, St. Louis, MO) and sulfuric acid treated water unless specifically described for experimental groups. Animals were confirmed to be free of adventitious viruses, parasites, and pathogenic enteric and respiratory bacteria through a quarterly dirty bedding sentinel monitoring program with diagnostic testing performed by IDEXX BioAnalytics (Columbia, MO).

Creation of Rat Strains

Both the em2 knock-out and T300A knock-in rat strains were developed using CRISPR-Cas9 genome editing technology by the Rat Resource and Research Center (Columbia, MO) and bred on site for these studies (Men et al., submitted). Briefly, zygotes from superovulated female F344/Hsd (Fischer 344; F344) and Hsd:Sprague Dawley® (SD) rats were collected 23 hours post-mating with stud males and cultured as described previously (K. Miyoshi, 1995). Two guide RNAs (gRNAs), one targeting exon 5 (5'-CACCGATTCTCCGCATTA AGGCGAT-3') and one targeting exon 13 (5'-CACCGACAATGCACGGATAGTCTC-3') of the rat *Atg16l1* gene, were designed for the

knock-out em2 strain. To generate animals carrying indels within the *Atg16l1* gene, pronuclear microinjection of both gRNAs (50 ng/μL each), and 100 ng/μL Cas9 mRNA of SD zygotes was performed. To generate the T300A knock-in strain, One gRNA (50 ng/μL; 5'-CCCAGTCCCCCAAGATGTCGTGG-3'), Cas9 protein (100ng/μL), and single-stranded oligonucleotide (ssODN) (100 ng/μL; 5' GCAGTCT GGTGGATACTGATGCTGTGCAGTTTTGTATGATGTCTGCCTCTGTTATTCCTTA GGAGACGCTCTGTCTCTTCCATCCCAGTCCCCCAAGATGTCGTAGAC**GCT**CAT CCTGCTTCTGGTAAAGATGTGAGAGTCCCAACTACTGCCTCGTATGTCTTTGT AAGTACGCTTTGTACCCAAGCCCCTCTGAGCCC 3') harboring the single base pair polymorphism of guanine to adenine in exon 10 (altered codon bolded in ssODN sequence), resulting in a threonine to alanine substitution at amino acid position 300, were used for pronuclear microinjection into F344 zygotes. One hour after injection, surviving zygotes were surgically transferred into pseudo-pregnant females. Resulting pups were screened at two-weeks of age for the mutations of interest. DNA was extracted from tail-snips using the DNeasy® Blood & Tissue Kit (QIAGEN, Valencia, CA). Indels were detected using the Surveyor® assay (Integrated DNA Technologies, Coralville, IA). High-resolution melt analysis with subsequent Sanger nucleotide sequencing was used to identify animals carrying the T300A polymorphism. Pups carrying the mutations of interest were bred to establish each strain/stock. The strains are available from the Rat Resource and Research Center (www.rrrc.us) as RRRC#896 (F344-Atg16l1^{em8Rrrc}) and RRRC#897 (SD-Atg16l1^{em2Rrrc}).

RNA Transcript Analysis

For each strain, tissue samples were collected from six wild type (WT) and six heterozygous (HET) rats (three males and three females per genotype) for RNA isolation. Tissues included: brain, thymus, esophagus, heart, lung, liver, kidney, spleen, stomach, jejunum, ileum, cecum, colon and gonad. Animals were euthanized with CO_2 overdose according to the 2013 *AVMA Guidelines for the Euthanasia of Animal* and subjected to full-body perfusion of phosphate-buffered saline (PBS, pH 7.4). Harvested tissues were immediately frozen in liquid nitrogen and stored at -80°C until processing.

RNA extraction was performed with the QIAGEN RNeasy Mini kit. Frozen tissue from each organ (30 mg) was individually placed into a sterile Red RINO lysis tube (Next Advance, Troy, NY) containing 600 μL of Buffer RLT (proprietary composition; a guanidine isothiocyanate binding buffer) and 6 μL β-mercaptoethanol. Samples were mechanically disrupted using the Bullet Blender® Storm Tissue Homogenizer (Next Advance, Troy, NY) for 3 minutes at speed level 12. Lysate was centrifuged for 3 minutes at 14,000 x g and the supernatant was carefully removed and transferred to a new microcentrifuge tube. One (1) volume of 70% ethanol was added to the supernatant and mixed by pipetting. Up to 700 uL of lysate, including precipitants that formed after addition of ethanol, was loaded on to the RNeasy spin column. The columns were centrifuged for 15 seconds at 10,000 rpm and the flow through was discarded. If the sample exceeded 700 uL the procedure was done again using the same spin column. Buffer RW1 (350 uL; 20% ethanol, 900 mM guanidine thiocyanate, 10 mM Tris-HCl (pH 7.5)) was added to the column and centrifuged at 10,000 rpm for 15 seconds. On-column DNase digestion was

performed by adding 10 uL of DNase I (Thermo Fischer Scientific, AM2222; Waltham, MA) to 70 uL buffer RDD (proprietary composition) and adding directly to the column membrane. Columns were incubated at room temperature for 15 minutes. Another 350 uL of buffer RW1 was added to the spin column and centrifuged at 10,000 rpm for 15 seconds, then flow through was discarded. To wash the membrane, 500 uL of buffer RPE (80% ethanol, 100 mM NaCl, 10 mM Tris-HCl (pH 7.5)) was added to the spin column and centrifuged for 15 seconds at 10,000 rpm. The wash step was performed again with centrifugation parameters of 2 minutes and 10,000 rpm. The spin column was placed in a new collection tube and the columns were centrifuged for 1 minute at 16,000 rpm to dry the membrane. RNA was eluted by centrifugation at 16,000 rpm using 30 uL of RNase-free water into new 1.5 mL microcentrifuge tubes. RNA concentrations were determined using the Experion™ Automated Electrophoresis System and Experion™ RNA StdSens chips (Bio-Rad Laboratories, Hercules, CA). Only RNA samples with a purity > 0.8 were used for transcript identification. RNA samples were stored at -80°C until further analysis.

Two-step RT-PCR was performed using the Superscript® IV First-Strand Synthesis System (Invitrogen, Carlsbad, CA). Two (2) μg of total RNA from each tissue sample, 1 uL random hexamer primers (50ng/μl; Thermo Fisher Scientific), 1 uL 10 mM dNTP mix (10 mM each), and DEPC-treated water (final volume 13 uL) were combined and mixed briefly for each tissue sample. Mixtures were heated at 65°C for 5 minutes then immediately incubated on ice for 2 minutes. In a separate tube, 4 uL 5x SSIV buffer 1 uL 100 mM DTT, 1 uL ribonuclease inhibitor, and 1 uL SuperScript IV reverse transcriptase (200 U/uL) for each sample was mixed to generate a master mix. The master mix was

capped, mixed and collected into the bottom of the tube using a benchtop mini centrifuge (MLX-106; Crystal Industries, Addison, TX). Each RNA sample was mixed with 7 uL of RT master mix. Reactions were incubated for 10 minutes at 23°C, 10 minutes at 55°C, and 10 minutes at 80°C. RNA was removed by adding 1 uL *E. coli* RNase H and incubating for 20 minutes at 37°C. Once the cDNA was made, gene-specific amplification was performed. Two (2) ul of cDNA was mixed with 2 uL PCR reaction buffer containing 20 mM $MgCl_2$, 3.2 uL dNTPs (1.25 mM), 0.3 uL forward primer (25 mM), 0.3 uL reverse primer (25 mM), and 0.2 uL FastStart™ Taq DNA polymerase (5 U/uL) (Sigma, St. Louis, MO). The reaction volume was brought up to 18 uL with nuclease-free water. Multiple gene-specific primer sets were used to identify WT rat *Atg16l1* splice variants. The primer sequences and amplification parameters can be found in Table 2.1.

Amplified products were separated by gel electrophoresis using 1X Tris-acetate EDTA (TAE) agarose gels and 1X Tris-acetate EDTA (TAE) running buffer (see Table 2.1). Amplicons were gel-purified using the QIAquick Gel Extraction Kit (QIAGEN). DNA bands were excised with a sterile scalpel and weighed in pre-weighed 1.5 mL microcentrifuge tubes. Buffer QG (5.5 M guanidine thiocyanate, 20 mM Tris-Cl (pH 6.6)) was added in a ratio of 3 volumes QG to 1 volume gel (100 mg gel ~ 100 uL). Samples were incubated at 50°C for 10 minutes with intermittent vortexing to melt the agarose gel. One (1) gel volume of 100% isopropanol was added to each sample and mixed. The samples were individually applied to QIAquick spin columns and DNA was bound to the membrane by centrifugation at 13,000 rpm for 1 minute at room temperature. The flow through was discarded, and another 500 uL buffer QG was added to the column and

centrifuged again at room temperature for 1 minute at 13,000 rpm. Flow through was discarded. To wash, 750 uL of buffer PE (10 mM Tris-Cl (pH 6.6), 80% ethanol) was added to the column and centrifuged at room temperature for 1 minute at 13,000 rpm and flow through was discarded. The column was centrifuged again at room temperature for 1 minute at 13,000 rpm to dry the membrane. Fifty (50) uL of buffer EB (10 mM Tris-Cl, pH 8.5) was applied to the membrane and allowed to incubate at room temperature for 1 minute followed by elution of the DNA into a new 1.5 mL microcentrifuge tube via centrifugation at room temperature for 1 minute at 14,000 rpm.

DNA concentrations and purity were measured using the Nanodrop 8000 Spectrophotometer (Thermo Fisher Scientific) and samples were sent to the University of Missouri DNA Core (Columbia, MO) for nucleotide sequence analysis. Resulting sequences were analyzed with SnapGene software (GSL Biotech LLC, Chicago, IL) and compared to the reported full-length *Rattus norvegicus Atg16l1* sequence (Ensembl *R. norvegicus* assembly: Rnor_6.0; ENSRNOT00000024445.3)

Table 2.1. Primers, PCR and gel electrophoresis conditions for WT *Atg16l1* splice variants and genetically modified em2 and T300A strain allele

Primers					PCR Conditions			Electrophoresis Conditions		
Primer Set		Primer Sequence (5' → 3')	Exon	Size of PCR Product (bp)	Denaturation	Anneal	Extension	% Agarose Gel	Voltage	Time (hr)
1	Forward	GGTGTGGAGAGGTGAGGTTC	1	612	94°C; 30s.	60°C; 30s.	72°C; 40s.	2	50	4.5
	Reverse	CATCGGTTGGTCTGGGACTT	5							
2	Forward	CAGATGCAGCAGAAGGACAA	4	419 167 (Δ5)	94°C; 30s.	58°C; 30s.	72°C; 30s.	3	35	5.5
	Reverse	GTCTAGTGTGTCTTCTCTGGAG	7							
3	Forward	CAGCAAAGGAACCTCTACCT	6	683 (FT) 634 (Δ 9) 577 (Δ 8, 9)	94°C; 30s.	58°C; 30s.	72°C; 45s.	3	35	7.5
	Reverse	GAGTTTGAGACCCTAGAGGC	14							
4	Forward	CGAATCTGGACTGTGGATGA	13	723	94°C; 30s.	59°C; 30s.	72°C; 45s.	2	50	4.5
	Reverse	ACTACACAGGAGGGTCTCTT	19							
5	Forward	CACAAGAAGCGTGGGGAGTTAG	3	798 750 (Δ 9) 693 (Δ 8, 9) 546 (Δ5)	94°C; 30s.	60°C; 30s.	72°C; 45s.	3 (High Res.)	40	4.5
	Reverse	CCAAAGTTTAACCCTGCGGTCC	11							

FT = full transcript; Δ = loss of specified exon(s)

Generation of Splice Variant Clones

Ten (10) ng of the vector pEGFP-N1 (V12024; NovoPro Bioscience, Inc., Shanghai, China) was transformed into 50 uL One Shot TOP10 competent cells (Invitrogen) and grown on LB-agar plates with kanamycin (50 ug/mL) overnight at 37°C. Ten colonies were selected from each plate and used to 1) streak for isolated colonies on LB-agar plates with kanamycin (50 ug/mL) for future use as well as 2) inoculate capped sterile tubes containing

3 mL LB broth+ kanamycin (50 ug/mL). Plates were incubated overnight at 37°C. Broth samples were grown overnight at 37°C in a shaking incubator set at 225 rpm.

Plasmid DNA was recovered from broth cultures the following morning. Bacterial cultures were transferred to sterile 15 mL conical tubes for centrifugation at 2500 rpm and 4°C for 10 minutes to pellet the bacteria. The supernatant was removed, and the pellet was resuspended in 500 uL ice-cold STE solution (8% (w/v) sucrose, 50 mM Tris-HCl (pH 8.0), 50 mM EDTA (pH 8.0)) and transferred to a 1.5 mL microcentrifuge tube. The samples were centrifuged at 4°C and 5000 rpm for 5 minutes. The supernatant was removed completely, and the pellet was resuspended completely by vortexing in 350 uL room temperature STET solution (8% (w/v) sucrose, 50 mM Tris-HCl (pH 8.0), 50 mM EDTA (pH 8.0), 5% (w/v) Triton® X-100). Twenty-five (25) uL of previously frozen lysozyme (10 mg/mL lysozyme in 10 mM Tris-HCl (pH 8.0)) was added to the STET suspension and mixed immediately for 5 seconds by pipetting up and down with a 1 mL pipette. The tubes were heated to 100°C for 45 seconds using a heat block and then removed and left to cool on the bench top to room temperature. Samples were centrifuged at 14,000 rpm and 4°C for 10 minutes. Pellets were removed using sterile toothpicks and an equal part of 100% isopropanol was added. The tube was inverted 6 times to mix and the samples were centrifuged at 14,000 rpm and 25°C for 30 minutes. Supernatant was removed completely and 500 uL of 70% ethanol was added to the pellet. The tubes were inverted 6 times to wash the pellet, and the samples were centrifuged at 14,000 rpm and 25°C for 10 minutes. The supernatant was removed completely, and the pellet was air-dried for 5 minutes. The

pellets were resuspended in 25 uL sterile, deionized water by incubation at 37°C for 20 minutes with brief, gentle vortexing every 5 minutes.

Table 2.2. Primers, PCR and gel electrophoresis conditions to verify nucleotide sequence of pEGFP-N1 vector

Primers				**PCR Conditions**			**Electrophoresis Conditions**		
Primer Set		Primer Sequence (5' → 3')	PCR Product (bp)	Denaturation	Anneal	Extension	% Agarose Gel	Voltage	Time (hr)
1	Forward	CTAGCGCTACCGGACTCAGA	798	94°C; 30s.	56°C; 30s.	72°C; 50s.	1	90	2
	Reverse	CAGCTCGTCCATGCCGAGAG							
2	Forward	CTGCTGGAGTTCGTGACCGC	1097	94°C; 30s.	58°C; 30s.	72°C; 75s.	0.7		
	Reverse	TAGGGGCGGGACTATGGTTG							
3	Forward	GTCAGCAACCATAGTCCCGC	1004	94°C; 30s.	55°C; 30s.	72°C; 60s.	0.7		
	Reverse	CTCGTCAAGAAGGCGATAGAAG							
4	Forward	CAGCGCATCGCCTTCTATCG	1059	94°C; 30s.	58°C; 30s.	72°C; 75s.	0.7		
	Reverse	GCGTGGCGCTTTCTCATAGC							
5	Forward	GATACCTACAGCGTGAGCTATG	966	94°C; 30s.	55°C; 30s.	72°C; 60s.	1		
	Reverse	GCAGAATTCGAAGCTTGAGCTC							

Overlapping primer sets across the entirety of pEGPF-N1 were used to sequence the plasmid (Table 2.2). Concentration of plasmid DNA was measured for sequencing using the NanoDrop™ 8000 Spectrophotometer (Thermo Scientific). The remainder of the samples were stored at -20°C.

The previously streaked and labeled LB-agar plate colony corresponding to a sequence-verified plasmid was used to grow up a stock of pEGFP-N1 plasmid to linearize and use in downstream applications. A sterile inoculation loop was used to collect a small subset of the previous streak and re-streak a new LB-agar plate. The plate was incubated at 37°C overnight to grow individual colonies from the saved streak. A sterile toothpick was used to inoculate 500 mL of LB broth + kanamycin (50 ug/mL) with bacteria and the culture was grown overnight at 37°C, shaking at 300 rpm. The following morning, an aliquot of 2.5 mL of bacterial suspension was used to create glycerol stocks (500 uL overnight culture to 500 uL 50% glycerol in 2 mL screw-cap tubes) to store at -80°C. The rest of the overnight culture was purified using the QIAGEN Plasmid Maxi Kit. Bacterial cells were harvested by centrifugation at 6000 x g for 15 minutes at 4°C in 50 mL conical tubes. The resulting bacterial pellets were resuspended in the same 10 mL of buffer P1 resuspension buffer (50 mM Tris-Cl (pH 8.0), 10 mM EDTA) containing LyseBlue® (43 mg/mL thymophthalein in 100% ethanol) and RNase A (100 ug/mL) by transferring the suspension from one tube to the next to incorporate all ten pellets. The new suspension was then placed in a 50 mL conical tube. Ten (10) mL of lysis buffer P2 (200 mM NaOH, 1% SDS (w/v)) was added to the sample and the tube was vigorously inverted 6 times and incubated at room temperature for 5 minutes. After incubation, 10 mL of chilled (4°C) neutralization buffer P3 (3.0 M potassium acetate, pH 5.5) was added to the suspension and vigorously inverted 6 times to mix. The tube was chilled on ice for 20 minutes. The sample was then centrifuged at 20,000 x g for 30 minutes at 4°C and the supernatant was removed immediately and placed into a new 50 mL conical tube. The supernatant was centrifuged

again at 20,000 x g for 15 minutes at 4°C and the supernatant was removed and placed into a new 50 mL conical tube. During centrifugation, a QIAGAN-500 tip was equilibrated by applying 10 mL of equilibration buffer QBT (750 mM NaCl, 50 mM MOPS (pH 7.0), 15% isopropanol (w/v), 0.15% Triton® X-100 (w/v)) and allowing the tip to empty by gravity flow. The supernatant was then added to the column and allowed to enter the resin by gravity flow. The column was washed with 30 mL buffer QC (1.0 M NaCl, 50 mM MOPS (pH 7.0), 15% isopropanol(w/v)) twice and allowed to empty by gravity flow before eluting the DNA with 15 mL of elution buffer QF (1.25 M NaCl, 50 mM Tris-Cl (pH 8.5), 15% isopropanol (w/v)) into a 50 mL conical tube.

Purified plasmid was linearized using a double-restriction endonuclease digest with *Eco*R1-HF and *Not*I-HF restriction enzymes in New England BioLabs® (NEB) Cutsmart® buffer (50 mM potassium acetate, 20 mM Tris-acetate, 10 mM magnesium acetate, 100 ug/mL bovine serum albumin; pH 7.9 at room temperature). One (1) ug of purified plasmid was incubated for 1 hour at 37°C with 1 uL of each restriction enzyme (20 units each) 2 uL 10X NEB Cutsmart® buffer and sterile deionized water to a total reaction volume of 20 uL. After 1 hour, restriction enzymes were heat inactivated for 20 minutes at 65°C. This restriction digest eliminated EGFP from the original plasmid since it was not needed for downstream cloning. The linearized plasmid was purified using the NucleoSpin Gel and PCR Clean-Up Kit (Takara Bio.) The sample volume was adjusted to 50 uL with nuclease-free water. One (1) volume of sample was mixed with 2 volumes of buffer NTI (proprietary composition; guanidine thiocyanate and sodium iodide-based dissolving buffer) and loaded into the NucleoSpin column. The sample was centrifuged for 30 seconds at 11,000 x g and

the flow through was discarded. Buffer NT3 (700 uL; (proprietary composition; an ethanol-based wash buffer) was added to the column and centrifuged for 30 seconds at 11,000 x g. Flow through was discarded and the wash step with NT3 was repeated. The column membrane was dried by centrifugation for 1 minute at 11,000 x g, and the DNA was eluted with 30 uL nuclease-free water into a new 1.5 mL microcentrifuge tube. Plasmid was stored at -20°C.

cDNA representing each WT *Atg16l1* splice variant was amplified in two fragments each using CloneAmp HiFi PCR Premix (proprietary composition; Takara Bio.). Primers were designed with 15 bp extensions (5') that were complementary to the ends of either the linearized vector or fragment ends (Table 2.3). A master mix of 10.35 uL nuclease-free water, 12.5 uL CloneAmp PCR Premix, 0.075 uL forward primer (100 uM stock) and 0.075 uL reverse primer (100 uM stock) for each sample was divided into 25 uL aliquots in 1.5 mL microcentrifuge tubes. One hundred (100) ng of template cDNA for each WT splice variant was added to each reaction. Amplicons were separated by gel electrophoresis and purified using the NucleoSpin Gel and PCR Clean-Up kit (Takara Bioscience Inc.). Parameters for PCR and gel extraction can be found in Table 2.3.

Table 2.3. Primers, PCR and gel electrophoresis conditions to amplify *Atg16l1* for generating splice variant clones

Primers				**PCR Conditions**			**Electrophoresis Conditions**		
Primer Set		Primer Sequence (5' → 3')	PCR Product (bp)	Denaturat.	Anneal	Extension	% Agarose Gel	Voltage	Time (hr)
1	Forward	CTCAAGCTTCGAATTATGTCGTCGGGCCTCC	1019	98°C; 10s.	58°C; 30s.	72°C; 65s.	1	90	2
	Reverse	CCGTCATGTGCATCAAAGACATACG							
2	Forward	TGATGCACATGACGGAGAGGTC	871	98°C; 10s.	60°C; 30s.	72°C; 55s.	1		
	Reverse	TCTAGAGTCGCGGCCGGTGGGTGCCATATAGCT							

DNA bands were excised from the agarose gel with a clean scalpel blade and placed into pre-weighed 1.5 mL microcentrifuge tubes. The weight of each agarose piece was taken, and 200 uL of buffer NTI was added per each 100 mg of agarose gel. The samples were incubated at 50°C for 10 minutes with brief vortexing every 2-3 minutes to melt the agarose. Once melted, all subsequent steps were performed at room temperature. The samples were placed individually into NucleoSpin Gel and PCR Clean-up Midi columns and centrifuged for 30 seconds at 11,000 x g. The flow through was discarded and the column was placed back into the collection tube. The column membrane was washed with 700 uL buffer NT3 and centrifuged for 30 seconds at 11,000 x g. The flow through was discarded and the collection tube replaced. The column was centrifuged again for 1 minute at 11,000 x g to dry, and the DNA was eluted in 30 uL nuclease-free water into a new 1.5 mL microcentrifuge tube after a 1-minute room temperature incubation.

Nucleotide sequence analysis of each variant was performed by the University of Missouri DNA Core and sequences were checked for accuracy using SnapGene software comparing full-length *Rattus norvegicus Atg16l1* (Ensembl *R. norvegicus* assembly: Rnor_6.0; ENSRNOT00000024445.3) to each variant. Variants were stored at -80°C until use.

Cloning was performed using the In-Fusion® HD Cloning Plus system (Takara Bio, Kutsatsu, Shiga Prefecture, Japan). After nucleotide sequence of the plasmid and each WT splice variant fragment was verified, In-Fusion reactions were set up, including 2 uL In-Fusion HD enzyme Premix (proprietary composition), purified PCR fragments, the linearized vector, and deionized water to a total volume of 10 uL. The molar ratio of each

of the inserts was 2:2:1 with regards to the linearized vector. Reactions were incubated for 15 minutes at 50°C and then immediately placed on ice. Reactions were then used to transform Stellar competent cells (Takara Bio). Cells kept at -80°C were thawed on ice just before use. Tubes of cells were tapped gently to evenly distribute and split into 25 uL aliquots in 1.5 mL microcentrifuge tubes. An aliquot (2.5 uL) of each In-Fusion reaction was added to 25 uL of cells and placed on ice for 30 minutes. The mixtures were then heat-shocked for exactly 45 seconds at 42°C and immediately placed on ice for 2 minutes. Warmed (37°C) SOC medium was added to a final volume of 500 uL and tubes were incubated for 1 hour at 37°C in an incubator shaking at 225 rpm.

Fifty (50) uL and 100 uL of each mixture was plated onto 2 LB-agar plates + kanamycin (50 ug/mL). The remainder of the sample was stored at -20°C overnight. Plate were incubated overnight at 37°C. The next morning, 10 individual colonies were selected for each WT splice variant and streaked onto labeled LB-agar + kanamycin plates. Each colony was also used directly for PCR screening to assess proper orientation and inclusion of the DNA fragments.

Protein Expression

HEK293 cells (ATTC, Manassas, VA) were grown in 75 cm^2 sterile flasks (Thermo Scientific) containing minimum essential media (MEM; Thermo Scientific) with fetal bovine serum (FBS; final concentration 10%; Sigma), and penicillin-streptomycin (P-S; final concentration 1%; Sigma) at 37°C and 5% CO_2. Cells were seeded into 25 cm^2, sterile, vented cap, non-treated culture flasks (NEST Scientific; Rahway, NJ) at 700,000 cells/flask

24 hours before transfection. Cells were between 70-80% confluence at the time of transfection. Transfection was performed using the Lipofectamine® 3000 reagent protocol (Invitrogen). Experimental groups included: each of the four splice variant overexpression plasmids (1 µg each), EGFP-N1 positive transfection control (1 µg), Lipofectamine® reagent only negative control, and cells-only negative control to give a total of 8 experimental groups performed in triplicate (24 flasks). Cells were incubated for 8 hours at 37°C and 5% CO_2 post-transfection and then the media was removed and replaced with 5 mL of fresh growth media (MEM + 10% FBS + 1% P-S) per flask. Cells were incubated for another 40 hours.

After incubation, cells were treated with TrypLE™ Express enzyme (1X with phenol red; Cat No: 12605010; Gibco) and centrifuged at 1250 x g for 10 minutes at 4°C. Cell pellets were washed with ice cold PBS, spun again at 1250 x g for 10 minutes at 4°C and resuspended in 500 uL ice-cold RIPA lysis buffer (150 mM sodium chloride, 1.0% Triton® X-100, 0.5% sodium deoxycholate, 0.1% sodium dodecyl sulfate (SDS), and 50 mM Tris-HCl pH 8.0) with fresh protease inhibitor cocktail (MFCD00677817; 5µL per mL RIPA), phenylmethylsulfonyl fluoride (PMSF; 20 µL of 100 mM stock per 1 mL RIPA) and sodium orthovanadate (10 µL of 20 µM stock per 1 mL RIPA) added to buffer immediately before use. Cell membranes were mechanically disrupted by pipetting the sample through a 1 mL pipette tip 10 times and vortexing for 10 seconds before incubation on ice for 30 minutes. Lysed samples were centrifuged at 14,000 x g for 15 minutes at 4°C to pellet the cell debris, and the supernatants were transferred to microcentrifuge tubes and stored at -20°C.

Protein was measured using the Pierce™ BCA Protein Assay Kit (Thermo Scientific) following the Pierce™ BCA kit microplate procedure. Bovine serum albumin (BSA) standards diluted in RIPA buffer were used for the assay (2000, 1500, 1000, 750, 500, 250, 125, 0 ug/mL). Briefly, reagent A (proprietary; contains sodium carbonate, sodium bicarbonate, bicinchoninic acid and sodium tartrate in 0.1 M sodium hydroxide) and B (proprietary; contains 4% cupric sulfate) were mixed in a 50:1 ratio with a resulting volume of 200 µL working reagent per sample. Working reagent and 10 µL of sample was added to each well (1:20 dilution of sample). The plate was covered and incubated at 37°C for 30 minutes. Absorbance was measured at 562 nm on the SpectraMax M3 microplate reader with SoftMax Pro 6.2 microplate data analysis software (Molecular Devices, Sunnyvale, CA).

Proteins were separated using ExpressPlus™ PAGE (polyacrylamide) gels (10x8, 12%, 12 well; GenScript, Jiangsu Province, China) at 140 V for 75 minutes in Tris-MOPS running buffer (M00138; GenScript). Briefly, 20 mg of total protein for each sample was added to 8 µL 5x sample buffer (MB01015; Genscript) and ddH_2O to a total volume of 40 µL. Samples were incubated at 70°C for 10 minutes to denature proteins and immediately placed on ice for 2 minutes to cool. Molecular weight of proteins was assessed using Precision Plus Protein™ Kaleidoscope™ Prestained Standards (Bio-Rad Laboratories). Proteins were considered fully separated once the sample buffer marker ran completely off the bottom of the gel (approximately 75 minutes).

Polyvinylidene difluoride (PVDF) membranes were presoaked in 100% methanol for 10 seconds, then transferred to soak in transfer buffer (M00139; GenScript) containing 10% methanol for 5 minutes at room temperature. PAGE gels, filter paper (Cat No: 84783; Thermo Scientific™), and foam pads were also presoaked in transfer buffer containing 10% methanol for 5 minutes at room temperature. Tank transfer sandwiches were assembled and placed into wet transfer tanks containing transfer buffer with 10% methanol surrounded by an ice bath, and proteins were transferred from the gel to the PVDF membrane at 100 V for 90 minutes (Bio-Rad Laboratories).

PVDF membranes were rinsed in distilled water three times for 5 minutes each prior to blocking. Blocking was performed in 1X TBST (pH 7.6; 20 mM Tris, 150 mM NaCl, 0.1% Tween 20) with 3% BSA for 4 hours at room temperature. Primary anti-ATG16L1 antibody (1:1000; TA306513, Origene, Rockville, MD) and secondary anti-rabbit IgG antibody (1:100,000; A0545, Sigma) were diluted in TBST with 1% BSA and 0.1% Tween 20 for membrane incubation overnight at 4°C and for 90 minutes at room temperature, respectively. Protein detection was performed with SuperSignal® West Pico Kit Chemiluminescent Substrate (Thermo Scientific). An equal volume of stable peroxide solution and luminol/enhancer solution were mixed (3.5 mL each) and added to the membrane. Membranes were incubated for 5 minutes in the dark at room temperature. The membrane was removed, and excess solution was drained. Protein bands were visualized on the ChemiDoc™ XRS+ System with Image Lab™ Software #1708265 (Bio-Rad).

Atg16l1 antibody was stripped from the membrane using Restore™ stripping buffer (Thermo Scientific) and the membranes were re-processed for detection of β-actin protein. Briefly, membranes were washed in room temperature TBS and incubated in stripping buffer for 15 minutes with agitation. Membranes were rinsed under cold tap water and washed in TBST (0.1% Tween) three times for 10 minutes each before blocking in TBST with 3% BSA for 4 hours. Primary anti-β-actin antibody (1:2000; ab8227; Abcam, Cambridge, UK) and secondary anti-rabbit antibody (1:100,000; A0545) were diluted in TBST with 1% BSA for incubation at room temperature for 1 hour and 90 minutes, respectively. Protein detection was performed as described previously.

Intestinal Permeability

Four groups of rats (SD WT, F344 WT, em2 HET, and T300A HET) were evaluated for intestinal permeability. Forty-eight, 6-week-old rats (6 males and 6 females for each group) were fasted for 12 hours (no feed or water) for baseline intestinal permeability analysis. After fasting, rats were weighed and immediately gavaged with 50 mg/kg fluorescein isothiocyanate (FITC) dextran (4,000 Da, 50 mg/mL in sterile water; Sigma) Four hours after gavage, animals were humanely euthanized by CO_2 asphyxiation and cardiac exsanguination. Three milliliters of blood were collected into gel serum separator tubes (SST) with clot activator (Becton Dickinson, Franklin Lakes, NJ) and shielded from light. Tubes were inverted gently 6 times and placed upright at room temperature for 30 minutes to ensure proper clot formation. Serum was separated by centrifugation at 1,300 x g for 12 minutes in a swinging-bucket rotor centrifuge. Serum (500 µL) was collected into a new microcentrifuge tube and diluted with equal parts sterile PBS.

Diluted serum (100 µL) was added to a Greiner CELLSTAR® black polystyrene plate with black polystyrene flat bottoms (Sigma) in triplicate. The concentration of FITC in individual serum samples was determined by fluorescence (excitation of 485 nm and emission of 528 nm) on the SpectraMax M3 microplate reader with SoftMax Pro 6.2 microplate data analysis software. Serially diluted FITC-dextran (0, 125, 250, 500, 1000, 2000, 4000, 8000 ng/mL in 1X PBS) was used as standards. Standards were run in triplicate to ensure proper linear concentration.

Histology

Ileum and proximal colon from six T300A HET rats and six WT littermates (three males and three females per group) were collected for histologic analysis. Fresh tissues were fixed in 10% formalin for at least 24 hours prior to being embedded in paraffin. Slides of each tissue were processed for analysis using a hematoxylin and eosin stain (H&E), Alcian blue stain at pH 2.5 with a Period Acid Schiff (PAS) counterstain, and lysozyme immunohistofluorescence (IFA) stain. H&E and Alcian blue/PAS measurements and cell counts were conducted on an Olympus BX41 microscope (Shinjuku, Tokyo, Japan) and images were captured using the Excelis HDS camera and monitor system (Accu-Scope, Commack, NY). IFA measurements were conducted on a Leica DMI4000 B automated inverted microscope and Leica TCS SPE confocal using the Leica Advanced Fluorescence application suite software (Wetzlar, Germany).

H&E and alcian blue/PAS staining was performed by IDEXX BioAnalytics histology services (Columbia, MO). Ileum and proximal colon were assessed with H&E stain to observe differences in villus length and crypt height. The length of each villus was measured from the top of the villus to the crypt transition (the invagination between two villi). Crypt height was measured from the crypt transition to the muscular layer. The lengths of 50 villi and heights of 50 crypts were measured, in triplicate, per animal. Alcian blue and PAS stain was used for ileal PC counts as well as ileal and proximal colon goblet cell counts. H&E and Alcian blue measurements were performed by a single trained observer.

Lysozyme IFA was used to observe differences in lysozyme staining within PCs. Deparaffinization and rehydration of tissues was completed using a standard xylene and ethanol wash procedure (Abcam IHC deparaffinization protocol; https://www.abcam.com/protocols/ihc-deparaffinization-protocol). Rehydrated slides were rinsed in cold tap water and placed in antigen retrieval buffer (10mM Tris Base, 1mM EDTA solution, 0.05% Tween 20, pH 9.0) overnight in a 60°C water bath. Slides were cooled to room temperature and rinsed in PBST (0.05% Tween 20) two times for 5 minutes each and blocked in TBS with 10% normal goat serum (NGS) and 3% bovine serum albumin (BSA) for 4 hours at room temperature. Slides were incubated in rabbit lysozyme polyclonal primary antibody (1:1000; 15013-1-AP, Proteintech, Chicago, IL) and goat anti-rabbit IgG (H+L) Alexa Fluor Plus 488 secondary antibody (1:1000; #A32731, Invitrogen) diluted in 1% BSA blocking buffer overnight at 4°C and for 1 hour at room temperature, respectively. Slides were mounted using VECTASHIELD HardSet Antifade

Mounting Medium (Vector Laboratories, Burlingame, CA) and kept in the dark at 4°C for up to one week before analyzing.

Microbiome

Twelve HET T300A rats and 12 WT littermates (equal sexes) were used for fecal microbiome analysis. Fecal samples were collected from each animal beginning at 4 weeks of age and then 6 and 12 weeks later. Individual rats were placed in empty autoclaved cages between the hours of 7AM and 9AM and allowed to defecate. Fecal pellets were collected with autoclaved, sterilized toothpicks and placed into sterile microcentrifuge tubes. Samples were immediately frozen and stored at -80°C.

Microbial DNA was extracted according to a published protocol (Ericsson et al., 2015). Previously frozen fecal samples (30 mg) were placed in 800 μL of lysis buffer (500 mM NaCl, 50 mM tris-HCl, 50 mM EDTA, and 4% SDS), homogenized for 5 minutes at speed level 12 using the Bullet Blender® Storm Tissue Homogenizer (Next Advance), and incubated at 70°C for 20 minutes. Samples were centrifugation at 5000 x g for 5 minutes at room temperature. The supernatant was mixed with 200 μL of 10 mM ammonium acetate, incubated on ice for 5 minutes, and centrifuged at 16,000 x g for 10 minutes at room temperature. A 750 μL aliquot of supernatant was mixed with equal volumes of chilled isopropanol and incubated for 30 minutes on ice. Samples were centrifuged at 16,000 x g, 4°C for 15 minutes to pellet DNA. Pellets were rinsed twice with 70% ethanol and re-suspended in 150 μL Tris-EDTA. Proteinase K (15 μL) and buffer AL (200 μL; 10 mM Tris-Cl, 0.5 mM EDTA (pH 9.0); DNeasy Kit, QIAGEN) were added and samples

were incubated at 70°C for 10 minutes. 100% ethanol (200 μL) was added and samples were transferred to a QIAGEN DNeasy spin column. Columns were centrifuged at 12000 x g for 1 minute at room temperature and flow through was discarded. Buffer AW1 (500 uL; proprietary, a stringent wash buffer with low concentration of quanidine) was added to each column and centrifuged for 1 minute at 10,000 rpm at room temperature. Buffer AW2 (500 uL; proprietary, Tris-based ethanol solution to remove salts) was added to the column and centrifuged at 14,000 x g for 3 minutes at room temperature. Samples were eluted into new 1.5 mL microcentrifuge tubes in 100 μL EB buffer (QIAGEN) and dsDNA yield was measured using Qubit® dsDNA BR assay kits and fluorometery (Qubit 2.0, Life Technologies, Carlsbad, CA). With one thin-walled 0.5 mL clear PCR tube per sample, 190 uL of Qubit® working solution (Qubit® dsDNA BR reagent 1:200 in Qubit® dsDNA BR buffer) was added to each tube. Ten (10) uL of sample was added for a total final volume of 200 uL. Two standards (0 ng/uL and 100 ng/mL) were prepared in a similar way, with 190 uL working solution plus 10 uL standard. All tubes were incubated at room temperature for 2 minutes before measuring. Each standard and sample was vortexed immediately prior to measurement on the Qubit® 3.0 fluorometer.

Library construction and sequencing was performed at the University of Missouri DNA Core facility. All DNA samples were normalized for PCR amplification. Bacterial 16S ribosomal DNA libraries were constructed by amplification of the V4 hypervariable region of the 16s rRNA gene with universal primers (U515F/806R) flanked by Illumina standard adapter sequences and the following parameters: 98°C (3 min.) + [98°C (15 sec.) +50°C (30 sec.) +72°C (30 sec.)] × 25 cycles +72°C (7 min.). Amplicons were pooled for shotgun

metagenome sequencing by Illumina MiSeq and V2 chemistry with 2x250 base pair paired end reads, as described previously (Ericcson, 2015).

Informatics analysis was conducted at the MU Informatics Research Core Facility (Columbia, MO). Quality-controlled reads were merged into contiguous sequences (contigs) using FLASh software (Magoč & Salzberg, 2011). Qiime v1.8 software (Kuczynski et al., 2011) was used to remove chimeric sequences and remaining contigs were binned and assigned to operational taxonomic units (OTUs). Taxonomic assignment was conducted using BLAST (Johnson et al., 2008) against the SILVA database (Quast et al., 2013) of aligned 16S rRNA gene sequences and taxonomy. Principle component analyses were performed on non-transformed OTU relative abundance data using Past v3.2 (O. Hammer, D. A.T. Harper, & Ryan, 2001).

All results were considered statistically significant for p values ≤ 0.05. Principal component analysis was performed using a non-linear iterative partial least squares algorithm to evaluate β-diversity and its association with sex and genotype (WT or HET) through Metaboanalyst (Chong, Wishart, & Xia, 2019); (Chong et al., 2018). Metaboanalyst was also used to develop heat map data, and significant OTU outliers were evaluated by Kruskal Wallis test at $p < 0.01$. Statistical analysis for measures of intestinal permeability were performed by two-way ANOVA examining the effect of sex and genotype on intestinal permeability. Statistical analysis for histologic measurements were performed using the Analysis ToolPak for Microsoft Excel 2016. Differences for histology were determined using two-tailed independent *T*-tests for genotype (WT and HET).

Acute Environmental Exposure

Sixteen (16) HET T300A rats and 16 WT littermates (equal sexes) between 10 and 11 weeks of age were randomly split between control groups and diclofenac (COX1 and COX2 non-specific non-steroidal anti-inflammatory; NSAID) treatment groups. Rats were co-housed by sex and treatment group in pairs with one WT and one HET per cage. Prior to experimental treatment, all rats were weighed, and a fecal sample was collected from each rat as described previously. Rats in the NSAID treatment groups were then orally gavaged with 10.0 mg/kg diclofenac (10 mg/mL in sterile water) between 8AM and 9AM. Rats in the control groups were orally gavaged with an equivalent amount of sterile water based on their weight. Rats were weighed every day to track possible weight loss (rats losing > 20% weight were euthanized and immediately necropsied) and ensure proper dosing. Twenty-four hours after the last treatment, rats were euthanized and grossly evaluated for signs of NSAID toxicity. A fecal sample, ileal scrape, blood sample, and samples of ileum and proximal colon were collected. Fecal samples and scrapes were immediately frozen at -80°C. To isolate serum, blood samples in serum separator tubes (SST; Becton Dickerson) were incubated at room temperature for 30 minutes and then processed by centrifugation at 1,200 x g for 20 minutes. Serum was stored at -80°C until use. Tissue samples were oriented into Swiss gut rolls, placed in tissue embedding cassettes, and placed into 10% formalin overnight to fix (Moolenbeek & Ruitenberg, 1981).

Rats were assessed for signs of NSAID toxicity, including, but not limited to, body fat wasting, liver necrosis, abdominal fibrosis suggestive of intestinal perforation, and free

blood within the abdominal cavity. Any changes were qualitatively noted and *in situ* images were taken for each animal prior to sample collection.

Swiss gut rolls including ileum, ileocecocolic junction, and proximal colon were processed by IDEXX BioAnalytics (Columbia, MO) using an H&E stain as previously described. Samples were analyzed independently by two laboratory animal veterinarians with training in histology, both blinded to sex, genotype, and treatment group of each sample. Each sample was given a score of 0-48 based on a previously developed inflammatory bowel disease rating system for mucosal and inflammatory changes (Figure 2.1). Samples were assessed for statistical significance using a three-way ANOVA for sex, genotype, and treatment group using GraphPad Prism 8 (San Diego, CA).Fecal samples and ileal scrapes were processed as described previously for DNA extraction, genomic library construction and 16S rRNA sequencing, and informatics. Principle component analyses were performed on non-transformed OTU relative abundance data using Past v3.2 (O. Hammer et al., 2001). Principal component analysis was also performed using a non-linear iterative partial least squares algorithm to evaluate β-diversity and its association with sex and genotype (WT or HET) through Metaboanalyst (Chong et al., 2019); (Chong et al., 2018). Metaboanalyst was also used to develop heat map data, and significant OTU outliers were evaluated by Kruskal Wallis test at $p < 0.01$.

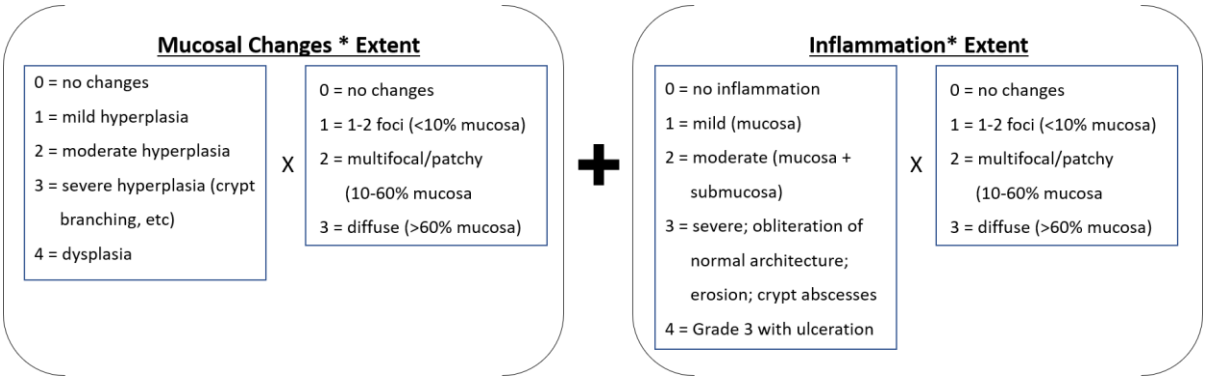

Figure 2.1: Inflammatory bowel disease scoring chart. Tissue samples, in Swiss-roll formation, were evaluated for mucosal changes and inflammation. Two blinded veterinarians trained in laboratory animal pathology scored tissues independently and scores were checked for consistency. Mucosal change or inflammation score was multiplied by the extent score to give a total of 12 for each category. Scores were added together for a final score of up to 24 for each tissue sample.

All reagents were prepared as described in the protocol for the S100 Calcium Binding Protein A8/A9 Complex (S100A8/A9), ELISA Kit (Cat No: MBS036184; MyBioSource, San Diego, CA). All reagents and samples were warmed to room temperature prior to assay, and the provided 20X wash solution was diluted to a 1X working wash solution. Standards (50 µL) and samples (50 µL) were added to their respective wells in triplicate, and sample diluent (50 µL) was added as a plate blank/control. HRP-conjugate (100 µL) was added to each well and the plate was covered and incubated for 60 minutes at 37°C. The plate was manually washed 4 times by dumping the mixtures out of the wells and filling completely with 1X wash solution and letting stand for 1 minute each time. Solution A (50 µL) and solution B (50 µL) were added to each well and incubated in the dark for 15 minutes at 37°C. Stop solution (50 µL) was added to each well (color change from blue to yellow). Within 15 minutes of adding stop solution, the optical density of standards and samples was measured at 450 nm using the SpectraMax M3 microplate reader with

SoftMax Pro 6.2 microplate data analysis software (Molecular Devices). Samples were assessed for statistical significance using a three-way ANOVA for sex, genotype, and treatment group using GraphPad Prism 8.

Chronic Environmental Exposure

Twenty-four (24) HET T300A rats and 24 WT littermates (equal sexes) were randomly split between a control group, a low-dose diclofenac treatment group, and an *ad libitum* Western diet formulated rodent chow (D12079B; Research Diets Inc., New Brunswick, NJ). All animals were weaned at 21 days of age and given 7 days to acclimate. At 28 days of age, rats were co-housed by sex and treatment group in groups of four (2 WT, 2 HET). At 6 weeks of treatment, males were split into pairs (1 WT, 1 HET) as per *The Guide* standards for cage sizing, for the remainder of the study. All animals were weighed prior to the beginning of the study and a fecal sample was collected as described previously and stored at -80°C until processing. Control animals were weighed weekly between 8AM and 9AM. No other treatments were conducted on control animals. Low-dose diclofenac treatment rats were orally gavaged with 1.25 mg/kg diclofenac diluted in sterile water between 6PM and 7PM on a 10 day on/7 day off treatment cycle and weighed weekly. Rats in the *ad libitum* Western diet groups were provided the specialty chow as their sole source of nutrients and weighed weekly. Fecal samples were collected from each group at 3, 6, 9, and 12 weeks of treatment and stored at -80°C. Ileal scrapes and tissue samples of the ileum and proximal colon were taken at the end of the 12-week study. Ileal scrapes were stored at -80°C until DNA extraction. Tissue samples were oriented into Swiss gut rolls, placed into tissue embedding cassettes, and incubated at room temperature in 10% formalin

overnight prior to tissue processing. Analysis of samples was performed comparing control vs. diclofenac treatment and control vs. diet treatment as separate experiments.

Weights were taken for all rats weekly between 8AM and 9AM. Statistical significance was determined using a two-way ANOVA comparing genotype and treatment for each experiment with a post-hoc Tukey test. Males and females were analyzed for each experiment separately due to known differences in weight between sexes.

Swiss gut rolls including ileum, ileocecocolic junction, and proximal colon were processed by IDEXX BioAnalytics (Columbia, MO) using an H&E stain as described above. Samples were analyzed independently by two laboratory animal veterinarians with training in histology, both blinded to sex, genotype, and treatment group of each sample. As we were not expecting the same severity of histologic changes as in our acute study, samples from the chronic study were first analyzed for qualitative changes based on distinct findings from both blinded observers. First read information was used to re-examine slides and categorize the qualitative findings into a 1-3 scoring system for each (mild, moderate, severe, respectively). These findings included: infiltration of white blood cells into the lamina propria, hyperplasia of the mucosal tissues, the presence of mucus in the intestinal lumen, and the presence of venous congestion Samples were assessed for statistical significance using a three-way ANOVA for sex, genotype, and treatment group using GraphPad Prism 8 (San Diego, CA).

Fecal samples and ileal scrapes were processed as previously described for DNA extraction, genomic library construction and 16S rRNA sequencing, and informatics. Principle component analyses were performed on non-transformed OTU relative abundance data using Past v3.2 (O. Hammer et al., 2001). Principal component analysis was also performed using a non-linear iterative partial least squares algorithm to evaluate β-diversity and its association with sex and genotype (WT or HET) through Metaboanalyst (Chong et al., 2018; Chong et al., 2019). Metaboanalyst was also used to develop heat map data, and significant OTU outliers were evaluated by Kruskal Wallis test at $p < 0.01$.

Functional in vitro Characterization of Atg16l1

pEGFP-N1 plasmid and WT splice variants were processed as described previously (Generation of Splice Variant Clones) to give four separate CMV-promotor overexpression plasmids containing one of the four WT splice variants.

HEK293 cells (ATCC; 100,000 cells seeded per well) were grown in Corning® Costar® 24 well plates (Sigma-Aldrich) in growth media (MEM + 10% FBS + 1% P-S) at 37°C and 5% CO_2 to 70-80% confluence. Transfection was performed using the Lipofectamine® 3000 reagent protocol (Invitrogen). Experimental groups included: each of the four splice variant overexpression plasmids (1 µg each), EGFP-N1 positive transfection control (1 µg), lipofectamine reagent only negative control, and cells-only negative control to give a total of 8 experimental groups performed in triplicate (24 wells). Experimental groups were analyzed in one of three treatment conditions: regular growth media (control), Earle's Balanced Salt Solution (starvation; 2 hours), or balfilomycin A1 (0.5 µM; inhibition of

autophagy). Cells were incubated for 8 hours at 37°C and 5% CO_2 post-transfection and then the media was removed and replaced with 5 mL growth media. Cells grown in growth media for 48 hours were used as the control group. For the starvation group, two hours prior to cell collection, growth media was removed, cells were washed with sterile, 37°C PBS and incubated in 5 mL of Earle's Balanced Salt Solution. To inhibit autophagy, balfilomycin A1 (0.5 μM; Cat No: 10-1379-0050; Focus Biomolecules, Plymouth Meeting, PA) was added to growth media after lipofectamine incubation and left for the entire 48-hour incubation.

Protein was extracted and analyzed as described previously above (*Protein Extraction* and *Protein Analysis*) with the following changes. Proteins extracted in RIPA buffer were separated using ExpressPlus™ PAGE gels (10x8, 12%, 12 well; GenScript) at 140 V for 50 minutes in Tris-MOPS running buffer (M00138; GenScript. The short running time prevents the small molecular weight LC3-I and LC3-II (approximately 17 and 15 kDa, respectively) proteins from running off the gel. Antibodies used for LC3 detection included: primary recombinant anti-LC3B antibody (1:1000; ab192890; Abcam) and secondary anti-rabbit IgG antibody (1:100,000; A0545, Sigma).

CHAPTER 3: THE *ATG16L1* GENE: CHARACTERIZATION OF WILD TYPE, KNOCK-IN, AND KNOCK-OUT PHENOTYPES IN RATS

Introduction

Crohn's disease (CD) is one of two chronic inflammatory bowel diseases (IBD) that affect the lining of the gastrointestinal (GI) system. Familial linkage, twin studies, and previously established genome-wide association studies confirm the important role of genetics in IBD (Barrett et al., 2008; Cleynen et al., 2013; Khor et al., 2011; Moller, Andersen, Wohlfahrt, & Jess, 2015). More than 230 genetic alleles have been linked to CD, one of the most common of which lies in the autophagy-related 16-like 1 (*ATG16L1*) gene (Cleynen et al., 2016; de Lange et al., 2017; Luo et al., 2017; Rioux et al., 2007). Individuals who possess a single, nonsynonymous adenine to guanine polymorphism resulting in a threonine to alanine substitution directly preceded by a caspase cleavage motif in the ATG16L1 protein (ATG16L1 T300A) have an increased predisposition for CD over those who retain a threonine in this position (ATG16L1 T300) (Hampe et al., 2007). This amino acid substitution causes increased sensitivity of the ATG16L1 protein to caspase 3-mediated cleavage during death-receptor activation and starvation-induced metabolic stress, resulting in decreased levels of full-length ATG16L1 protein and diminished macroautophagy, hereafter referred to as autophagy (Lassen et al., 2014; Lassen & Xavier, 2014; Murthy et al., 2014).

Autophagy is the evolutionarily conserved degradation pathway that delivers unwanted cellular debris to the lysosome for destruction (Levine & Klionsky, 2004; Levine & Kroemer, 2008; Z. Yang & Klionsky, 2009). In the absence of stress, basal autophagy functions to eliminate and recycle damaged or long-lived cellular components that could

otherwise become toxic. During periods of cellular stress, autophagy is critical in cell survival by encapsulating and degrading intracellular bacteria and damaged cellular products to maintain homeostasis. ATG16L1 is necessary for formation of the double-membrane vesicle, the autophagosome, during autophagy (Cadwell et al., 2008; Mizushima et al., 2003; Salem, Ammitzboell, Nys, Seidelin, & Nielsen, 2015). Without proper autophagosome formation, there is no autophagy.

The mechanism by which the *ATG16L1* T300A polymorphism causes increased susceptibility to CD is still incompletely understood. Previous studies examining the role of *Atg16l1* in autophagy and CD have found that mice hypomorphic for *Atg16l1* (Atg16l1^{HM1}) and mice homozygous for the *ATG16L1* CD risk allele display the same abnormal PC granulation seen in CD patients homozygous for the T300A polymorphism (Cadwell et al., 2008; Lassen et al., 2014). Furthermore, mice carrying the *Atg16l1* T300A risk allele exhibit increased retention of bacteria within polymorphonuclear cells, greater bacterial replication and dissemination throughout the gut, and *Salmonella*-induced colitis (Gao et al., 2017). To further the research on the association of *ATG16l1* and CD, our laboratory developed the first rat model carrying a CD risk allele, *Atg16l1* T300A (F344-*Atg16l1*^{em8Rrrc}, referred to hereafter as T300A), as well as a knock-out rat model of *Atg16l1* (SD-*Atg16l1*^{em2Rrrc}, hereafter referred to as em2) using CRISPR-Cas 9 (Men et al., submitted).

The following describes the genotypic and phenotypic characterization of wild type (WT) rat *Atg16l1* as well as characterization of rats heterozygous for the *Atg16l1* T300A risk

allele and an *Atg16l1* knock-out model. We identified four wild type *Atg16l1* transcripts, two previously unknown, all with the capability to produce protein *in vitro* and with tissue-specific patterns of expression. We also show that our T300A rat strain has evidence of abnormal PC morphology and does not exhibit altered intestinal permeability, inherent gut microbiota differences compared to wild type animals, nor spontaneous inflammatory bowel disease. Given these phenotypic similarities to human CD patients, our T300A rat strain represents a useful new tool to further understand autophagy and its role in CD susceptibility in humans.

Results

Mutational Analysis

The knock-in modification in F344-*Atg16l1*^{em8Rrrc} introduces the human CD susceptibility variant (T300A) into the rat *Atg16l1* gene. The single adenine to guanine substitution in exon 10 creates a nonsynonymous codon change that results in replacement of amino acid threonine with alanine but does not affect the coding length of the full-length transcript (Figure 3.1). The knock-out modification in SD-*Atg16l1*^{em2Rrrc} results in a 709 base pair deletion starting in exon 5 and ending in exon 14. In the course of intercrossing heterozygous animals over the past four years, we noted that neither strain produced rats that were homozygous for their respective genetic alterations (Table 3.1). Consequently, all studies have been carried out in heterozygous animals and their wild type littermates. This apparent homozygous lethality has not been seen in humans or mice carrying the T300A mutation. (Cadwell et al., 2008) and was unexpected since the genomic and peptide sequences for *Atg16l1* are highly similar for humans, rats, and mice (Figure 3.2).

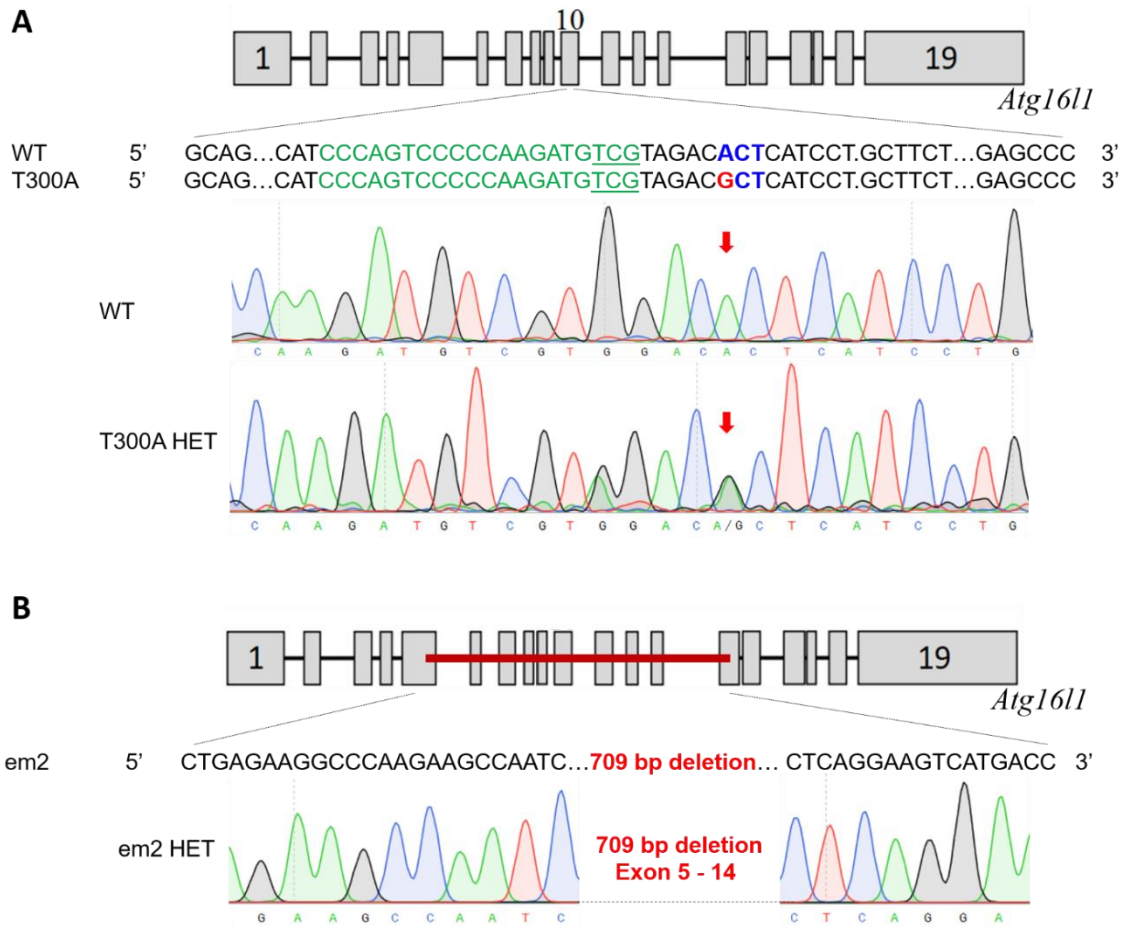

Figure 3.1: Mutational analysis of the genetic alterations in *Atg16l1* in the em2 and T300A rat strains. The nucleotide sequence of each mutant Atg16l1 allele was compared to the wild type Atg16l1 sequence. A. The rat Atg16l1 gene has 19 exons. The T300A allele has a single base pair change (A to G) in exon 10 (arrow). B. The em2 allele has a 709 bp deletion spanning exons 5 through 14.

Table 3.1. Genotypes for em2 and T300A litters

Rat Strain	Total # Pups	WT	HET	HOM	Litters
SD-*Atg16l1*^{em2}	221	85	136	0	29
F344-*Atg16l1*^{em8}	409	192	217	0	52

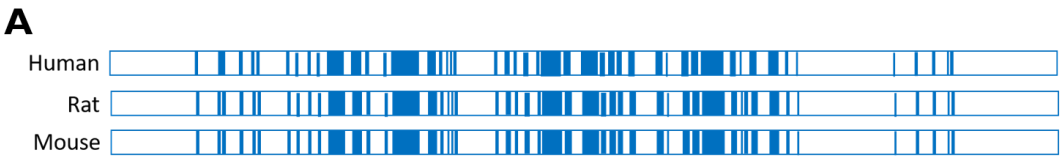

B

Species	Gene ID (Ensembl)	% Homology	%Coverage	Peptide ID (UniProt)	Peptide Length	% Identity
Rat (*Rattus norvegicus*)	ENSRNOG00000017913	89%*	100%	A0A0G2K9U6	623 aa	94%*
Mouse (*Mus musculus*)	ENSMUSG00000026289	89%*	100%	Q8C0J2-3	623 aa	94%*

*as compared to human gene and protein

Species	Gene ID (Ensembl)	% Homology	%Coverage	Peptide ID (UniProt)	Peptide Length	% Identity
Mouse (*Mus musculus*)	ENSMUSG00000026289	91.9%**	100%	Q8C0J2-3	623 aa	97.6%**

**as compared to rat gene and protein

Figure 3.2: Comparison of human, rat, and mouse Atg16l1. A) Comparison of genomic organization of the Atg16l1 genes. Blue areas represent exons; white areas represent introns. Adapted schematics of Atg16l1 for human (Uniprot; E7EVC7), rat (Uniprot; D3ZFK6) and mouse (Uniprot; G9M4M6). All 19 exons are represented in the human, mouse, and rat full-length transcripts. B) Comparison of homology at the DNA level and identity at the protein level for rat and mouse compared to human (top) and mouse compared to rat (bottom).

RNA Transcript Analysis

Four WT splice variants of Atg16l1 were identified by RT-PCR using overlapping primers (Table 3.1) and confirmed in both F344 and SD rats. From start to stop codon, these transcripts include: Atg16l1-A (full length, 1872 bp), and three alternative transcripts: Atg16l1-B (no exon 9; 1824 bp), Atg16l1-C (no exons 8 and 9; 1767 bp), and Atg16l1-D (no exon 5; 1620 bp) (Figure 3.3A). Atg16l1-B and Atg16l1-C were present in all tissues tested. Atg16l1-A was only present in brain, heart and esophageal tissue and Atg16l1-D was only expressed in brain tissue (Figure 3.3B & C). Alternative transcripts Atg16l1-C and Atg16l1-D have not been reported previously in the rat.

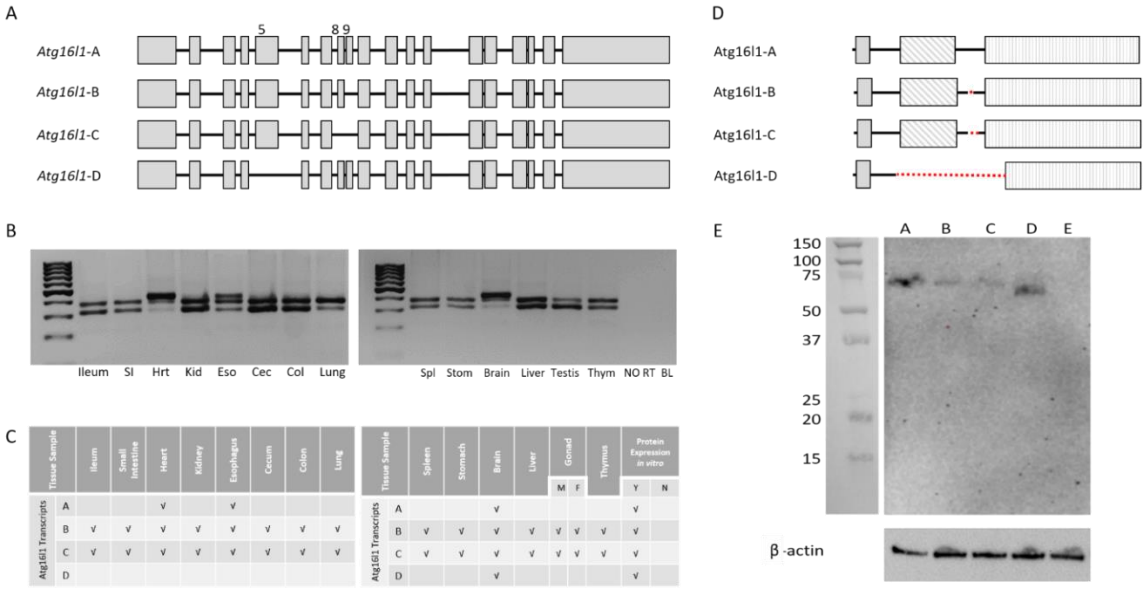

Figure 3.3: WT splice variant DNA and protein analysis. A) Representative schematic of the four WT splice variants of rat Atg16l1. Gray boxes designate exons. B). Representative agarose gel images depicting splice variants detected in different tissues. C) Summary of WT splice variants detected in various tissues D) Representative schematic of predicted protein isoform for each splice variant. Dotted lines denote the area of each protein isoform missing relative to the full-length protein (Atg16l1-A). shaded box = ATG5 binding motif; diagonal hashmark box = coiled coil domain; vertical hashline box = WD40 repeat domains (7 total). E) Representative western blot image showing protein expression when DNA constructs coding for each splice variant were transfected into HEK293 cells. A = Atg16l1-A; B = Atg16l1-B; C = Atg16l1-C; D = Atg16l1-D; E = non-transfected HEK293 cells (negative control). Ladder: Precision Plus Protein™ Kaleidoscope™ Prestained Protein Standards (1610375; BioRad); Loading control: β-actin.

Protein Expression

Full length rat Atg16l1 protein contains 623 amino acids (Atg16l1 -A; Figure 3.3D). Individual splice variants code for protein isoforms of 607 (Atg16l1-B), 588 (Atg16l1-C) and 540 (Atg16l1-D) amino acids respectively. It is not possible to effectively resolve these various isoforms by electrophoresis due to their similar sizes. To verify that protein could be produced from each splice variant, we cloned the coding region representing each alternative transcript into a mammalian expression vector and performed transfections in

cell culture. All four Atg16l1 transcripts were translated into protein in vitro in HEK293 cells (Figure 3.3E).

Intestinal Permeability

One of the most common theories on the initiation of IBD and CD is that damage to the epithelial lining of the gastrointestinal tract causes breaks in the luminal barrier and increases GI permeability thereby increasing the capacity for unwanted luminal bacteria to enter the gut tissues and cause inflammation (Michielan & D'Incà, 2015). Therefore, we wanted to investigate whether the *Atg16l1* em2 and T300A mutations fit this narrative and cause increased permeability. The non-digestible fluorescein isothiocyanate (FITC dextran) molecule passively crosses the intestinal epithelium and, when measured in the plasma via fluorescence, represents a measure for paracellular permeability of the intestinal epithelium. We found that 6-week-old HET rats from the em2 and T300A strains do not show increases in intestinal permeability over WT littermates (Figure 3.4). There were no statistically significant differences for two-way ANOVA examining the effect of sex and genotype on intestinal permeability for either em2 (genotype $p = 0.58$; sex $p = 0.78$) or T300A (genotype $p = 0.58$; sex $p = 0.78$) rat strains. The retention of epithelial integrity as shown by normal intestinal permeability in both the HET em2 and HET T300A rats mimic findings in human patients with the T300A variant who also do not show an increased intestinal permeability (Büning et al., 2007).

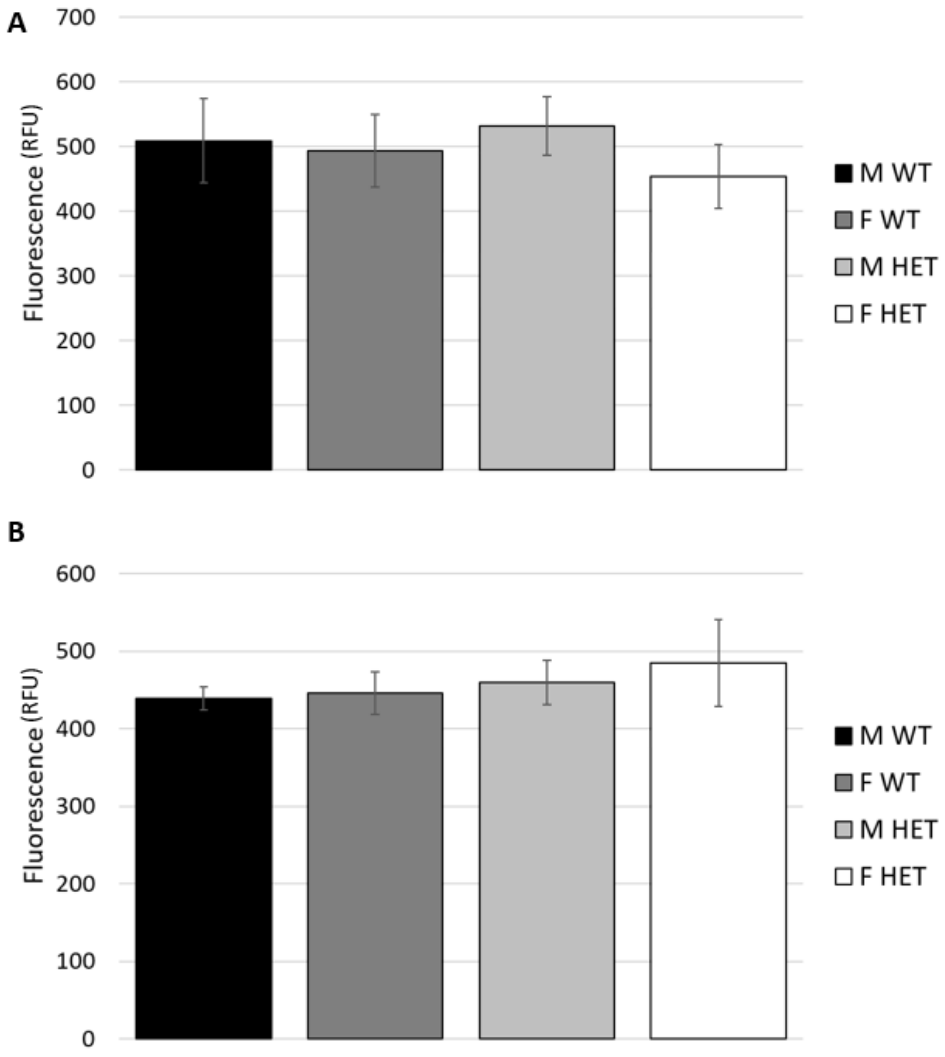

Figure 3.4: FITC fluorescence for WT and HET em2 (A) and T300A (B) rat strains. Average FITC fluorescence in relative fluorescence units (RFU) +/- Standard Deviation. M = male; F = female; WT = wild type; HET = heterozygous; n = 6 for each group; samples were run in triplicate.

Histology

The gold standard for characterizing IBD in animal models is to visualize changes to the gastrointestinal tract at the macroscopic and microscopic level. However, to understand any changes that may occur by subjecting our model to environmental triggers of IBD, we

first need to understand the changes to this model due solely to the underlying genetic modification. It has been shown that samples of pre-disease human tissue display changes to PC morphology and granulation pattern, and we wanted to investigate whether this was the case for our rat model as well. Samples of the ileum and proximal colon were taken to evaluate changes to the intestinal epithelium, including ileal villus length, ileal crypt height, colonic mucosal thickness, and ileal PC counts and granulation patterns (Figure 3.5). Six rats of each genotype (T300A strain, equal sexes) were evaluated, and the same cohort of animals was used for all histologic measurements.

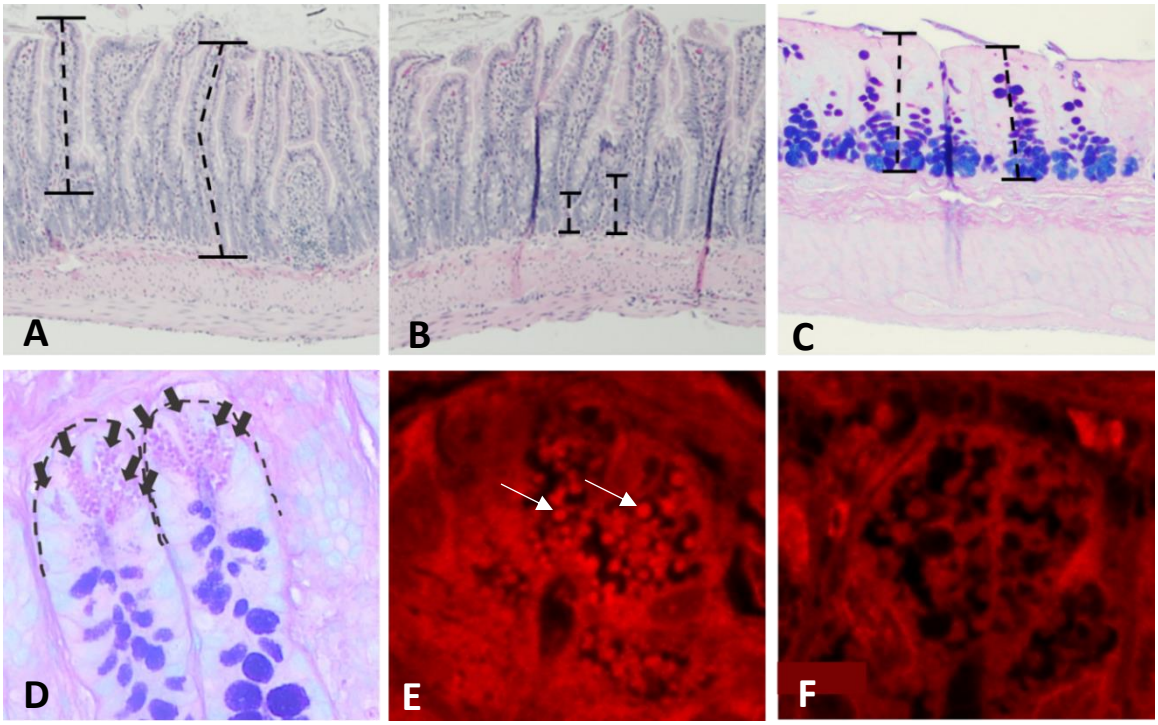

Figure 3.5: Representative histologic images from intestinal characterization. A) Villus length measurement (M WT 100x; H&E). Villi were measured parallel to the center of the villus from the luminal tip to the crypt transition. B) Crypt height measurement (F WT 100x; H&E). Crypts were measured from the crypt transition to the muscular layer. C) Colonic mucosal thickness (M WT 100x; Alcian blue/PAS). D) Paneth cell (PC) count (M WT; 400x; Alcian blue/PAS). E & F) Lysozyme IFA of ileal crypt PC. F WT, 630x (E) and F HET, 630x (F) HET rats exhibit inherent defects in PC granule packaging and number of granules present within the cytoplasm. Dotted lines (A-C) represent examples of how measurements were taken. Arrows (D) highlight individual PCs. Arrows (E) mark a few of many granules present. M = males; F = female; WT = wild type; HET = heterozygous.

Ileal villus length and crypt height as well as colonic mucosal thickness were analyzed using a H&E stain (Figure 3.5A & B). We found no statistically significant differences between WT and T300A HET animals for either measurement at 3 weeks ($t = 2.31$, $p > 0.05$) or 6 weeks ($t = 2.26$, $p > 0.05$) of age (Figure 3.6A). Fifty individual measurements were taken, in triplicate (50 randomly selected measurements per animal were taken three separate times on three separate days), for colonic mucosal thickness, measuring perpendicular from the luminal surface to the submucosal layer (Figure 3.5C). Again, we found no significant differences in mucosal thickness between WT and T300A HET rats at either 3 weeks ($t = 1.31$, $p > 0.05$) or 6 weeks ($t = 1.19$, $p > 0.05$) of age (Figure 3.6B). These findings phenocopy those seen in healthy tissues from human patients with the T300A variant (Cadwell et al., 2008).

PC counts were performed using an Alcian blue stain (pH 2.5) with a Periodic Acid-Schiff (PAS) counterstain (Figure 3.5D). Twenty-five crypts per animal were evaluated, in triplicate, only if aligned along the longitudinal axis such that the lumen of the crypt could be seen along its length. Counts were performed at a constant magnification (400X) in 2 ways: 1) by counting the number of PCs per crypt; and 2) by a differential count of at least 500 crypt cells with the results expressed as PCs per 100 crypt cells. No significant differences were shown in the frequency of PCs between WT and T300A HET rats at 3 or 6 weeks of age, regardless of the counting method used (per crypt at 3 weeks, $t = 1.69$, $p > 0.05$; 6 weeks, $t = 1.69$, $p > 0.05$; or per 100 crypt cells at 3 weeks, $t = 1.70$, $p > 0.05$; 6 weeks, $t = 1.70$, $p > 0.05$) (Figure 3.6D).

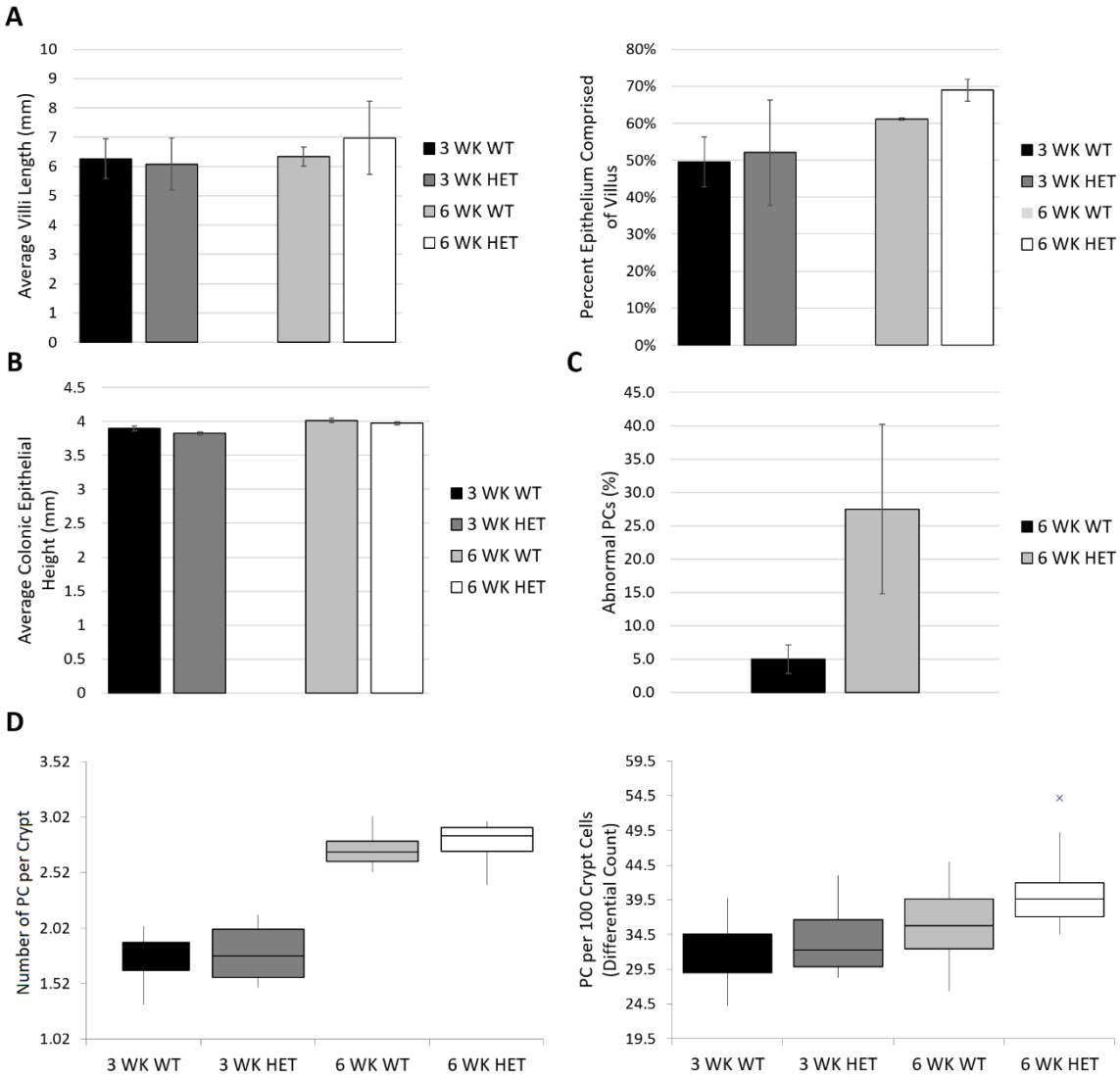

Figure 3.6: Quantitative intestinal histology. A) Villus length as measured from the tip of the villus (luminal side) to the beginning of the crypt transition as measured by average villus length for WT and HET males and females and percent of epithelium comprised of the villus (villus length / villus length + crypt height). B) Average colonic epithelium height as measured parallel from the luminal surface of the colonic mucosa to the base of the epithelium in contact with the muscular layer. C) Abnormal Paneth cells (PC) on lysozyme IFA with results measured as abnormal (yes) or normal (no) and reported as the percentage of cells with abnormal PC granulation. D) PC counts as measured by both number of PC per crypt and a differential count of PC per 100 crypt cells. n = 6 for all groups; x in panel D represents a single outlier for the 6 WK HET group. Student's t-tests between 3 WK rats and between 6 WK rats used. WK = weeks.

Finally, we used lysozyme IFA to determine whether our 6-week-old T300A HET rats had greater expression of abnormal PCs than WT littermates. Fifty PCs per animal, in triplicate, were counted and abnormal granulation, defined as aberrant and disorganized granules, was recorded as either yes or no for each cell (Figure 3.5E& F). We noted a significant increase in the number of abnormal PCs in tissues from T300A HET rats ($t = 20.69$, $p < 0.0001$) (Figure 3.6C). Instead of the distinct, bright, spherical granules located within the cytoplasm of most WT PCs, many HET cells contained diffuse, finely granular staining with no visible granules present within the cytoplasm of the cell. This abnormal PC finding is consistent with results from human patients with the T300A CD susceptibility variant as well as mouse models with a hypomorphic variant of *Atg16l1* (Atg16l1^{HM}) (Cadwell et al., 2008; Lassen et al., 2014).

Microbiome Analysis

Previous studies have shown that IBD risk alleles can affect gut microbial composition (Knights et al., 2014). Due to the role of *Atg16l1* in autophagy and the processing of intracellular bacteria, we evaluated whether the T300A variant could alter the gut microbiota in 16-week old conventionally housed HET T300A rats versus their WT littermates. This age point was chosen because it falls well within the age range of "adult" for F344 and SD rats, and CD tends to be a disease developed in late adolescence to young adulthood. We found no apparent significant differences between the genus-level OTU (operational taxonomic unit; clusters of organisms grouped by DNA sequence similarity which represent pragmatic proxies for "genus") for WT and HET T300A rats (Figure 3.7A). Principal component analyses in the PC1 x PC2 and PC1 x PC3 directions also

reveal overlapping, and therefore similar, microbiome compositions for each group (Figure 3.7B). One-way PERMANOVA for the effect of sex and genotype on microbiome revealed no statistically significant difference between WT and HET groups for males or females. On heat map analysis, which compares the 25 most prevalent OTUs in our study between individual rats from all experimental groups, we found that our males and females grouped together based on sex, regardless of genotype. This suggests a difference in gut microbiota composition between males and females in our study (Figure 3.7C). This microbiome difference between sexes has been confirmed in past studies and is not unique to our model; therefore, further qualitative and quantitative analysis of males vs. females was not conducted (J. Miyoshi et al., 2018); (Fransen et al., 2017); (Elderman et al., 2018).

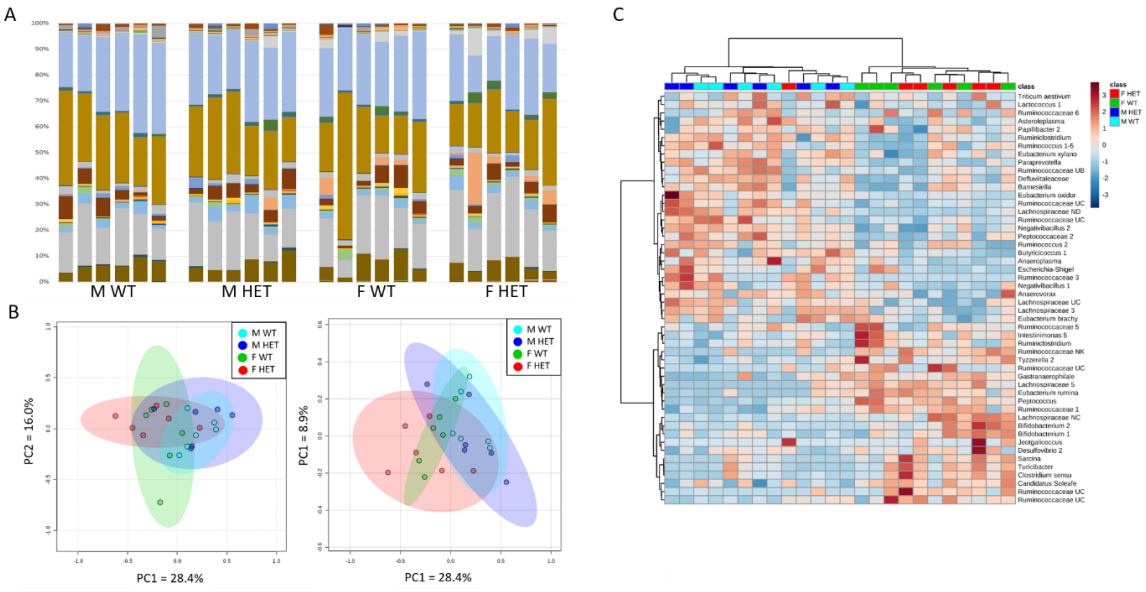

Figure 3.7: Gut microbiome analysis for 16-week old WT and HET T300A rats. A) Stacked bar charts of genus-level OTUs for each rat per group. Each color represents a unique OTU in each group. B) Principal component analysis plots. The amount of distance between 95% confidence ellipses show the amount of difference between groups. No significant differences were found. C) Cluster heat map grouping samples based on the 25 most common OTUs present in the dataset from rats of WT and HET genotypes (n = 6/group, legend upper right) with samples arranged according to an unweighted pair group method with arithmetic mean (UPGMA) algorithm.

Discussion

Wild Type Atg16l1 in the Rat: We describe one of the first characterizations of wild type *Atg16l1* in the rat. The full-length wild type rat *Atg16l1* gene contains 19 exons, the same number of exons found in the human and mouse full-length genes. We identified four wild type rat *Atg16l1* alternative transcripts, all of which contain the codon involved in the T300A susceptibility variant. Two of these transcripts, *Atg16l1*-C (missing exons 8 and 9) and *Atg16l1*-D (missing exon 5) have not been previously described. The human *ATG16L1* gene has nine protein-coding alternative transcripts, four of which are the same as those we have found in the rat: one full-length transcript, one missing exon 9, one missing exons 8 and 9, and one missing exon 5. The mouse also has four protein-coding alternative transcripts, three of which are the same as those found in the rat: one full-length transcript, one missing exon 9, and one missing exon 5. Interestingly, the T300A CD susceptibility variant falls within exon 9 of the human and mouse genes but just at the beginning of exon 10 in the rat. This means that, while all wild type rat *Atg16l1* alternative transcripts carry the susceptibility variant, some wild type alternative transcripts of human and mouse do not. These transcripts which are not affected by the T300A variant in humans and mice may compensate for those that are and may provide an answer as to why humans and mice can be homozygous viable for the variant (Cadwell et al., 2008) while it is embryonic lethal in the rat.

By extracting total RNA from healthy rat tissue samples from different organs, we showed that the four wild type alternative transcripts are differentially expressed in different tissues, with heart and brain being the only tissues to express all four transcripts. We found

that all four of the wild type rat *Atg16l1* alternative transcripts could produce protein *in vitro* when individually transfected into HEK293 cells in a plasmid with an overexpression promotor (CMV). Since all four transcripts code for a protein product, it suggests that there are four protein isoforms with the potential to function at some capacity during autophagy. Future studies will be aimed at evaluating the function of each isoform during the autophagy process to understand why we see differential tissue expression of the various alternative transcripts.

Knockout Atg16l1: We have genotypically and phenotypically characterized a new knock-out rat strain with a 709 bp deletion in *Atg16l1* (SD-*Atg16l1*^{em2Rrrc}). This is the first rat strain described to date with a deletion in the *Atg16l1* gene. While there is no evidence to suggest that a knockout of *ATG16L1* exists as a CD susceptibility variant in humans, our knockout model is an important resource for understanding the overall function of the *Atg16l1* gene and how the autophagy process is impacted in the absence of *Atg16l1*. We were able to produce 29 litters from HET x HET matings of the em2 strain, none of which produced a homozygous pup (Table 1), suggesting that this genotype is embryonic lethal and that *Atg16l1* plays a vital role during embryonic development. We also found that this knockout strain does not possess any inherent intestinal permeability as confirmed by FITC-dextran permeability assay (Figure 4A). Due to its homozygous lethality, our knockout rat cannot be used to evaluate the effect of a complete absence of *Atg16l1* on autophagy, and we did not proceed further with characterization of this model.

Atg16l1 T300A Variant: We have generated and characterized a rat model carrying the T300A susceptibility variant for CD in the *Atg16l1* gene. This is the first rat strain described to date that carries an IBD susceptibility variant in the *Atg16l1* gene. We maintained a breeding colony of HET x HET T300A rats, resulting in 52 litters of pups. No pups born from these crosses were homozygous for the T300A variant, suggesting that this single amino acid substitution is embryonic lethal. Interestingly, the numbers of HET animals produced in T300A HET X HET matings was also less than expected. It is possible that inheritance of the T300A allele is associated with embryonic lethality in both homozygous and heterozygous rats. Alternatively, there may be some selective disadvantage in gametes that carry the T300A allele that results in no homozygous and fewer heterozygous offspring being produced. Further studies would be necessary to determine the reason for the skewed genotypic ratios observed in these crosses.

Phenotypic characterization of T300A rats focused on whether this model presents with alterations in gut permeability, microbiota composition, or histologic features – three of the most common metrics in IBD and CD studies. It is important to understand any phenotypic characteristics that present solely due to inheritance of the susceptibility variant itself in the absence of environmental triggers of disease.

Like human patients carrying the *Atg16l1* T300A susceptibility variant (Büning et al., 2007)., our rat strains do not have inherent increases in intestinal permeability as measured by the FITC-dextran permeability assay. The mechanism by which *Atg16l1* is thought to initiate CD lies within its role in regulation of homeostasis of the gastrointestinal lumen,

not permeability (Barker, 2014). *Atg16l1* is vital for proper exocytosis of PC granules which encapsulate α-defensins, lysozyme, and other antibacterial modulators and release them into the intestinal lumen as part of the mucosal immune barrier. When the T300A variant is present, ATG16L1 protein is sensitive to caspase-3 mediated cleavage. Increased cleavage results in reduced concentrations of ATG16L1 protein, limiting the release of antibacterial modulators into the intestinal lumen. The luminal microbiome, now unburdened by immunomodulators, has a high propensity for dysbiosis, which is hypothesized to be the cause of CD in susceptible individuals. Thus, the finding of no permeability changes is unsurprising.

Analysis of the microbiome of T300A WT and HET rats shows differences between males and females; however, this sex-dependent difference is not unique to our T300A strain and is a common feature of many rat models (Kim, Unno, Kim, & Park, 2020). There does not appear to be any significant differences in the microbiome of 16-week-old WT and HET rats carrying the T300A variant. It is surprising that we did not see a gut microbiota shift related to genotype in our rat model when differences exist in pre-disease CD patients with the *Atg16l1* susceptibility variant; however; many disparities between human and rat host factors exist, such as diet, environment, and features of the gastrointestinal system itself (differences in small intestine: colon ratios, size of the cecum, etc.) which could explain why the rat gut microbiota may be less susceptible to changes based on the T300A variant alone. There are also several differences between the rat and human gut microbiota that could explain its heartiness against T300A variant changes (Nagpal et al., 2018). Outbred rats have a higher prevalence of *Prevotella* and fecal lactate than humans. The gut

microbiota of rats appears to be dominated by *Bacteroidetes* over *Firmicutes*, whereas, human gut microbiota composition demonstrates equal to slightly higher numbers of *Firmicutes*. Recently, it was found that gnotobiotically-raised mice expressing the T300A variant that received feces from patients with active CD exhibit an increase in *Bacteroides* abundance compared to WT mice (Lavoie et al., 2019). This technology could be used in rat models as well to understand the implications of *Atg16l1* variants on the gut microbiota. Future studies in the T300A rat strain will seek, in part, to determine what microbiome changes are revealed in rats with active CD and whether they are comparable to human patients with active CD.

Intestinal histology from F344-*Atg16l1*^{em8Rrrc} WT and HET rats shows PC abnormalities like those seen in human patients and mice carrying the *Atg16l1* T300A variant (Cadwell et al., 2008). These PCs display diffuse lysozyme staining throughout the cytoplasm of the cells as shown by lysozyme IFA staining. These cells also display a significant decrease in granules (vesicles) within the cytoplasm, suggesting that production of alpha defensins and other host defense proteins packaged within granules in the PCs is working, but the packaging process is not. PC function by exocytosis of their granules into the intestinal lumen to release these defense proteins to modulate the luminal environment (Burgoyne & Morgan, 2003). This process requires the membrane of the vesicle to fuse with the PC membrane. Without granule formation, these enzymes cannot escape the PCs and cannot perform their intended function. Further studies on the role of *Atg16l1* in PC packaging and exocytosis and the effect during CD are needed.

Overall, the characterization of this *Atg16l1* T300A rat strain supports its use in future CD studies. While a mouse model carrying the *Atg16l1* susceptibility variant exists, there are many benefits to a larger rodent model with characteristics mimicking human CD patients. The larger size of the rat makes them preferable for applications that may involve tissue sampling or serial sampling. Rats are also a much easier model in which to perform surgery, and, given the high likelihood of CD patients to undergo at least one surgical procedure to address disease symptoms, this makes the rat an appealing CD model for future therapies and treatments. Like human CD patients carrying the T300A variant, the T300A rat strain exhibits inherent abnormalities in PCs, including abnormal packaging of antibacterial lysozyme and an overall decrease in PC granules. Future studies utilizing this model will examine the potential to induce CD-like lesions using known environmental triggers of CD. Overall, both new rat models will facilitate further studies into the mechanism of *Atg16l1* in autophagy and CD.

CHAPTER 4: THE *ATG16L1* GENE: CHARACTERIZATION OF WILD TYPE, KNOCK-IN, AND KNOCK-OUT PHENOTYPES IN RATS

Introduction

Crohn's disease (CD) is known to have a multifactorial etiology including genetic predisposition, immune regulation, microbiome composition, and exposure to known environmental triggers of disease. Most research on CD has been invested in understanding the genetic susceptibility of disease, an endeavor which has relied heavily upon large-scale genetic studies that have implicated several genes related to autophagy (Barrett et al., 2008; Hampe et al., 2007). Autophagy is the ubiquitous, evolutionarily conserved pathway required to rid cells of unwanted debris and intracellular bacteria (Glick et al., 2010; He & Klionsky, 2009; Levine & Kroemer, 2008). Without functional autophagy, programmed cell death (apoptosis) is increased at basal levels, and stressed cells are more likely to become overwhelmed, resulting in necrosis and inflammation (Qian, Fang, & Wang, 2017). One of the most common genetic variants to cause CD lies within the gene *ATG16L1*, an autophagy gene responsible, in part, for formation of the double-membrane bound autophagosome vital to the process of macroautophagy (a subcategory of autophagy, hereby referred to as autophagy).

We previously generated a knock-in rat model using CRISPR-Cas9 in which the *Atg16l1* gene contains a comparable point mutation to the common CD susceptibility variant found in human patients (T300A) (Men et al., submitted) This variant alters a highly conserved amino acid residue from threonine to alanine, resulting in increased susceptibility to caspase-3 mediated protein cleavage (Murthy et al., 2014). In our initial characterization

of the T300A strain, no homozygous (HOM) pups were born in over 50 litters from heterozygous (HET) X HET pairings. This apparent embryonic lethality in rats is not seen in human patients or the mouse model of the T300A variant (Chesney et al., submitted; (Cadwell et al., 2008). This suggests a vital role for *Atg16l1* in embryonic development in the rat. T300A HET rats show aberrant PC granulation patterns in non-diseased tissues like human patients with this similar genetic variant (Cadwell et al., 2008). Our initial characterization, and *Atg16l1* research conducted previously, suggest that *Atg16l1* is a necessary mediator of intestinal immunity, and the T300A variant can cause undesirable disease manifestation when combined with other etiologic agents of CD (Lavoie et al., 2019; T.-C. Liu et al., 2018).

While great emphasis has been placed on understanding the genetic susceptibility of CD, little information has been gathered regarding other aspects of disease etiology, particularly the environmental factors contributing to disease. What little information has been gathered on environmental etiologic agents has been heavily targeted toward artificial bacterial and viral infection (Boada-Romero et al., 2016; Cadwell et al., 2010). While these studies have shown an increased susceptibility to certain infectious agents, very few studies have been conducted evaluating less innocuous environmental triggers of disease. One study evaluating the exposure of mice with the T300A variant to cigarette smoke found that mice homozygous for the variant were susceptible to smoking-induced PC defects (T.-C. Liu et al., 2018). This suggests that animal models can be used to understand the combined role of genetics and environmental factors in disease manifestation.

The current studies are the first of their kind to evaluate whether rats carrying the T300A variant elicit signs of disease when exposed to acute or chronic oral doses of the non-specific, non-steroidal anti-inflammatory (NSAID), diclofenac, or a Western diet formulated rodent chow. First, we evaluated whether rats heterozygous for the T300A variant were more susceptible to NSAID toxicity by subjecting them to a short course of high-dose NSAID to mimic short-course NSAIDS given to human patients for acute, severe pain. Then, we determined whether chronic exposure to either low-dose NSAID, such as those at a dose given for over-the-counter daily use in human patients, or a Western diet formulated feed could result in disease signs in rats heterozygous for the T300A variant. In all cases, rats heterozygous for the T300A variant elicited signs of disease, supporting the model's use in future studies of CD.

Results

Acute Exposure to High-Dose NSAID Causes Disease Signs in HET T300A Rats

The mean scores for weight change (Figure 4.1) were not found to be statistically significant for males when using an ANOVA with repeated measures with a Greenhouse-Geisser correction (F (3.9, 47.1) = 1.0, $p > 0.05$). Females did have a statistically significance difference in weight change between groups when using an ANOVA with repeated measures with a Greenhouse-Geisser correction (F (6.0, 22.131) = 70.2, $p < 0.05$). Post hoc tests using the Games-Howell correction for unequal variances revealed that female HET rats on NSAID treatment lost significantly more weight compared to both control and female WT NSAID treatment groups with time points at 6 and 7 days statistically significant ($p < 0.05$).

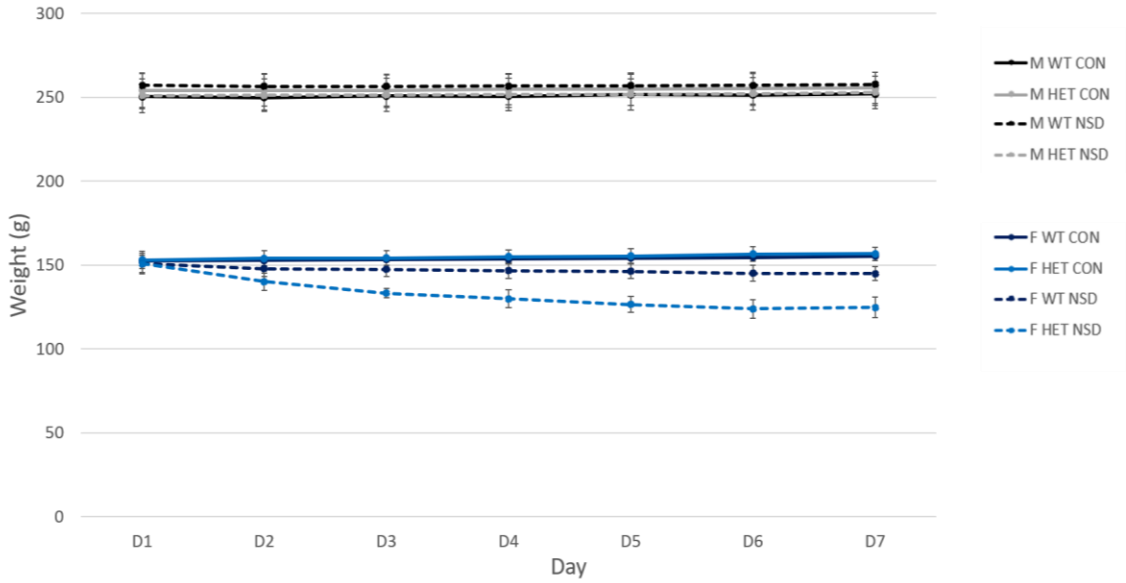

Figure 4.1: Rat weights (+/- standard deviation) through the duration of acute NSAID exposure. Weights were significantly different on days 6 and 7 for female HET rats on NSAID treatment. M = male; F = female; WT = wild type; HET = heterozygous; CON = control group; NSD = diclofenac NSAID treatment group**.**

Gross and Histologic Analysis

Changes to the *in situ* abdominal organs were apparent in 3 of the 4 HET females give high-dose NSAID during our acute study (Figure 4.2). Upon retraction of the abdominal wall, these HET females presented with a moderate amount of straw color serous fluid in the cavity. In addition, these females had jaundiced, fibrotic omentum adhered to the intestine, stomach, and liver. No gastrointestinal perforation was visible grossly. One out of 4 HET females also presented with multifocal hepatic necrosis.

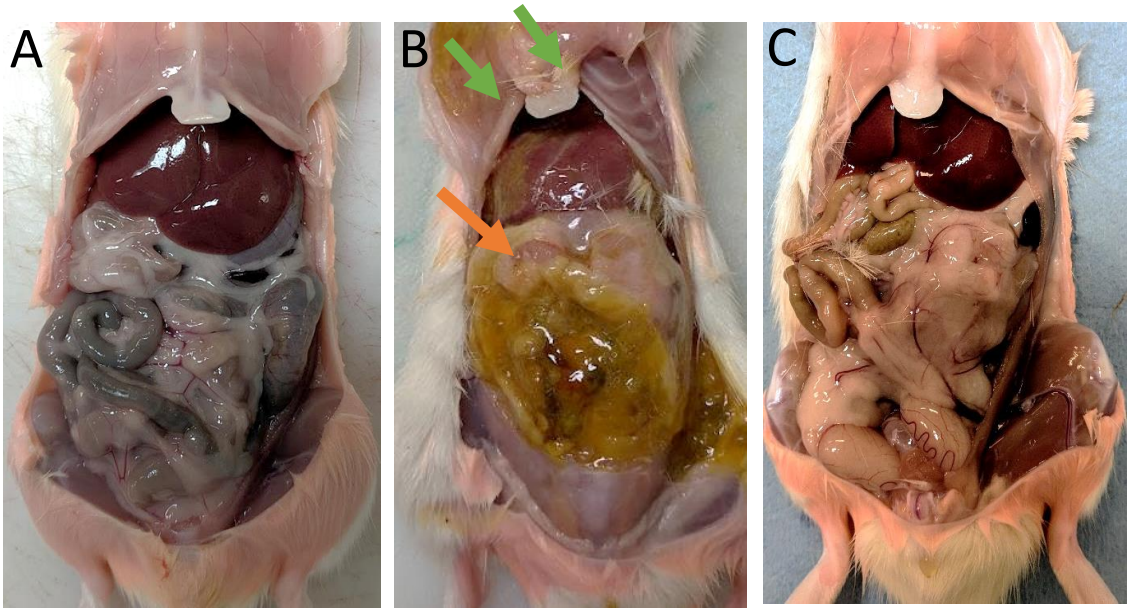

Figure 4.2: Acute study gross necropsy. A) Female HET control; *in situ* abdominal organs; no signs of disease; B) Female HET NSAID treatment; jaundiced/fibrotic omentum (orange arrow), moderate straw-colored ascites, multifocal hepatic necrosis (green arrow). Findings consistent in 3/4 HET females on NSAID treatment. C) Male HET NSAID treatment rats (3/4) displayed mild fibrosis of the omentum but no jaundice or hepatic necrosis.

Histologic analysis (Figure 4.3) of intestinal tissues revealed significant changes in tissues from HET rats on high-dose NSAID. Three-way ANOVA was run on our sample of 40 rats to examine the effect of genotype, sex, and treatment on histologic score (Figure 4.4). ANOVA uncovered statistical differences between WT and HET ($F(1, 32) = 69.9$, $p < 0.0001$), between males and females ($F(1, 32) = 7.3$, $p = 0.01$), and between control and NSAID treatment ($F(1, 32) = 49.2$, $p < 0.0001$). Additionally, we found an interaction between genotype and treatment ($F(1, 32) = 26.3$, $p < 0.0001$) as well as an interaction between sex and treatment ($F(1, 32) = 4.7$, $p = 0.04$). Post-hoc Bonferroni testing for the genotype and treatment interaction revealed a significant difference in scores between HET control and HET NSAID treated rats ($p < 0.05$) as well as a trend toward significance for the comparison of HET NSAID treated and WT NSAID treated rats ($p = 0.06$). Additional

post-hoc Bonferroni testing for the sex and treatment interaction uncovered significant differences between scores for female controls and female NSAID treated rats ($p < 0.0001$) as well as significant differences in score between male NSAID treated and female NSAID treated rats ($p < 0.0001$).

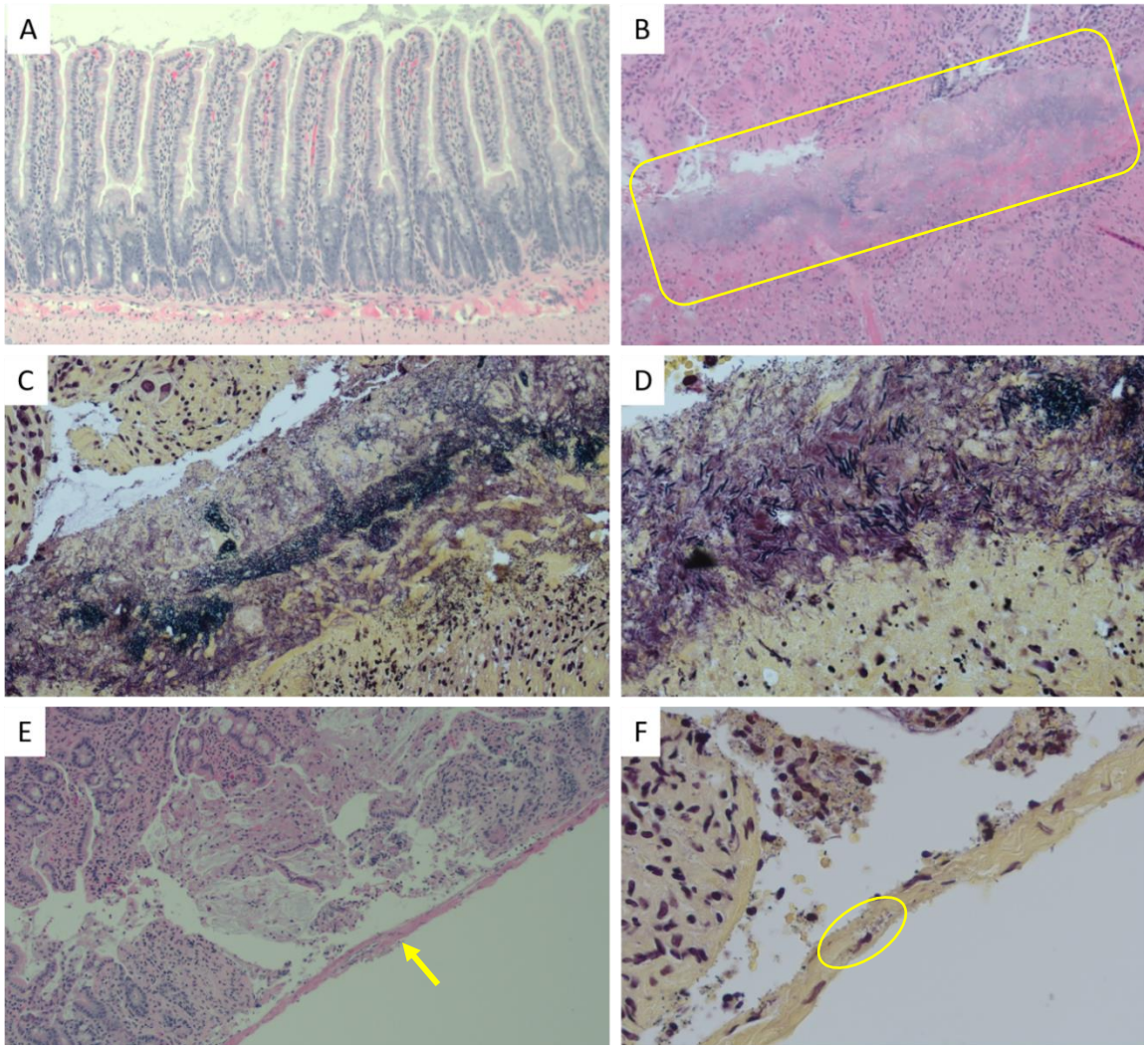

Figure 4.3: Representative histologic images from control HET (A) and NSAID-treated HET (B-F) females. A) Female HET control (200X), normal ileal sample; B) Female HET post-NSAID treatment (40X), large area of necrosis (box) with suspected bacterial infiltration; C) Female HET post-NSAID treatment (100X; close-up of B; Gram stain), confirmation of bacterial infiltration into mucosal and muscularis tissues; D) Female HET post-NSAID treatment (630X); visualization of rods and cocci present within tissues confirms presence antemortem; E) Female HET post-treatment (100X); complete sloughing of mucosa and submucosa from muscularis (arrow); F) Female HET post-treatment (630X; close-up of E; Gram stain); confirmation of bacterial involvement within tissues (circle).

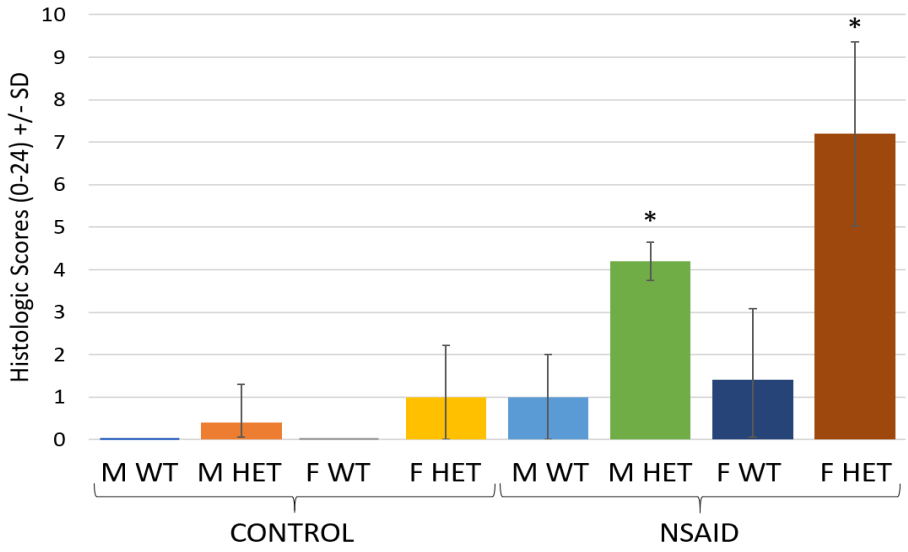

Figure 4.4: Histologic scores of intestinal tissues from acute NSAID exposure study. HET male and female rats given high-dose diclofenac exhibited more signs of inflammation and mucosal changes in the ileum and proximal colon than all other groups. M = male, F = female; WT = wild type littermates; HET = heterozygous. SD = standard deviation. * = groups with a $p < 0.05$ from all other groups; n = 4 per group.

To evaluate the GM composition of WT and HET control and NSAID-treated rats, we developed bar charts in Microsoft Excel (Figures 4.5 and 4.6; Microsoft, Redmond, WA) and performed principal component analysis (PCoA) in Past (Past v. 4.03; Hammer & Harper, Oslo, Norway) at the OTU level to visually inspect the data (Figure 4.7). On qualitative analysis of bar chart data, there were some changed between WT and HET animals in control and NSAID groups. Most notably, an increase in Bacteroidaceae and a decrease in Muribaculaceae in post-treatment fecal samples of HET animals in the NSAID group. There was also an increase in Peptostreptococcaceae in ileal samples, but this increase appears to be consistent between NSAID treated groups irrespective of genotype. In PCoA, the more similar samples are to each other, the closer they appear. Overlapping data points suggest similar microbiota composition. There were no visual differences in the composition of the microbiome before treatment, after treatment, or at the level of the ileum between groups. All groups clustered together, indicating similar β-diversity. Heatmap

analysis using the 25 most common OTUs between all samples revealed two relatively distinct clusters for NSAID treated animals and one cluster for all control animals (Figure 4.8).

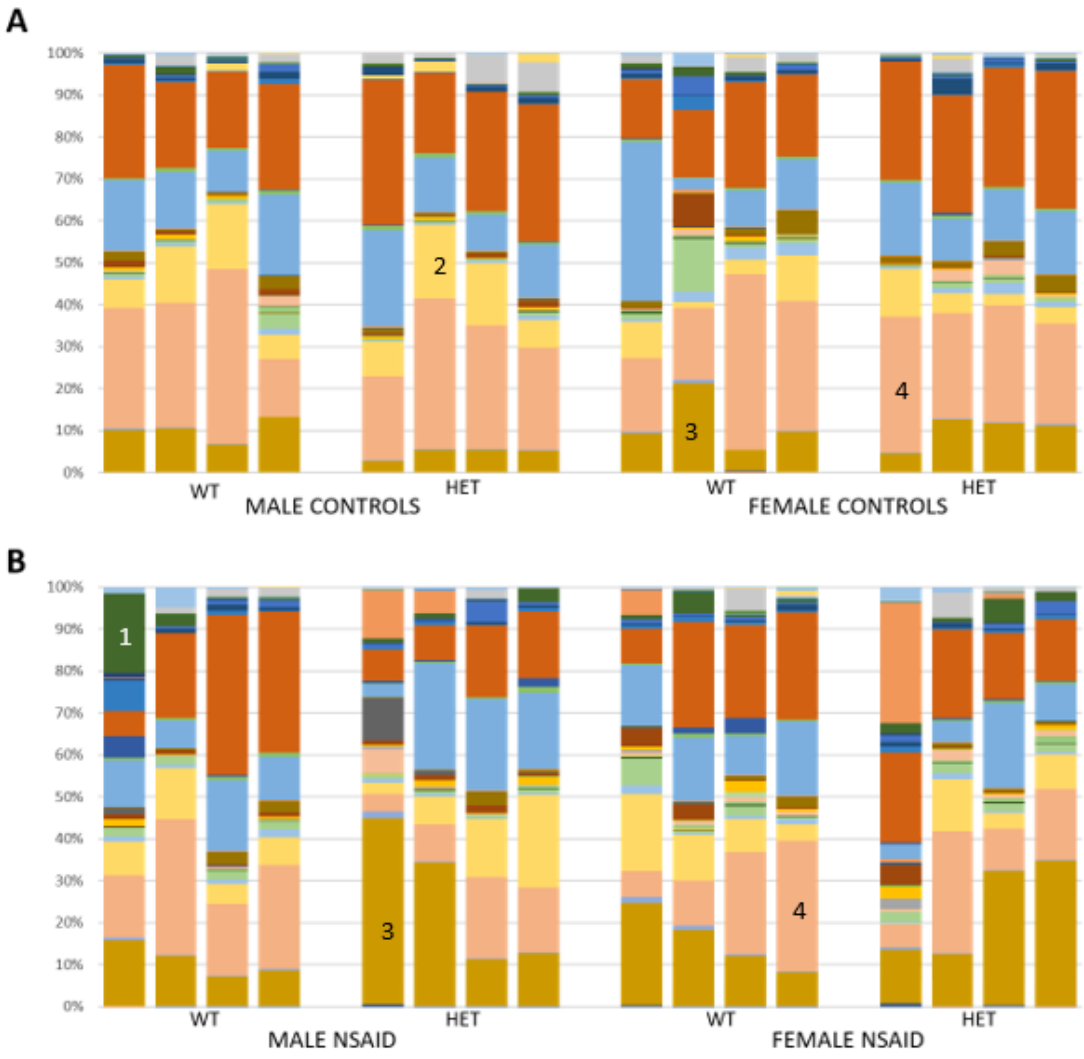

Figure 4.5: Fecal microbiome OTU graphs for post-treatment acute exposure samples. A. Controls. B. NSAID-treated. Each bar represents the post-treatment fecal microbiota profile for one animal in each group. OTUs of interest are depicted. Like colors denote identical OTU for each animal: 1 = Burkholderiaceae; 2 = Prevotellaceae; 3 = Bacteroidaceae; 4 = Muribaculaceae. WT = wildtype; HET= heterozygous.

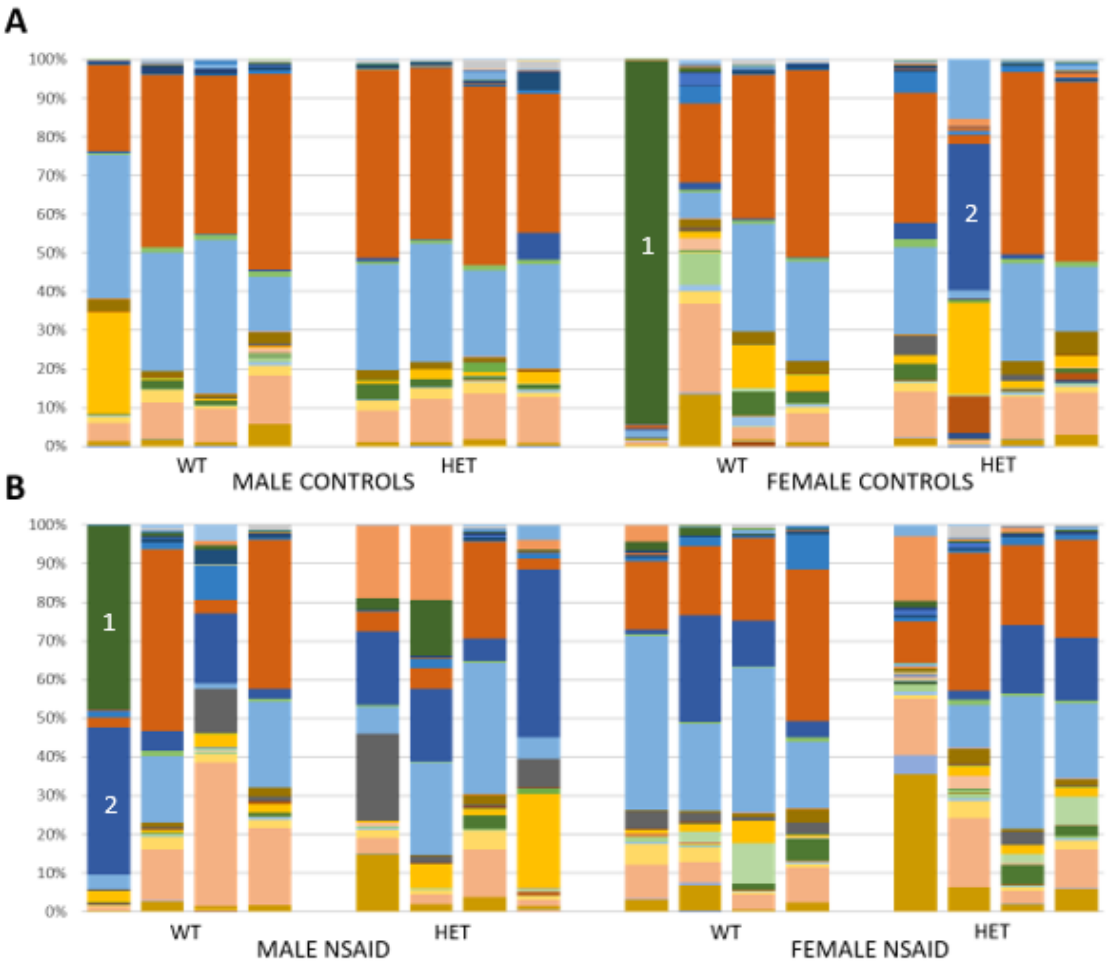

Figure 4.6: Ileal microbiome OTU graphs for acute exposure samples A. Controls. B. NSAID-treated. Each bar represents the post-treatment fecal microbiota profile for one animal in each group. OTUs of interest. Like colors denote identical OTU for each animal: 1 = Burkholderiaceae; 2 = Peptostreptococcaceae. WT = wildtype; HET= heterozygous.

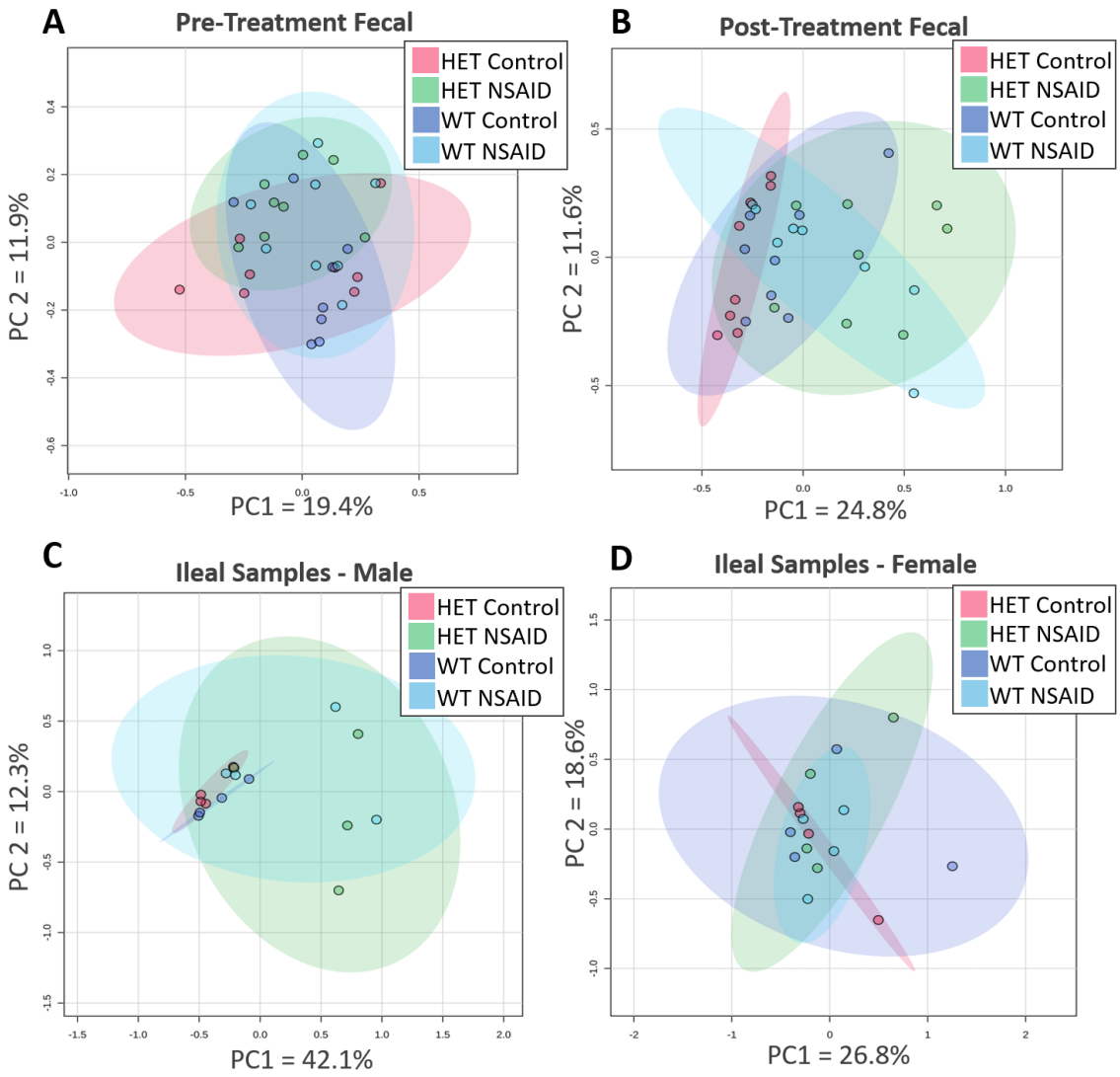

Figure 4.7 : Principal component analyses (PCoA) for acute exposure to high-dose diclofenac. The principle component percentage for each axis corresponds to the amount of difference between samples that is accounted for by that component. The further the spread between samples, the greater the difference. Overlapping samples are considered to have no to very limited differences. A) Fecal samples from each rat prior to treatment; B) Fecal samples from each rat upon euthanasia immediately upon completion of the acute study; C and D) Ileal scrape samples from C) male and D) rats immediately upon completion of the acute study. WT = wildtype; HET= heterozygous; n = 4 per group.

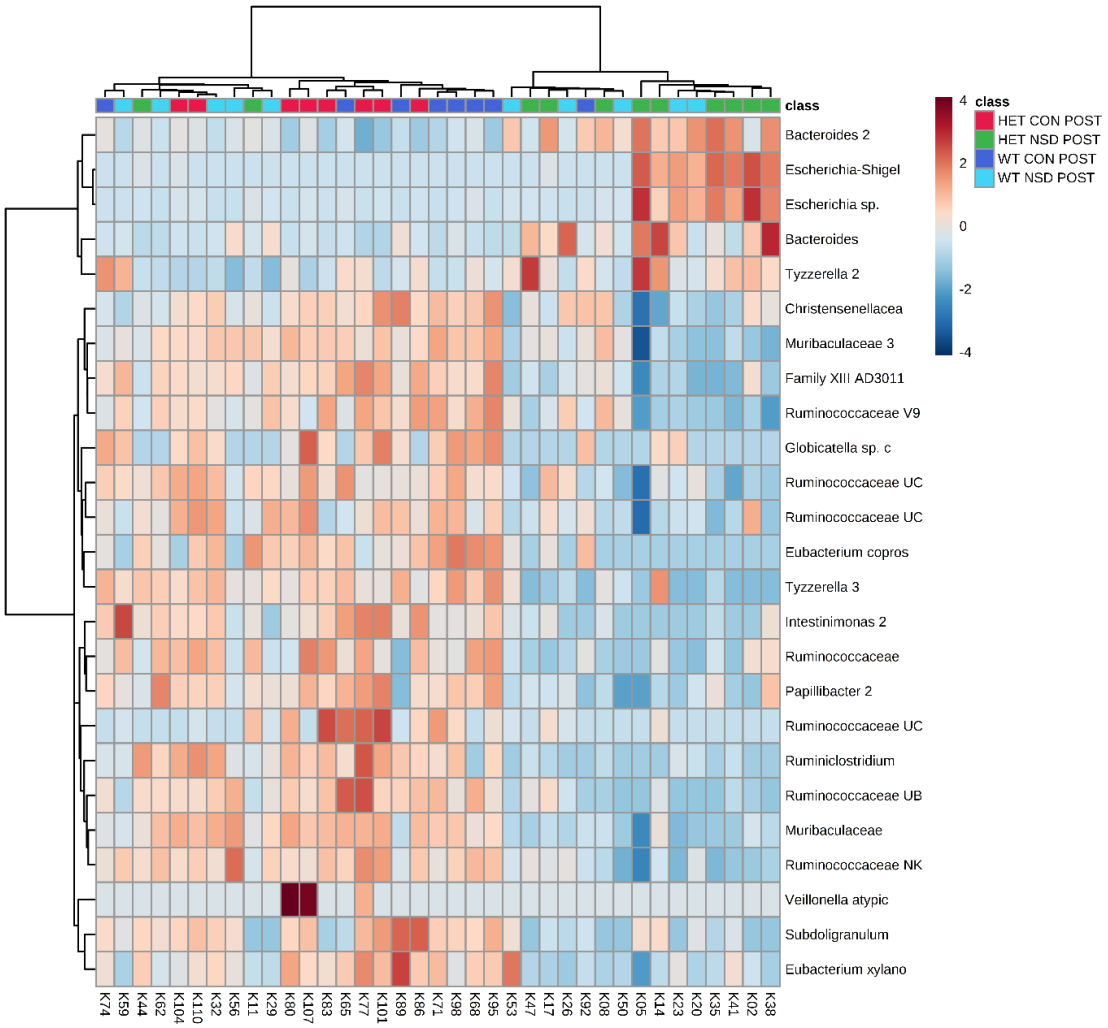

Figure 4.8: Post-treatment heatmap for acute exposure fecal samples. The darker the blue coloring of the data point, the less of that OTU is present in that sample compared to the average of all samples. The darker the red, the greater the abundance of that OTU present in that sample compared to the average. HET = heterozygous; WT = wild type; CON = control; NSD = non-steroidal anti-inflammatory; POST = post-treatment. X-axis contains individual designators for each rat in the study. Y-axis shows the top 25 OTUs that account for the most difference between individuals. n = 8 for CON groups, 12 for NSD groups.

Chronic Exposure to Environmental Triggers Results in Mild Histologic Changes

The mean scores for weight change (Figure 4.9) were not found to be statistically significant at any time point for males or females from any of our treatment groups when

using an ANOVA with repeated measures with a Greenhouse-Geisser correction: M WT vs NSD (F (3, 20) = 2.1, $p > 0.05$); M CON vs DIET (F (3, 20) = 0.12, $p > 0.05$); F CON vs NSD (F (3, 20) = 0.79, $p > 0.05$); F CON vs DIET (F (3, 20) = 0.42, $p > 0.05$).

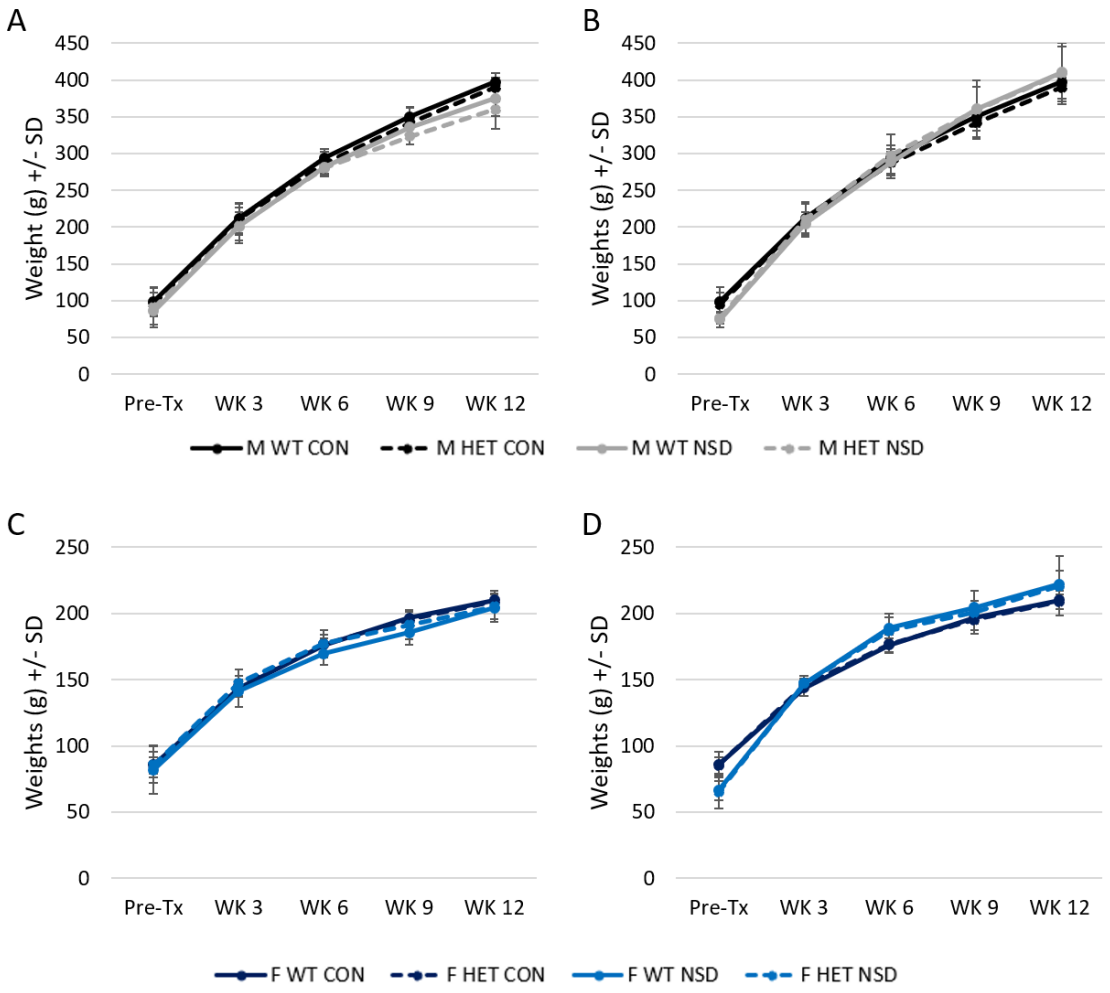

Figure 4.9: Rat weights during chronic treatment. A) Male (M) wild type (WT) and heterozygous (HET) rats, control (CON) vs diclofenac (NSD) treatment; **B)** M WT and HET rats, CON vs. Western diet (DIET) treatment; **C)** Female (F) WT and HET rats, CON vs. NSD; **D)** F WT and HET rats, CON vs DIET treatment. Pre-Tx = pre-treatment; WK = week; SD = standard deviation. n = 6 per group.

Histologic ileal and proximal colon samples taken from all rats on our chronic study were evaluated for effects of treatment on infiltration, hyperplasia, presence of mucus, and

presence of venous congestion (Figure 4.10). Two three-way ANOVAs were conducted to determine the effects of sex, genotype, and treatment on infiltration and hyperplasia scores, respectively, for both control versus NSAID treated and control versus diet treated animals (Figure 4.11). No interactions existed for hyperplasia scores between control and NSAID treated or control and diet treated groups. A statistically significant three-way interaction of sex, genotype, and treatment was revealed for infiltration between control versus diet treated animals ($F(1, 42) = 5.38$, $p < 0.05$). An additional significant interaction between genotype and treatment was found for control versus diet treated animals ($F(1,42) = 4.73$; $p < 0.05$) with scores for HET rats on diet treatment higher than all other groups (HET control: $p = 0.00005$; WT controls: $p = 0.00001$; WT diet treated: $p = 0.00003$). No three-way interaction was noted for control versus NSAID treated animals; however, a statistically significant interaction was noted between genotype and treatment for the control versus NSAID treated group ($F(1,38) = 4.43$, $p < 0.05$) with significantly higher scores for HET rats on NSAID treated than all other groups (HET controls: $p = 0.01$; WT controls: $p = 0.003$; WT NSAID treated: $p = 0.004$).

Multiple four-way loglinear analyses were performed to determine hierarchical unsaturated models for the associations between sex, genotype, treatment (CON vs NSD and CON vs DIET), and either mucus presence or venous congestion. Unsaturated models were chosen using SPSS Statistics' hierarchical loglinear model selection procedure with a backwards elimination stepwise procedure. The loglinear model revealed 3 two-way interactions between treatment and mucus, genotype and mucus, and treatment and congestion for our NSAID treated groups. Each model had a Pearson goodness-of-fit ratio of $\chi^2 (9) = 0.67$, p

= 1.00 (presence of mucus) and χ^2 (10) = 5.80, p = 0.83 (presence of venous congestion). The loglinear model also revealed a three-way interaction between treatment, genotype, and congestion and 2 two-way interactions between treatment and mucus and treatment and congestion for our diet treated groups. Each model had a Pearson goodness-of-fit ratio of χ^2 (10) = 0.67, p = 1.00 (presence of mucus) and χ^2 (7) = 0.34, p = 1.00 (presence of venous congestion).

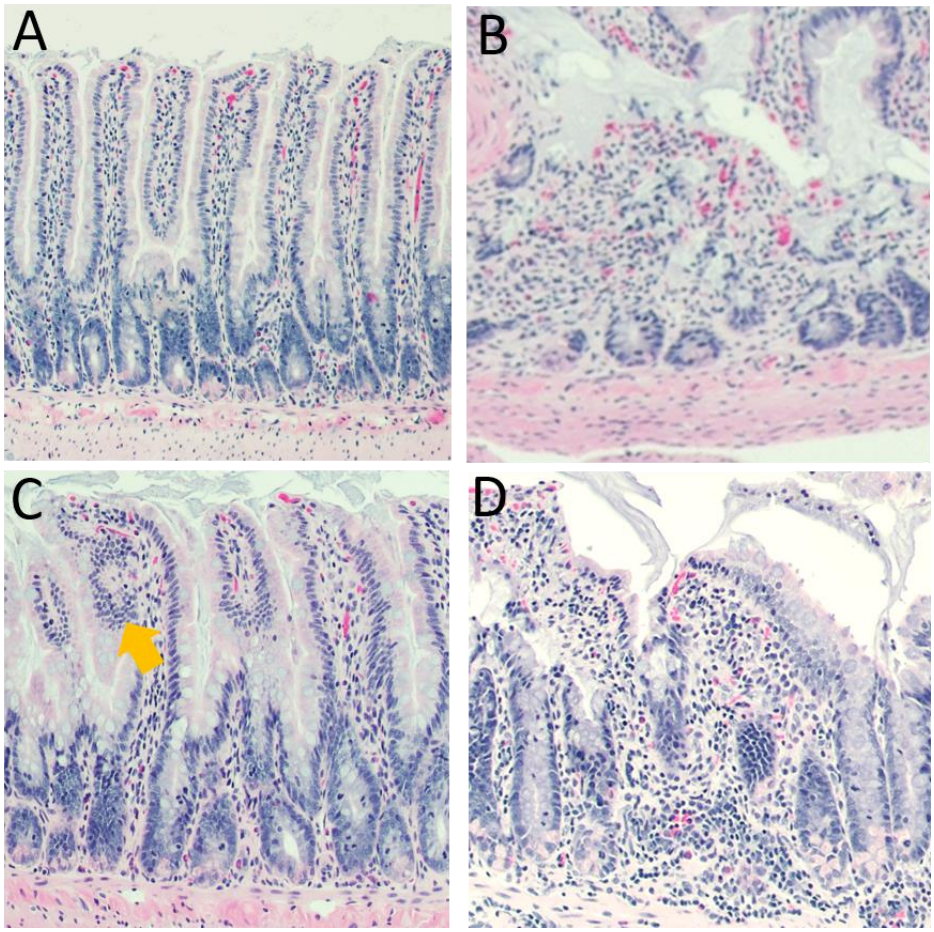

Figure 4.10: Representative images of ileal histology from control HET (A) and HET rats from treatment groups (B-D). A) Male HET control (200X), normal ileum; B) Female HET post-diet treatment (200X), dysplastic epithelium (abnormal development of cells); C) Male HET post-diet treatment (200X), arrow indicates area of mild epithelial hyperplasia (increase in reproductive rate of cells); D) Female HET post-NSAID treatment (200X), inflammatory infiltration within the lamina propria (plasma and mononuclear cells). WT = wild type; HET = heterozygous.

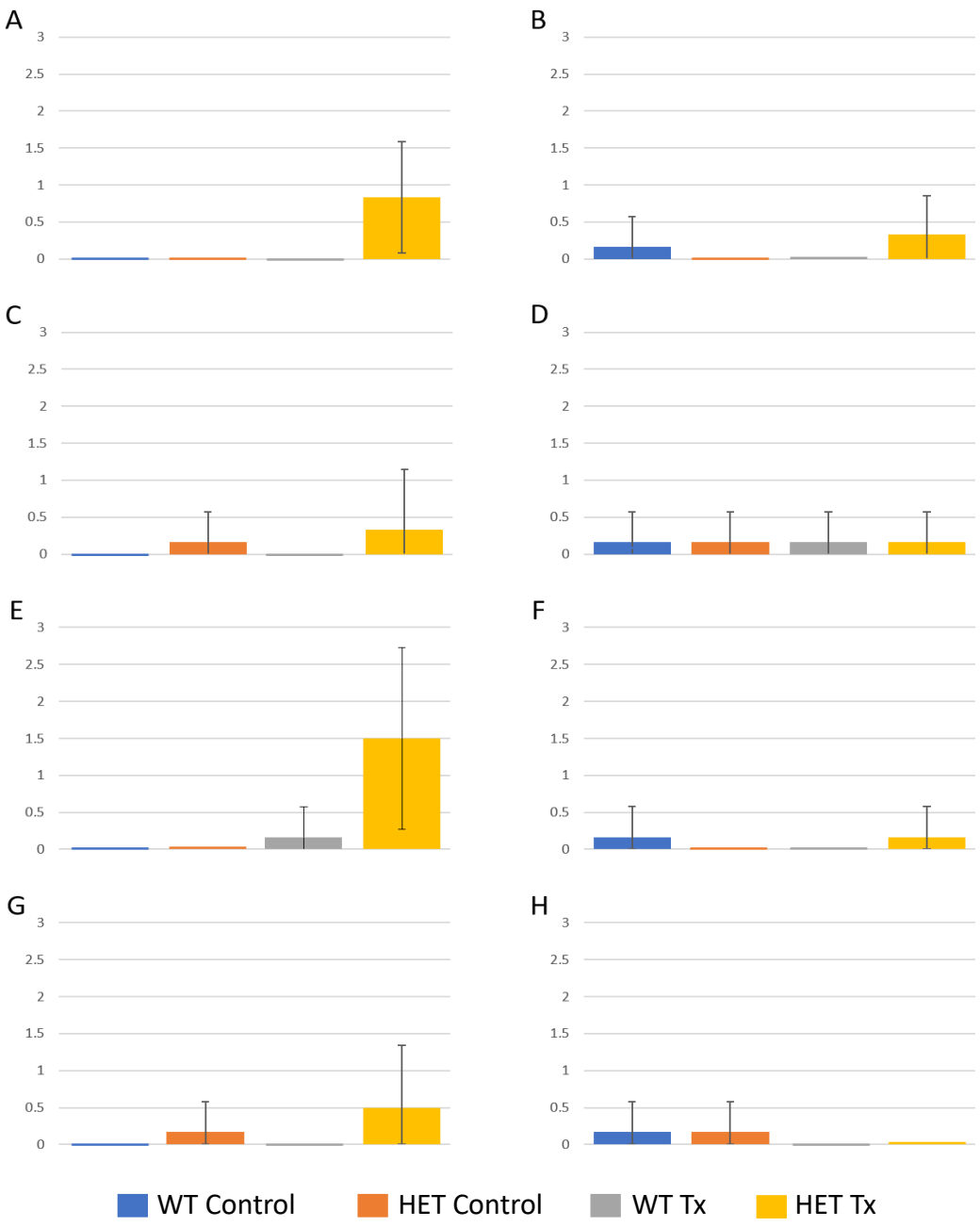

Figure 4.11: Histologic Scores for chronic exposure to low-dose diclofenac or *ad lib* Western diet. A) Male control vs NSAID infiltration; **B)** Male control vs NSAID hyperplasia; **C)** Female control vs NSAID infiltration; **D)** Female control vs NSAID hyperplasia; **E)** Male control vs diet infiltration; **F)** Male control vs diet hyperplasia; **G)** Female control vs diet infiltration; **H)** Female control vs diet hyperplasia. WT = wild type; HET = heterozygous; n = 6 per group.

For gut microbiome analysis, groups were visually inspected for descriptive analysis of consistency between animals using generated bar graphs in Microsoft Excel (Figures 4.12 and 4.13). Pre-treatment fecal samples from both WT and HET rats in all groups appear similar with no OTU standing out and significantly different between animals (Figure 4.12). However, there are major differences shown via bar chart for the post-treatment samples. Specifically, it appears that, regardless of genotype, there is a loss of Bacteroides and a bloom of Firmicutes in our diet groups. This is denoted by a loss of Muribaculaceae and an increase in Lachnospiraceae, Christensenellaceae, and Ruminococcaceae (Figure 4.13). In addition, we see a bloom of Lactobacillaceae in our NSAID-treated groups, especially in females, and a bloom of desulfovibrionaceae in our diet groups, particularly the males. Additional qualitative analysis by clustering of animals within groups using principal coordinate analysis (PCoA) in Past revealed differences in overall microbiome composition. In terms of post-treatment fecal samples, there were no distinct differences between control and NSAID-treated animals as noted by the overlap of convex hulls for all groups (Figure 4.14). However, PCoA shows that Western diet has a significant effect on the microbiome in both male and female animals regardless of genotype. Due to the distinct separation between the control and diet treated animals, additional PCoA graphs were created to observe any separation of WT and HET diet treated animals, but none existed for either sex (graphs not shown). The only significant separation noted between ileal scrape samples was found in male HET rats on the diet treatment (Figure 4.15C).

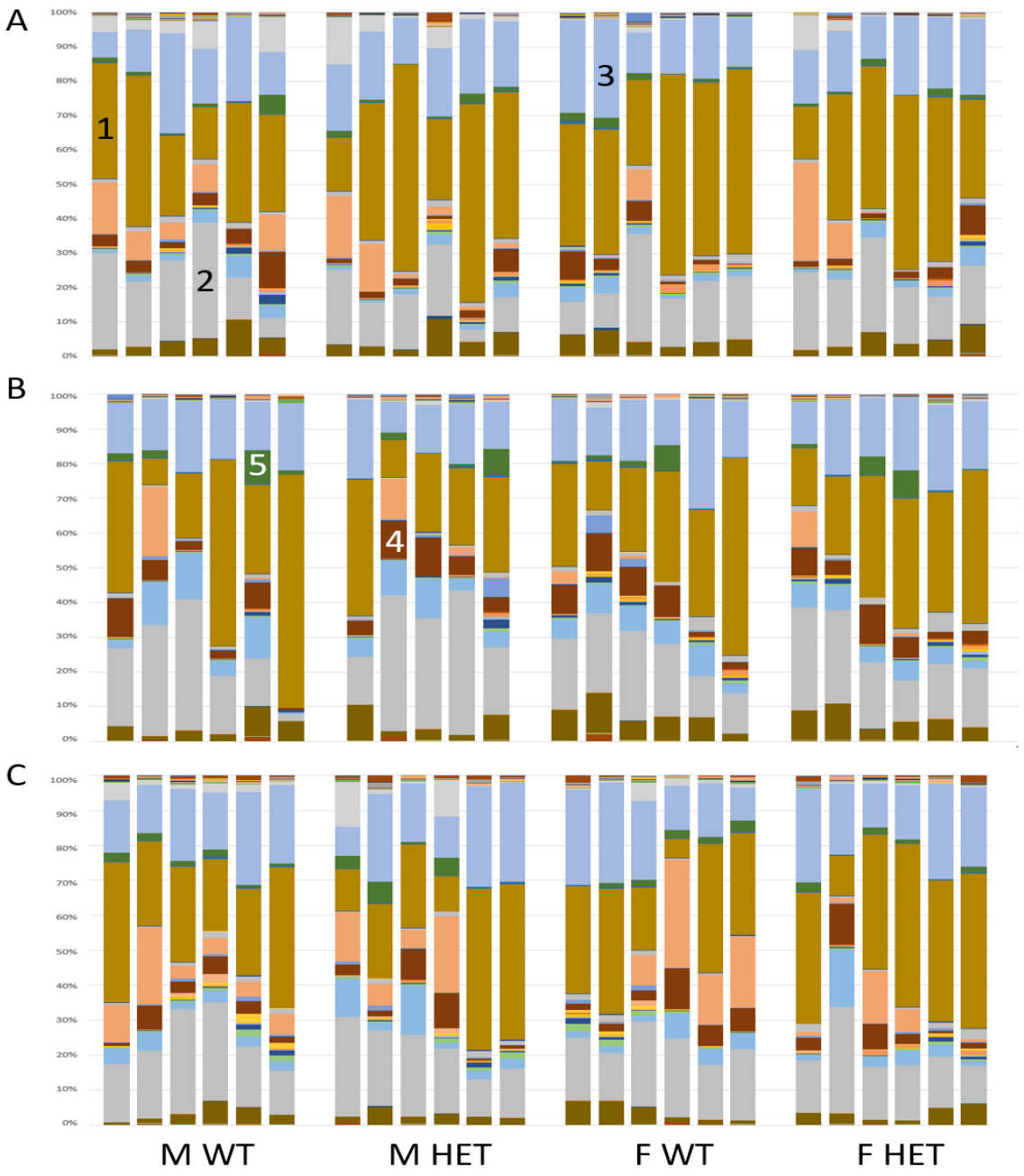

Figure 4.12: Pre-treatment microbiome OTU graphs for chronic exposure samples. Each bar represents the pre-treatment fecal microbiota profile for one animal in each group. Like colors denote identical OTU for each animal. Major OTUs include: 1: Lachnospiraceae; 2: Muribaculaceae; 3: Ruminococcaceae; 4: Lactobacillaceae; 5: Peptostreptococcaeceae **A)** Control animals; **B)** NSAID-treated animals; **C)** Western diet treated animals. M = male; F = female; WT = wild type; HET = heterozygous.

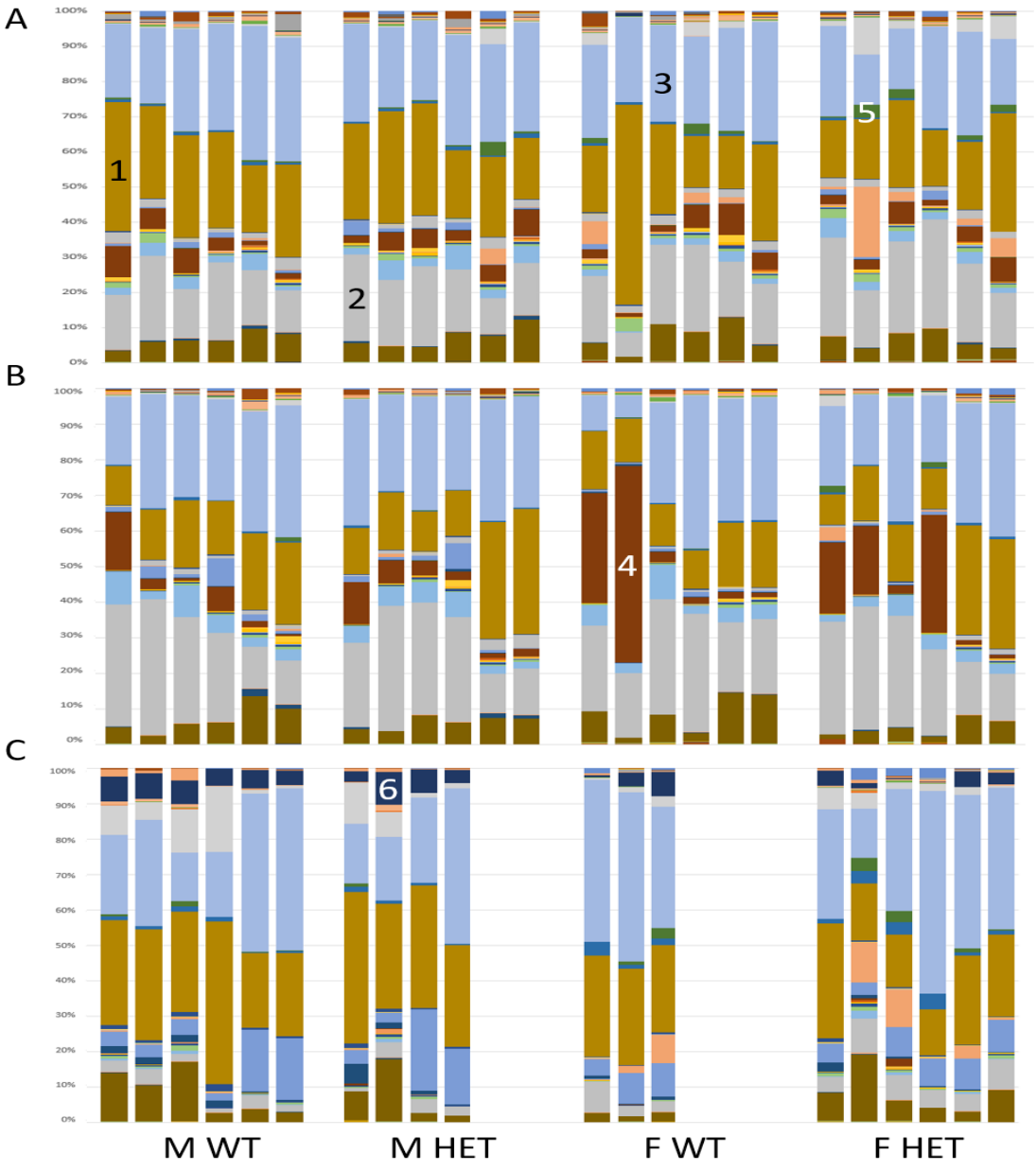

Figure 4.13: Week 12 post-treatment microbiome OTU graphs for chronic exposure samples. Each bar represents the pre-treatment fecal microbiota profile for one animal in each group. Like colors denote identical OTU for each animal. Major OTUs include: 1: Lachnospiraceae; 2: Muribaculaceae; 3: Ruminococcaceae; 4: Lactobacillaceae; 5: Peptostreptococcaceae; 6: Desulfovibrionaceae **A)** Control animals; **B)** NSAID-treated animals; **C)** Western diet treated animals. Note, some samples from our Western diet groups came back with significantly low read counts and were eliminated from the final analysis. M = male; F = female; WT = wild type; HET = heterozygous.

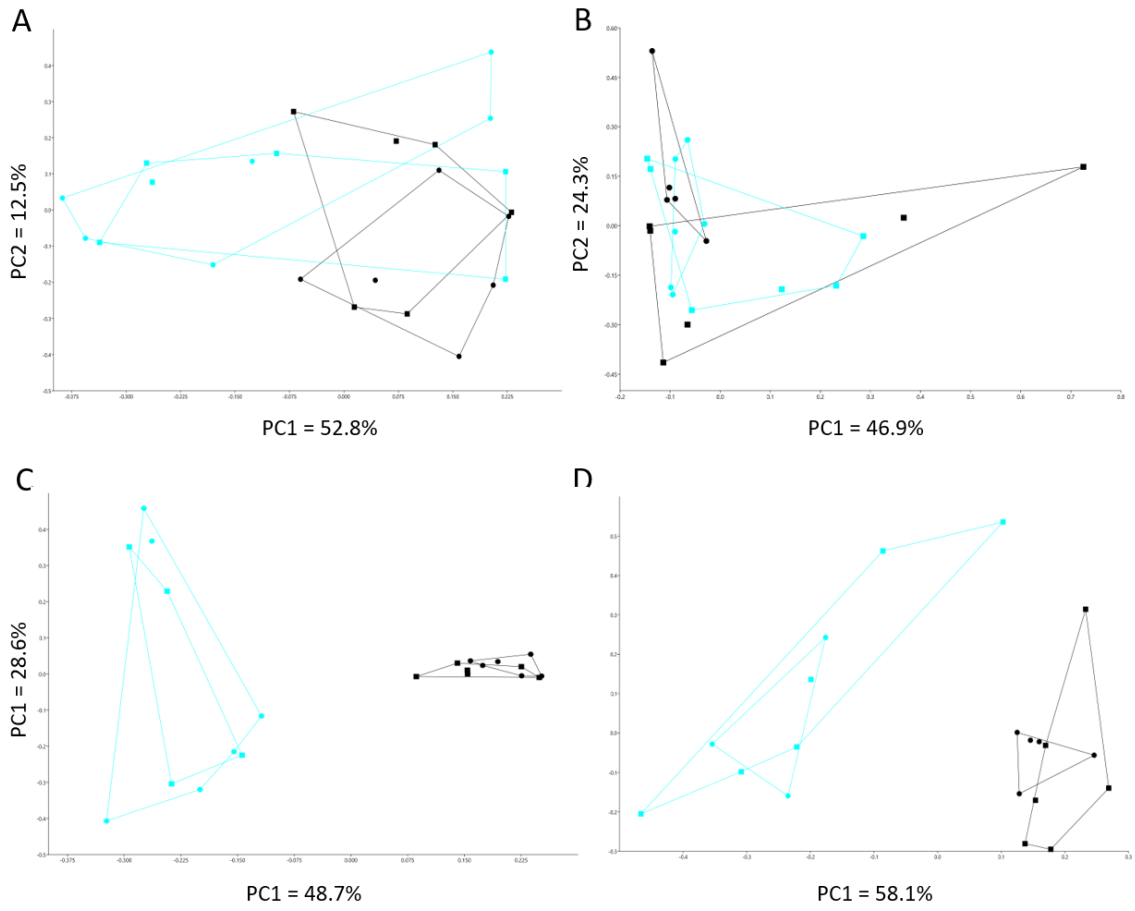

Figure 4.14: Principle component analyses (PCoA) for chronic exposure to diclofenac and Western diet, post-treatment fecal samples. The principle component percentage for each axis corresponds to the amount of difference between samples is accounted for by that component. For each graph: black dot = WT control; black square = HET control; blue dot = WT treatment; blue square = HET treatment. All graphs are control animal compared with the following: **A)** Male NSAID treated; **B)** Female NSAID treated; **C)** Male diet treated; **D)** Female diet treated. PC = principle component; WT = wild type; HET = heterozygous; n = 6 per group

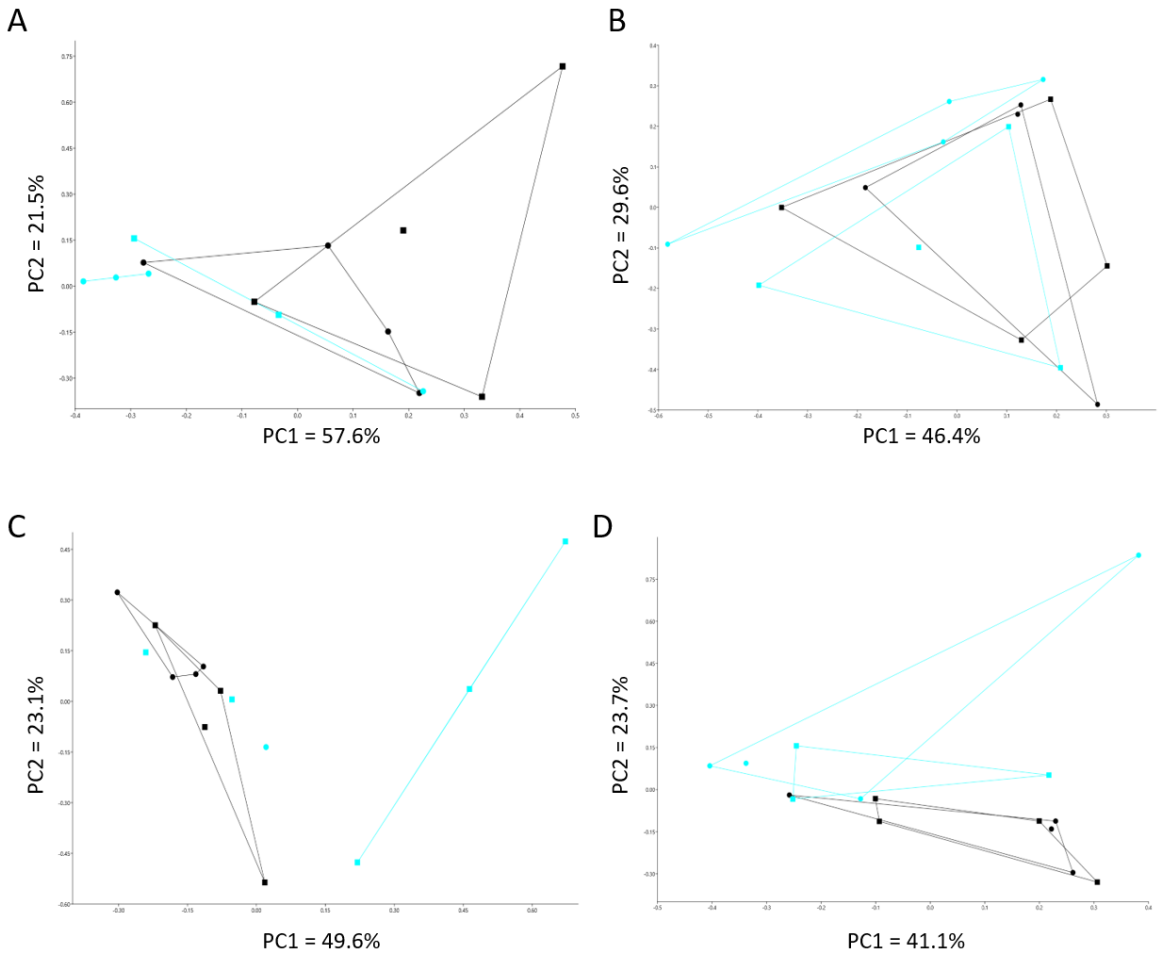

Figure 4.15: Principle component analyses (PCoA) for chronic exposure to diclofenac and Western diet, ileal samples. The principle component percentage for each axis corresponds to the amount of difference between samples is accounted for by that component. For each graph: black dot = WT control; black square = HET control; blue dot = WT treatment; blue square = HET treatment. All graphs are control animals compared with the following: **A)** Male NSAID treated; **B)** Female NSAID treated; **C)** Male diet treated; **D)** Female diet treated. PC = principle component; WT = wild type; HET = heterozygous; n = 6 per group.

Discussion

The goal of the current study was to determine whether rats carrying a genocopy of the human T300A *ATG16L1* susceptibility variant would show signs of disease when exposed to known environmental triggers of Crohn's disease (CD). We accomplished this by

performing both an acute study whereby rats HET for the T300A variant and their WT littermates were given high-dose oral diclofenac once a day for 7 days and a chronic study whereby HET rats and their WT littermates were either exposed to low-dose diclofenac or *ad lib* Western diet for 12 weeks. We evaluated the effects of treatment by microbiome analysis, gross and microscopic pathology, and weight changes

Non-steroidal anti-inflammatories are known to be an environmental trigger of CD in humans (Vedamurthy & Ananthakrishnan, 2019). The goal of our acute exposure study was to identify whether HET T300A rats exhibited a greater susceptibility to NSAID toxicity than their WT littermates. Our week-long study indicates that females carrying the rat version of the human T300A variant do show signs of significant NSAID toxicity after 7 days of high-dose diclofenac treatment.

Only two of our four female HET rats on NSAID treatment reached the 7-day dosage endpoint. One had lost over 20% of its body weight when weighed on day 5 of treatment and the other had lost over 20% of its body weight on day 6. Therefore, only three females were included in the weight average for day 5 and only two for day 7. We still noted a statistically significant difference in weight for HET females on NSAID when compared to all other female groups (Figure 4.1). In addition, signs of severe NSAID toxicity were noted at gross necropsy (Figure 4.2). While no perforations were found on gross examination or histologic analysis in the intestinal tract, the jaundiced and fibrotic omentum and straw-colored fluid within the abdominal cavity suggested this may have been the case. The presence of multifocal hepatic necrosis is also highly suggestive of

NSAID toxicity. Diclofenac, like other NSAIDs, is metabolized through the liver, and drug metabolism, reactive metabolite formation, and poor clearance of the drug are all factors in hepatotoxicity in humans (Bessone, 2010). Histologic findings of erosion, ulceration, and bacterial infiltration into the ileal tissues were apparent in the two female HET rats on high-dose NSAID that were euthanized prior to our study end-point (Figure 4.3). Higher histologic scores for male and female rats were consistent with increased acute inflammatory infiltrate, mainly neutrophils and macrophages, and varying degrees of bacterial proliferation (Figure 4.4).

Interestingly, qualitative microbiome data was no different between groups for our acute study. However, we did note clustering on heatmap analysis of the 25 most prominent OTUs in the samples (Figure 4.8). Two clusters were present for NSAID-treated animals. After returning to the raw data, it was discovered that animals clustering on the right side of the heatmap had higher scores for mucosal change and inflammation within their respective group. This suggests that the microbiome changes associated with NSAID administration are correlated with gross and histologic changes we noted from supposed NSAID toxicity in our HET animals. Considering the T300A variant is only a susceptibility variant and is found in both healthy and CD affected people, it is reasonable to assume that experimental disease expression does not have a 100% penetrance either.

As expected, our chronic exposure study revealed much more mild signs of disease than the acute NSAID toxicity study (Figure 4.10). Weight change and gross necropsy

findings were not significant for any of our treatment groups. Given the expected mild form of disease in our chronic treatment groups, the histologic assessment performed focused on a broader array of changes than the acute study, including overall white blood cell infiltration, overall hyperplasia of the mucosal tissues, and the presence of mucous and venous congestion in the lumen and vasculature, respectively. We did find significant results for infiltration of white blood cells in HET rats on both NSAID and diet treatment. This infiltration included mainly mononuclear cells (plasma cells, lymphocytes, etc.) found in chronic human IBD cases. Both mucous production and venous congestions were elevated in animals receiving either the NSAID or diet treatment independent of sex or genotype. Microbiome samples were not significantly different for either treatment groups; however, we noted a large shift in the fecal microbiome of animals receiving the diet treatment versus control animals (Figure 4.14) but not for ileal samples (Figure 4.15).

This study is the first of its kind to not only evaluate these two environmental triggers of CD, but also to evaluate any triggers of CD in a rat model carrying a human CD susceptibility variant. Our findings show that this rat model which carries the human T300A *ATG16L1* CD susceptibility variant does in fact show disease signs when exposed to known triggers of CD. The overt susceptibility to NSAID toxicity in our model gives further support to non-specific NSAIDs as a trigger for disease, and, more specifically, a trigger for individuals with this susceptibility variant in *ATG16L1*.

When viewed in the context of several studies reporting strong phenotypes associated with complete knock-out of autophagy genes in certain cell types (Patel & Stappenbeck, 2013), and severe signs of disease in models artificially exposed to opportunistic and pathogenic bacterial and viral strains (Cadwell et al., 2010; Kuballa et al., 2008), our chronic study results highlight a potential model to evaluate more mild cases of CD in a long-term capacity, allowing for very slight changes in intestinal and microbial environments to be uncovered. The finding of increased lymphocytes and plasma cells within the lamina propria of HET animals on both chronic treatments is one major sign of IBD in humans (Panaccione, 2013). The fact that it was seen without additional signs may suggest early stages of CD and that this chronic study was too short to result in true IBD manifestation. Future studies should evaluate whether a more long-term study could elicit additional finding in this rat model.

Overall, the T300A rat model is a valuable tool for both acute and chronic environmental studies of IBD. The presence of the human T300A variant as well as the ability to produce disease signs with environmental triggers of CD in humans will make it an important contributor to future CD and IBD research.

CHAPTER 5: *IN VITRO* FUNCTIONAL ASSESSMENT OF RAT *ATG16L1* AND AUTOPHAGIC FLUX

Introduction

In its classical form, the autophagy pathway is responsible for sequestration of unwanted cytoplasmic materials into a double membrane bound vesicle called the autophagosome. The autophagosome delivers these unwanted components to the lysosome for either recycling of cellular materials into their original building blocks or lysis, in the case of intracellular bacteria. This process is conserved in all eukaryotic species, occurs even at basal levels in nearly all cell types, and is increased by several intracellular and extracellular cues.

Formation of the two vesicular components of autophagy – the autophagosome, which develops from a double membrane fragment called the phagophore, and lysosome – involved 16-20 different autophagy (*ATG*) genes categorized into different functional groups based on the step of autophagy during which their respective protein products work (Figure 5.1) (Pyo, Nah, & Jung, 2012; C.-W. Wang & Klionsky, 2003). The ULK1 serine threonine complex is stimulated by one of a number of cell stressors (starvation, abnormal pH, damage, etc.) and induces autophagy and phosphorylates the downstream Beclin 1 complex. Beclin 1 and its associated protein are responsible for autophagosome nucleation, or the first step in formation of the new autophagosome structure via self-assembly/self-organization (Mariño & López-Otín, 2004). Once the membrane fragment is initiated, the ubiquitin-like protein conjugation complex ATG12-ATG5-ATG16L1 localizes the

autophagosome machinery inside the vesicle and fuses the double membrane to form the structure. It is during this step that *ATG16L1* is vital in the autophagy process.

When ATG12-ATG5 conjugate with ATG16L1, the binding site of ATG5 is exposed to allow ATG12 to interact with the phagophore, or the initial autophagosome membrane fragment (Figure 5.2A). This interaction between ATG12 and LC3-ATG3 complexes on the membrane signals phosphatidylethanolamine (PE) and results in lipidation of LC3, converting it from LC3-I to LC3-II. This step is vital to elongation of the phagophore and fusion of the membrane to create the autophagosome vesicle (Figure 5.2B).

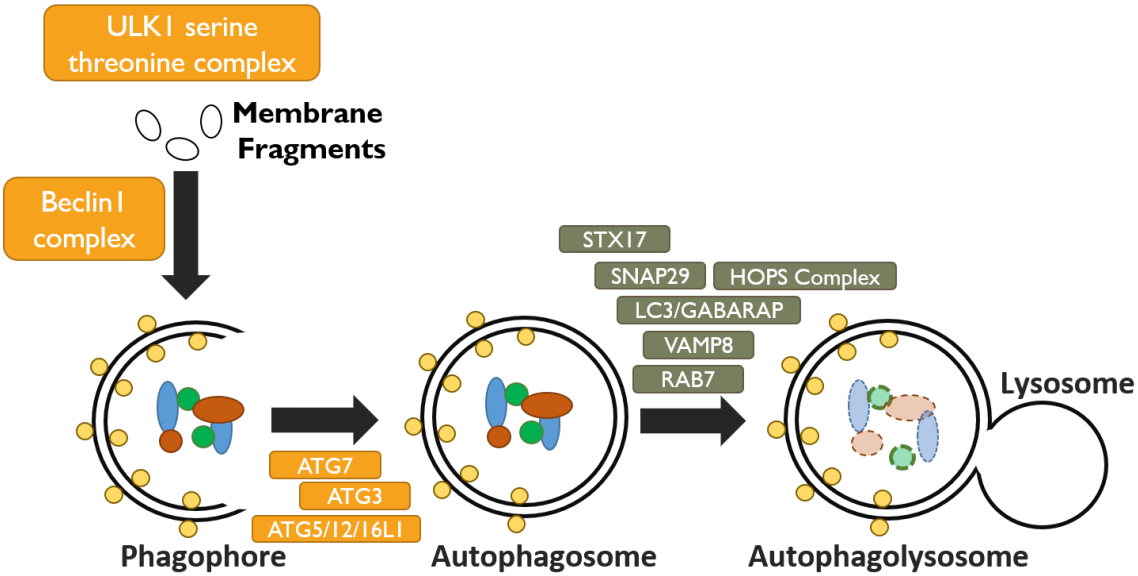

Figure 5.1: The pathway of classic degradative autophagy. Initiation of autophagy is caused by a cell stressor which triggers the ULK1 serine threonine kinase complex to initiate membrane formation and phosphorylate the Beclin 1 complex. Beclin 1 and associated proteins are responsible for autophagosome nucleation. After the phagophore is formed, expansion involves the ubiquitin-like protein conjugation complex ATG12-ATG5-ATG16L1. This complex is responsible for membrane localization of the autophagy machinery and generation of the autophagosome. The final step of autophagy requires fusion of the autophagosome to the lysosome. The lysosome contains degradative enzymes, also called acidic hydrolases, which degrade materials sequestered in the autophagolysosome.

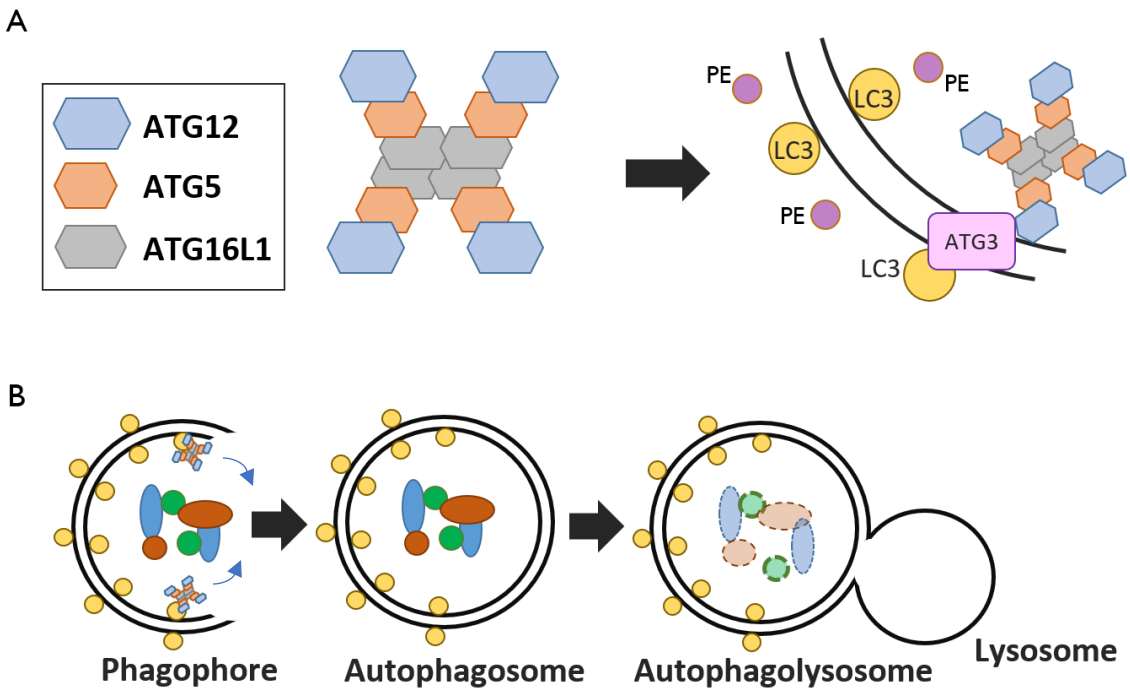

Formation of the autophagosome by the ATG5-ATG12-ATG16L1 complex. A) Formation of the ~350kDa ATG5-ATG12-ATG16L1 multimeric protein complex results in ATG5 and ATG12 residues forming a highly conserved, continuous functional region to which ATG3 binds at the phagophore. Binding of ATG3 causes lipidation of LC3-I to LC3-II and elongation of the phagophore. PE = phosphatidylethanolamine B) The phagophore elongates to sequester unwanted cellular debris within the vesicle structure. Upon fusion of the membrane to form the complete vesicle, it is called the autophagosome. This autophagosome then fuses with the lysosome to form the autophagolysosome. The membranes of the autophagosome are degraded during fusion to release lysosomal acidic hydrolases inside the autophagosome.

Autophagic flux studies use LC3 to measure autophagic degradation activity (du Toit, Hofmeyr, Gniadek, & Loos, 2018). LC3 is a unique component of the autophagic machinery, because it is incorporated into the autophagosome membrane but then degraded along with the autophagosome contents after lysosomal fusion. During autophagy, cytosolic LC3-I is conjugated to form LC3-II, the form of LC3 that conjugates to the autophagosome membrane. It then degrades with autophagosome fusion; therefore, lysosomal turnover of LC3-II reflects the rate of induced autophagy.

The current study focuses on understanding the effect of wild type *Atg161* splice variants on autophagic flux. The rat *Atg16l1* has four WT splice variants, all which produce a protein *in vitro* (Chapter 3). This study revealed that these WT variants are found in different combinations in different tissues of the body, which suggests that these splice variants may have different effects during autophagy. A previous *in vitro* study analyzing the effect of overexpression of three out of nine human WT splice variants of *ATG16l1* on autophagic flux noted that there were differences in autophagosome counts and duration of heightened autophagy after stressors were introduced depending on the splice variant. (Jiang, Qin, He, Lin, & Ding, 2013).

To begin investigating the effects of the rat splice variants on autophagic flux, we performed transfections of each of the four splice variants into HEK293 cells. Transfected cells were 1) treated for 4 hours with balfilomycin A1, an inhibitor of autophagosome-lysosome fusion, 2) subjected to starvation conditions for 12 hours, or 3) were starved for 12 hours with the addition of balfilomycin during the last 4 hours (Figure 5.3). Additionally, we speculated that cells transfected with the other three variants and subjected to stressors would show decreased autophagic flux compared to cells over-expressing the full-length transcript. The rationale for this is that compared to the full-length transcript, the other three variants have deletions of exons that lead to isoforms with alterations in protein structure that might be expected to inhibit their full function during autophagy. The loss of exon 5 results in a partial loss of the coiled coil domain of the

protein. This domain is responsible for protein binding specificity and its loss is expected to reduce the ability for the variant to bind to Atg5 and Atg12 during autophagy. The loss of exon 9 or exon 8 and 9 results in a shortening of the linker region between the coiled coil domain and WD 40 repeat domain of the Atg16l1 protein. While this does not have any effect on the functional domains of the protein, because Atg16l1 is used in a multimeric protein complex, we hypothesize that the shortening of this region alters the tertiary and quaternary structures of the protein vital for proper formation of the multimeric Atg5-Atg12-Atg16l1 complex.

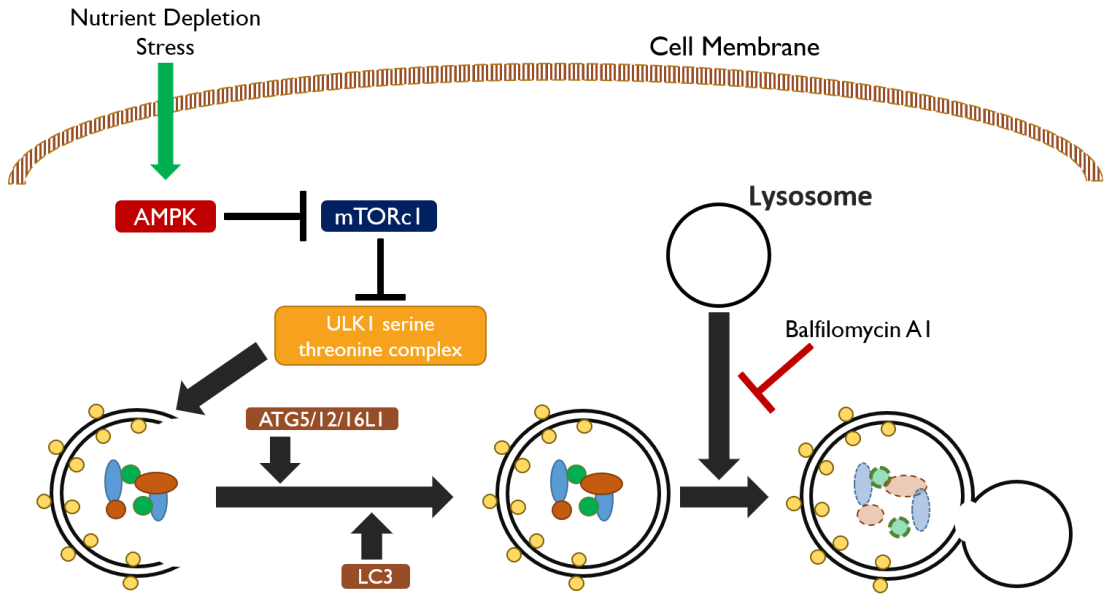

Figure 5.3: Example of the effect of cellular stressors on autophagic flux. Cellular stressors, such as nutrient depletion or damage, trigger a downstream cascade of autophagy (ATG) proteins which result in initiation of the phagophore by ULK1 and Beclin 1 complexes. Through conjugation of the ATG5-ATG12-ATG16L1 complex and LC3-I conversion to LC3-II, the phagophore fuses to surround sequestered materials for degradation. The resulting autophagosome can be experimentally inhibited from fusing with the lysosome by using antibiotics and chemicals, such as balfilomycin A1 or chloroquine. This leads to a build-up of autophagosomes in the system and therefore LC3-II, which would normally be degraded along with sequestered materials, can be quantified to assess autophagic flux.

Results

Qualitatively, we were able to confirm that experimental treatments were successful in manipulating the rate of autophagy in each cell culture since we observed the expected increases and decreases in protein band density for LC3-II (Figure 5.4). Non-treated cells in growth media were used as the control for cells treated for four hours with balfilomycin A1, an inhibitor of autophagosome – lysosome fusion. Starved cells were used as a control for starved cells treated with balfilomycin A1 for four hours into 8 hours of starvation. We expected that balfilomycin-treated cells would have an increase in LC3-II, because the inhibition of lysosomal fusion results in a build-up of otherwise degraded LC3-II when the autophagosome fuses with the lysosome. We also expected that starved cells overall would have a greater densitometric ratio than fed cells given the presence of a cell stressor inducing autophagy.

Quantitative comparisons between bands for each transfection with a rat *Atg16l1* splice variant were performed using ImageJ software (National Institutes of Health, Bethesda, MD) by taking the area under the curve for the density of each LC3-II band per blot. The densitometric ratios for each set of experiments done in triplicate were analyzed using a Student's T-test comparing the densitometric ratio of fed cells to starved cells for each group. We found no statistically significant difference between fed cells and starved cells in terms of ratio for non-transfected cells. However, all our transfection groups were statistically significant when comparing fed cells to starved cells ($p < 0.05$; Figure 5.5). Of the four transfected groups, autophagy was significantly increased by introduction of the

full-length *Atg16l1* splice variant and the splice variant missing exon 5. This effect was the most prevalent in cells transfected with the full-length variant with an over 3X increase in autophagy between fed and starved cells. Interestingly, autophagy was diminished by introduction of the splice variants missing exon 9 or exons 8 and 9.

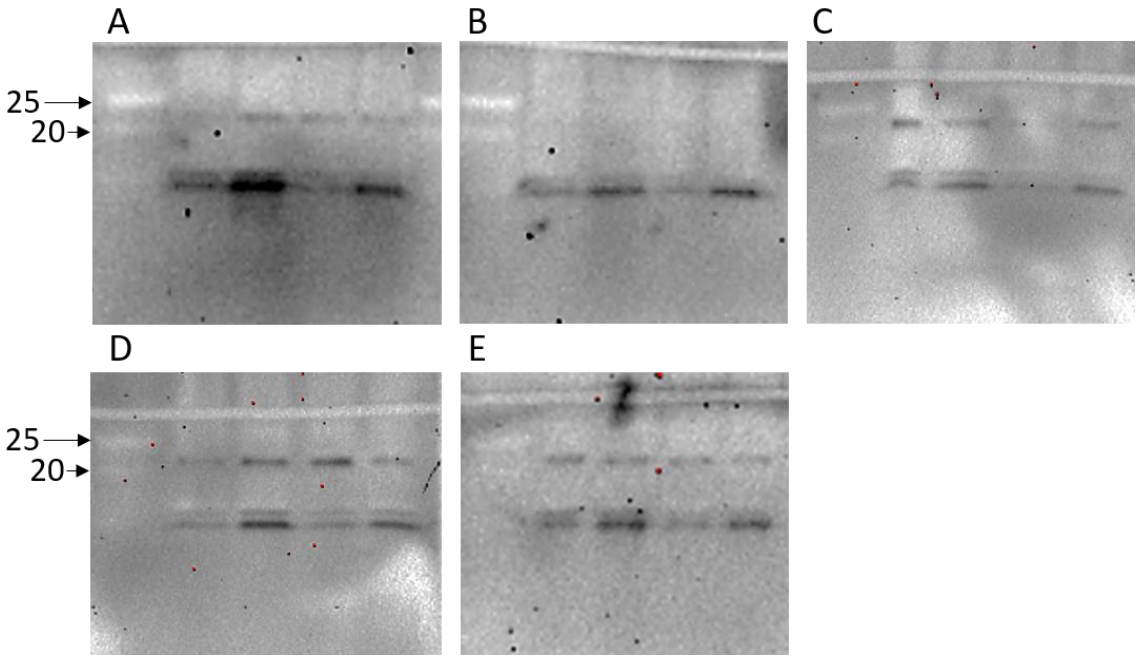

Figure 5.4: Representative Western blot images for detection of LC3 in transfected HEK293 cells with and without rat *Atg16l1* WT splice variants. Ladder with 20 kDa and 25 kDa in white on the far left of each blot. Protein bands at ~16 and ~14 kDa representative of LC3-I and LC3-II, respectively were detected. For each blot: Lane 1, untreated cells in growth media; Lane 2, balfilomycin treated (0.5 μM) cells in growth media; Lane 3, cells in Earle's balanced salt solution starvation media; Lane 4, cells in Earle's balanced salt solution starvation media + balfilomycin (0.5 μM). A) Non-transfected cells; B) Full-length transcript; C) Splice variant missing exon 9; D) Splice variant missing exons 8 and 9; E) Splice variant missing exon 5.

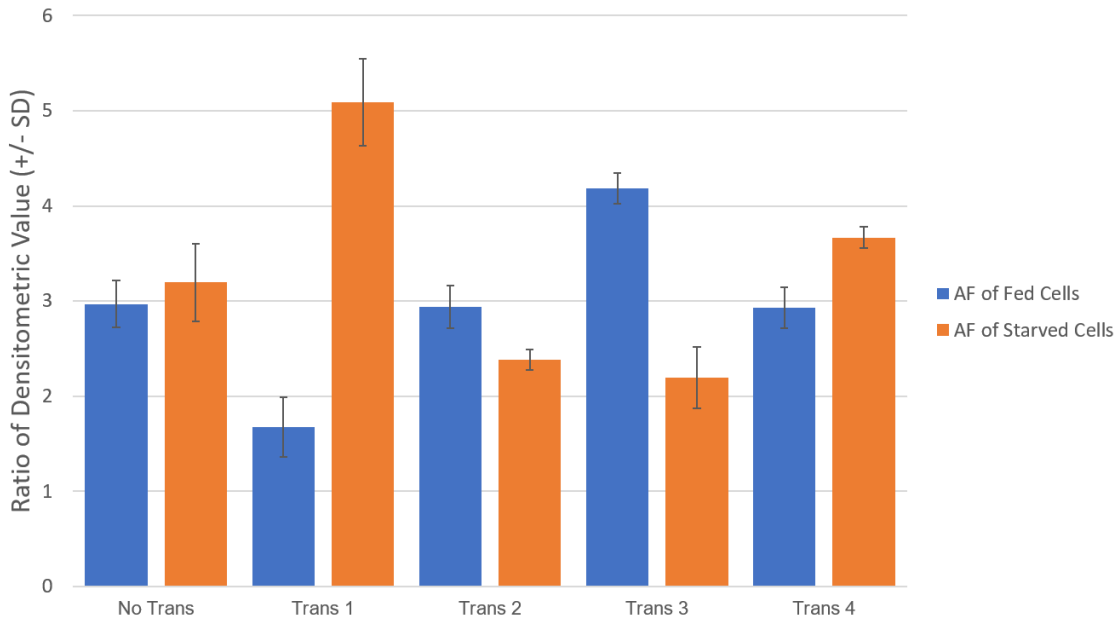

Figure 5.5: Comparison of densitometric value ratios for Western blot detection of LC3 in transfected HEK293. Blue bars = autophagic flux (AF) in fed cells; orange bars = autophagic flux in starved cells. A greater densitometric ratio means a higher rate of LC3 turnover (greater autophagy). For each pair of blue and orange bars, a higher orange bar indicates the transfected variant confers an increase in autophagic flux and a lower orange bar indicates a decrease. All but the non-transfected cells were statistically significant by Student's T-test. SD = standard deviation; No trans = no transfection; Trans 1 = transfection of full-length variant; Trans 2 = transfection of variant missing exon 9; Trans 3 = transfection of variant missing exons 8 and 9; Trans 4 = transfection of variant missing exon 5.

Discussion

In the present study, we performed Western blot analysis on HEK293 cells transfected with one of four WT rat *Atg16l1* splice variants to study the effects of WT rat Atg16l1 isoforms on autophagy. The degree of autophagy did indeed vary with different Atg16l1 isoforms.

Measurements of LC3-II are the gold standard quantitative index of autophagy in the classical, or macroautophagy, pathway (A. L. Wang et al., 2009). Our results show that

when the full-length splice variant and splice variant missing exon 5 are overexpressed *in vitro*, the amount of LC3-II increases. These data imply that overexpression of these isoforms influenced autophagy and can induce autophagosome formation. Alternatively, results from splice variants missing exon 9 or exons 8 and 9 revealed that overexpression of these isoforms leads to inhibited autophagosome formation. Previous studies, all which involve human ATG16L1 isoforms., have shown variable outcomes: an increase in autophagic flux (Jiang et al., 2013; Wildenberg et al., 2012), an inhibitory effect of Atg16l1 overexpression (Hwang et al., 2012), or no difference (Fukuda & Itoh, 2008). However, only one of these previous studies used individual splice variants of *Atg16l1*.

In the study conducted by Jiang et al., three of nine human splice variants (hereby referred to as *ATG16L1*-1, *ATG16L1*-2, and *ATG16L1*-3) revealed that all variants had a significant effect on autophagic flux *in vitro* under stress conditions. However, the amount of increase attributed to each variant was significantly different (2013). The human *ATG16L1*-1 and *ATG16L1*-2 are homologues of the splice variants in the rat missing exon 9 and exons 8 and 9. *ATG16L1*-3 does not match a splice variant in the rat; however, this variant does confer a similar effect to the protein structure as the rat variant missing exon 5. They both result in a loss of the coiled coil domain responsible for Atg5-Atg12 binding. The full-length human transcript of *ATG16L1* was not tested in the previous study, so we have no comparison for the effect of the full-length human variant versus the full-length rat variant.

Our findings validated our hypothesis that that *in vitro* overexpression of the full-length rat variant of *Atg16l1* increased autophagic flux as measured by an increase of LC3-II, the gold standard marker for autophagy, on Western blot analysis. The overexpression of full-length rat *Atg16l1* resulted in a 3X increase in LC3-II between fed cells and starved cells as measured by densitometric ratio using ImageJ (NIH, Bethesda, MD). The full-length splice variant of *Atg16l1* results in the most complete protein structure, which was expected to perform optimally during autophagy. The other three variants produce isoforms with altered protein structure, which was expected to affect the functionality of resulting protein during autophagy.

Like results from the human study evaluating three of nine splice variants of *ATG16L1* (Jiang et al., 2013), *in vitro* overexpression of the variant affecting the coiled coil domain of the resulting protein (the rat variant missing exon 5) resulted in a diminished increase in autophagy. We found only a 1.25X increase in autophagy when comparing fed cells to starved cells. Previous structural analysis of the ATG16L1 protein has found specific, conserved amino acid residues within the coiled coil domain necessary for proper binding of ATG5 and ATG12 during protein complex formation (Travassos et al., 2010). This suggests that the entirety of the coiled coil domain may not be necessary for binding, and explains why a truncated coiled coil domain, like that from the rat variant missing exon 5, is still functional to some degree.

Interestingly, our results for the rat splice variants missing exon 9 and exons 8 and 9 were contradictory to the human study evaluating homologues of these variants in the human (Jiang et al., 2013). We saw a decrease in LC3-II production when we overexpressed these splice variants *in vitro*, both of which shorten the linker region between the coiled coil domain and the WD 40 repeat domain of the resulting protein. Some studies have shown that transiently expressed human ATG16L1 inhibits autophagosome biogenesis, potentially due to incorrect stoichiometry of the ATG16L1 complex components (Fujita et al., 2008; Li, Chen, Stang, & Gao, 2017). We speculate that these isoforms are unable to form proper protein complexes *in vitro.* It is likely that these two WT splice variants do not form a functional Atg5-Atg12-Atg16l1 complex with the correct stoichiometry when transiently expressed *in vitro* to be used in the formation of the autophagosome. Future studies evaluating the structure of the Atg5-Atg12-Atg16l1 complex should be performed to determine whether transient expression of each splice variant can lead to formation of a complex and whether that complex retains its proper quaternary structure.

Overall, studies of rat Atg16l1 isoforms are valuable in understanding the mechanism of *Atg16l1* in autophagy. Our findings that two WT splice variants conferred an increase in autophagy while two conferred a decrease leave much to uncover as to the mechanism of action for each isoform of Atg16l1 in the rat.

CHAPTER 6: CONCLUSIONS AND FUTURE DIRECTIONS

ATG16L1 has been a known autophagy gene for decades; however, the discovery of its role in CD susceptibility is relatively new (Hampe et al., 2007; Kuballa et al., 2008). The gene is responsible for making the ATG16L1 protein required for development of the double-membrane bound autophagosome vital to removing unwanted cellular debris and intracellular bacteria from the cell. Given the importance of the autophagy process for cell survival, it is not surprising that *ATG16L1* is found ubiquitously in eukaryotes with high structural and sequence similarity of the encoded protein across species (Xiong et al., 2018).

The *ATG16L1* susceptibility variant is a nonsynonymous adenine to guanine polymorphism that results in a threonine to alanine substitution in the amino acid sequence (T300A). Previous T300A knock-in and knock-out mouse models of the *Atg16l1* gene have been instrumental both in understanding the pre-disease effects of the T300A variant and confirming similarities in these pre-disease signs between human patients and mice (Cadwell et al., 2008). However, these models have never been subjected to environmental triggers of CD; rather, researchers have utilized exposure to artificial opportunistic and pathogenic bacteria or viruses to triggers severe disease signs (Cadwell et al., 2010; Salem et al., 2015). The purpose of developing a knock-in rat model with the T300A variant was to find a model to use for environmental studies and potential future therapeutics and treatments of CD. However, *Atg16l1* had never been fully characterized in the rat, and

initial characterization of this model was vital to any future work and was the basis of this dissertation.

This dissertation is the first comprehensive genetic characterization of *Atg16l1* in the rat. The goal of our work was to characterize the wild type *Atg16l1* rat gene and provide proof of concept that a novel rat model carrying the T300A human susceptibility variant of *ATG16L1* can be used as a tool to evaluate the mechanism of *ATG16L1* in Crohn's disease (CD). Current mouse models (both hypomorphic for *Atg16l1* and carrying the T300A variant) have successfully recapitulated certain pre-disease markers, such as PC granule malformation, as well as a sensitivity to bacterial infiltration (Cadwell et al., 2008). However, these models have never been shown to have a sensitivity to common environmental triggers of CD – a vital component to the multifactorial etiology of disease. The knock-out SD-*Atg16l1*$^{em2/RRRC}$ rat model and F344-*Atg16l1*^{em8RRRC} rat model carrying the T300A variant, developed by our laboratory, provide a means to identifying the relationship between *ATG16L1* CD genetic susceptibility and environmental triggers of disease.

Chapter 3 of this dissertation highlights the initial characterization of *Atg161* in the rat. During our characterization, we confirmed that the rat possesses similar pre-disease histologic abnormalities found in humans and mice carrying the T300A variant. Specifically, this included PC changes, both in granule concentration and morphology. However, we identified that the rat, unlike both humans and mice, cannot be homozygous

(HOM) for either a knock-out of *Atg16l1* or the T300A variant. This presents an interesting opportunity to understand the mechanism of *ATG16L1* and its role in autophagy and disease. All wild type splice variants of *Atg16l1* carry the T300A susceptibility variant in the rat. Given the presence of wild type *Atg16l1* splice variants in humans and mice that do not carry the exon harboring the T300A susceptibility allele, it suggests that perhaps these wild type variants compensate for the altered variants carrying the susceptibility allele and provide some protection for the systems which utilize ATG16L1. Future experiments should seek to uncover the stage in development where lack of unaltered wild type splice variants affects the process. Two experiments could help pinpoint the step where development is hindered. First, sperm and ova collected from wild type and heterozygous F344-*Atg16l1*^{em8RRRC} rats should be sequenced to determine whether the T300A variant affects either sex cell. It is known that functional autophagy is required for proper development of ectoplasmic specialization in Sertoli cells (C. Liu et al., 2016). It could then be hypothesized that males carrying the T300A variant cannot confer that variant to their offspring, because sperm development is hindered by a lack of ATG16L1 protein when the susceptibility variant is present. If phenotypically normal sperm can be developed carrying the T300A variant, these sperm should be evaluated for impregnation of the ova *in vitro* to confirm that this variant does not present any hinderance to mobility or function. Second, and if sperm production is not hindered by the T300A variant, embryos from F344-*Atg16l1*^{em8RRRC} HET x HET matings would be collected to determine at which stage of development HOM embryos die. It is apparent from our characterization that no HOM pups are born; however, the stage at which the variant causes embryonic lethality is unknown.

While we were able to confirm that our rat models were genetically faithful representations of CD susceptibility in human patients and presented with the same histologic feature of the T300A variant (abnormal PC granulation) in human CD patients, Chapter 4 aimed to extend this work to evaluate whether the F344-*Atg16l1*^{em8RRRC} rat model could develop signs of disease when exposed to known environmental triggers of CD in humans. These were the first experiments of their kind to determine whether triggers, specifically as the non-specific, non-steroidal anti-inflammatory (NSAID) Diclofenac and *ad libitum* Western diet formulated rodent chow, could cause disease signs.

While our acute study did not explicitly evaluate signs of CD, we successfully accomplished our goal to determine whether rats carrying the T300A variant were more susceptible to NSAID-related toxicity. HET rats given high-dose NSAID had weight loss, intestinal inflammation, erosions, ulcerations, and systemic signs of disease in the omentum and liver. Multiple mechanisms have been implicated as to how NSAIDs trigger CD, including increased mucosal permeability, formation of drug-enterocyte adducts, and NSAID-induced intracellular ATP deficiency, increased enterohepatic circulation, and prostaglandin synthesis (A. Klein & Eliakim, 2010). However, these mechanisms have yet to be tied to any specific genetic susceptibility variant. Knowing that our rat model does have increased susceptibility to NSAID-induced gastrointestinal toxicity, future studies in NSAID exposure and CD should be conducted to determine the precise mechanism of action relating the *ATG16l1* T300A variant, NSAID use, and onset of CD in humans. Of particular interest is the effect of NSAIDs on prostaglandin synthesis. Prostaglandins are vital in mucosal defense and modulation of the immune system in the colon (Wallace,

2001). ATG16L1 is also needed for proper mucosal defense and immune modulation via PC degranulation. It may be that while the deficiencies of the immune system solely with the T300A variant are manageable, the additional insult to the immune system by NSAIDs is enough to trigger acute CD.

In addition to our acute experiment, we also conducted a long-term exposure study using two known environmental triggers of CD (NSAID and Western diet) to see how exposure to these variables effected our F344-*Atg16l1*^{em8RRRC} rat model over time. Differences between our HET rats and their WT littermates were subtle. The purpose of this study was not to elicit NSAID toxicity signs or result in severe illness but rather to uncover those initial changes in histology and microbiome that precede serious, acute CD illness. Therefore, the subtle changes noted in this study were precisely the goal. However, there are potential pitfalls to our chronic study. This study did encompass the duration of the rat lifespan which includes much of the growth and development phase (ages 4 weeks to 4 months), which equates to approximately ages 1 – 12 years in a human (Andreollo, Santos, Araújo, & Lopes, 2012; Sengupta, 2013). However, given most CD cases in humans are diagnosed in the late teens/twenties (Quezada, Steinberger, & Cross, 2013), this study may not have been long enough to truly encompass an equivalent age in our model to see the full extent of exposure. Future experiments should be conducted to determine whether this is the case and whether chronic exposure needs to extend out to 12 months, or an equivalent age to 30 human years (Andreollo et al., 2012; Sengupta, 2013). Given the subtle changes in intestinal histology noted during our study, it suggests that our T300A rat model does have the potential to respond to these environmental factors. This is an area of CD study

that is sorely lacking in information and supports the positive effect our model could have on future CD studies.

One finding from the environmental exposure studies using the NSAID diclofenac that we did not anticipate was the difference in disease signs between males and females depending on whether exposure was acute or chronic. In the acute study, females were much more severely affected than males, showing signs of jaundice, ascites, and hepatic necrosis on gross exam and extensive erosion and ulceration with bacterial infiltration on histologic exam. However, only males presented with statistically significant signs of disease on histologic exam in the chronic study.

There has been a large push to examine sex differences in immunity within the last decade, and all the evidence supports a need to evaluate both sexes independently due to reported sex bias in the dynamic responses to invading pathogens (Ingersoll, 2017; Macleod & Mohan, 2019; Voelkl et al., 2020; vom Steeg & Klein, 2016). These responses are associated with direct effects of X- or Y-linked genes, indirect effects of sex hormones, and responses to environmental risk factors that act in a sex-specific manner (Markle & Fish, 2014). It has long been documented in humans, and mouse and rat models, that males are more susceptible to infectious disease than females, including bacterial, viral, and parasitic infection (Brabin & Brabin, 1992; Zuk & McKean, 1996). Much of this difference has been attributed to differences in the endocrine-immune interaction (S. L. Klein, 2000). Androgens in males and estrogen in females modulate multiple aspects of host immunity,

including gene behavior that influence susceptibility and resistance to infection (Alexander & Stimson, 1988; Grossman, 1989; S. L. Klein, 2000).

One of the most intriguing aspects of male vs. female immunity is the prevalence of the Th1 and Th2 response in each sex. In both humans and mouse models, females exhibit higher Th2 responses (Interleukin (IL)-4, IL-5, IL-6, and IL-10) than males (S. L. Klein, 2000). While limited evidence supports the Th1 response in male rats, extensive evidence exists in humans and mouse models. If male rats have the same high Th1 response, this could explain why male are more susceptible to a true, chronic "Crohn's-like" disease process as elicited in the chronic study, because the disease is dependent on that Th1 response. If, in males, the Th1 response is already elevated, combining that with dysfunction associated with the T300A susceptibility variant may have been enough to exceed the phenotypic threshold such that the male animals in the chronic study exhibited significant signs of disease. In contrast, female animals, already predisposed to a Th2 response, may not have produced a strong enough Th1 response over time to low-dose triggers and therefore, no significant disease-related changes occurred.

In addition to the Th1/Th2 response dichotomy, there is evidence supporting sex bias with NSAID use. Hypersensitivity to NSAID is already more prevalent in human and murine females than males (Rebelo Gomes et al., 2016). While peptic ulcer disease does not seem to be more prevalent in one sex over the other (Lanas & Chan, 2017), the compounding effects of sex-specific sensitivity, an abnormal Atg16l1 gene, and the type of immune

response mounted against invading bacterial pathogens (as seen in histologic imaging of female intestinal tissues) may have all contributed to increased sensitivity to high-dose NSAID during the acute study.

Unfortunately, human data pertaining to sensitivity and NSAID use is confounded by several different factors. Lifestyle, environment, socioeconomic factors, and longevity all contribute to the effects of NSAID over time. Our findings provide an interesting peek into how males and females may respond to triggers of Crohn's disease, and provide a foundation for future work in this area.

Chapter 6 highlights ongoing *in vitro* work which seeks to understand the effects of the rat *Atg16l1* T300A susceptibility variant on autophagy. An intriguing piece of data we uncovered during our characterization of *Atg16l1* in rats is that different combinations of the WT splice variants show up in different tissues in the body. This would suggest that they each do something slightly unique in the autophagy process. After *in vitro* confirmation that all four WT splice variants of the rat *Atg16l1* gene can produce a protein, these WT variants were used to transfect HEK293 cells and further our knowledge of their effect on 1A/1B-light chain 3 (LC3) turnover and autophagic flux.

Our first and only experiment currently in progress focuses on qualitative measurement of LC3. By collecting total protein from HEK293 cells transfected with one of the four WT splice variants of *Atg16l1* and performing Western blot analysis to probe for LC3-I and LC3-II, we could evaluate the effect on autophagy by visualizing the intensity of the

banding pattern under different conditions. LC3 is one of the definitive markers of autophagy (Tanida, Ueno, & Kominami, 2008). It is expressed as a protein precursor until activation when it is cleaved by ATG4 protease to form LC3-I. Initiation of autophagy causes the conversion of LC3-I to LC3-II through the addition of phosphatidylethanolamine (PE) to the C terminus. The lipophilic quality of PE also results in the insertion of LC3-II into the membrane of the autophagosome and its subsequent degradation as autophagosomes are turned over. An increase in LC3-II band intensity on Western blot is considered the hallmark of autophagy; however, this increase can be caused by a number of things, including enhanced autophagosome synthesis or reduced autophagosome recycling, so additional LC3 experiments beyond Western blot must be conducted to ensure characterization of the autophagy process is appropriate.

Western blot experiments were complicated by number of additional pitfalls common in LC3 studies. Initially, low yields of total protein resulted in too much total protein needed to fit our Western blot PAGE gels; therefore, we needed to refine our method to collect protein from cells grown in T75 flasks. LC3 also rapidly degrades after purification with total protein. Therefore, protein was kept in aliquots at -80°C to reduce denaturation from freeze/thaw cycles. Finally, LC3 antibodies used in Western blot analysis have varying degrees of affinity for LC3-I and LC3-II, and there are also significant differences in LC3 expression depending on the cell type used for *in vitro* work. Several LC3 antibodies were tested before finding one with a high enough affinity for LC3 in HEK293 cells to allow us to conduct appropriate ratios of LC3-II between treatment groups. What has resulted is an

appropriate method and initial results which can be continued in the laboratory in the future.

Additional future studies to evaluate LC3 and the effect of the WT *Atg16l1* splice variants on autophagic flux should include direct visualization of autophagosomes and other components of the autophagy process. For example, direct visualization of LC3 protein localization should be conducted using a tandem RPF-GFP sensor kit (such as the Premo™ Autophagy Tandem Sensor RFP-GFP-LC3B Kit (Invitrogen)) for cell culture transfected with each WT splice variant of rat *Atg16l1*. These kits use the inherent pH differences between the autolysosome (acidic) and the autophagosome (neutral) and the difference in pH sensitivities of RFP and GFP to monitor the progression of the autophagosome to autolysosome. Second, direct dual transfection of cell culture with an GFP-tagged LC3 vector and one of each WT rat *Atg16l1* should be performed to visualize and manually count LC3-II puncta present within cells to evaluate changes in autophagosome formation. These experiments, combined with the initial Western blot study performed as part of this dissertation, would provide a full picture for the effect of each WT rat *Atg16l1* splice variant on autophagy.

In summary, we presented the first studies on rat *Atg16l1* and genotypically and phenotypically characterized a knock-in rat model carrying the T300A human CD susceptibility variant in the *Atg16l1* gene as well as a knock-out *Atg16l1* rat model. We have also performed initial studies to evaluate the effects of WT rat *Atg16l1* alternative

splice variants on autophagy. This work has broad application to understanding the role of rat *Atg16l1* particularly in autophagy and it introduces new *Atg16l1* rat models that have utility for future CD research.

BIBLIOGRAPHY

Adegbola, S. O., Sahnan, K., Warusavitarne, J., Hart, A., & Tozer, P. (2018). Anti-TNF Therapy in Crohn's Disease. *International journal of molecular sciences, 19*(8), 2244. doi:10.3390/ijms19082244

Alexander, J., & Stimson, W. H. (1988). Sex hormones and the course of parasitic infection. *Parasitology Today, 4*(7), 189-193. doi:https://doi.org/10.1016/0169-4758(88)90077-4

Allais, L., Kerckhof, F.-M., Verschuere, S., Bracke, K. R., De Smet, R., Laukens, D., . . . Van de Wiele, T. (2016). Chronic cigarette smoke exposure induces microbial and inflammatory shifts and mucin changes in the murine gut. *Environmental Microbiology, 18*(5), 1352-1363. doi:10.1111/1462-2920.12934

Amre, D. K., D'Souza, S., Morgan, K., Seidman, G., Lambrette, P., Grimard, G., . . . Seidman, E. G. (2007). Imbalances in dietary consumption of fatty acids, vegetables, and fruits are associated with risk for Crohn's disease in children. *The American journal of gastroenterology, 102*(9), 2016-2025. doi:10.1111/j.1572-0241.2007.01411.x

Andreollo, N. A., Santos, E. F. d., Araújo, M. R., & Lopes, L. R. (2012). Idade dos ratos versus idade humana: qual é a relação? *ABCD. Arquivos Brasileiros de Cirurgia Digestiva (São Paulo), 25*, 49-51. Retrieved from http://www.scielo.br/scielo.php?script=sci_arttext&pid=S0102-67202012000100011&nrm=iso

Arora, U., Ananthakrishnan, A. N., Kedia, S., Bopanna, S., Mouli, P. V., Yadav, D. P., . . . Ahuja, V. (2018). Effect of oral tobacco use and smoking on outcomes of Crohn's disease in India. *Journal of Gastroenterology and Hepatology, 33*(1), 134-140. doi:10.1111/jgh.13815

Barker, N. (2014). Adult intestinal stem cells: critical drivers of epithelial homeostasis and regeneration. *Nature Reviews Molecular Cell Biology, 15*(1), 19-33. doi:10.1038/nrm3721

Barnich, N., Carvalho, F. A., Glasser, A.-L., Darcha, C., Jantscheff, P., Allez, M., . . . Darfeuille-Michaud, A. (2007). CEACAM6 acts as a receptor for adherent-invasive E. coli, supporting ileal mucosa colonization in Crohn disease. *The Journal of clinical investigation, 117*(6), 1566-1574. doi:10.1172/JCI30504

Barrett, J. C., Hansoul, S., Nicolae, D. L., Cho, J. H., Duerr, R. H., Rioux, J. D., . . . Daly, M. J. (2008). Genome-wide association defines more than 30 distinct susceptibility loci for Crohn's disease. *Nature genetics, 40*(8), 955-962. doi:10.1038/ng.175

Bayless, T. M., Tokayer, A. Z., Polito, J. M., Quaskey, S. A., Mellits, E. D., & Harris, M. L. (1996). Crohn's disease: Concordance for site and clinical type in affected family members--potential hereditary influences. *Gastroenterology, 111*(3), 573-579. doi:https://doi.org/10.1053/gast.1996.v111.pm8780559

Bernales, S., McDonald, K. L., & Walter, P. (2006). Autophagy Counterbalances Endoplasmic Reticulum Expansion during the Unfolded Protein Response. *PLOS Biology, 4*(12), e423. doi:10.1371/journal.pbio.0040423

Bessone, F. (2010). Non-steroidal anti-inflammatory drugs: What is the actual risk of liver damage? *World Journal of Gastroenterology, 16*(45), 5651-5661. doi:10.3748/wjg.v16.i45.5651

Biancone, L., Calabrese, E., Petruzziello, C., Capanna, A., Zorzi, F., Onali, S., . . . Pallone, F. (2014). A family study of asymptomatic small bowel Crohn's disease. *Dig Liver Dis, 46*(3), 276-278. doi:10.1016/j.dld.2013.11.003

Biedermann, L., Brülisauer, K., Zeitz, J., Frei, P., Scharl, M., Vavricka, S. R., . . . Schuppler, M. (2014). Smoking Cessation Alters Intestinal Microbiota: Insights from Quantitative Investigations on Human Fecal Samples Using FISH. *Inflammatory Bowel Diseases, 20*(9), 1496-1501. doi:10.1097/mib.0000000000000129

Biedermann, L., Zeitz, J., Mwinyi, J., Sutter-Minder, E., Rehman, A., Ott, S. J., . . . Rogler, G. (2013). Smoking cessation induces profound changes in the composition of the intestinal microbiota in humans. *PLOS ONE, 8*(3), e59260-e59260. doi:10.1371/journal.pone.0059260

Bloemendaal, F. M., Becker, M., Koelink, P. J., van der Bilt, J. D., Bemelman, W. A., D'Haens, G. R. A. M., . . . Wildenberg, M. E. (2020). DOP82 Macrophages in Crohn's disease mesentery are predominantly inflammatory and produce calprotectin. *Journal of Crohn's and Colitis, 14*(Supplement_1), S121-S122. doi:10.1093/ecco-jcc/jjz203.121

Boada-Romero, E., Serramito-Gómez, I., Sacristán, M. P., Boone, D. L., Xavier, R. J., & Pimentel-Muiños, F. X. (2016). The T300A Crohn's disease risk polymorphism impairs function of the WD40 domain of ATG16L1. *Nature Communications, 7*(1), 11821. doi:10.1038/ncomms11821

Bolotin, A., Quinquis, B., Sorokin, A., & Ehrlich, S. D. (2005). Clustered regularly interspaced short palindrome repeats (CRISPRs) have spacers of extrachromosomal origin. *Microbiology, 151*(8), 2551-2561. doi:https://doi.org/10.1099/mic.0.28048-0

Brabin, L., & Brabin, B. J. (1992). Parasitic Infections in Women and their Consequences. In J. R. Baker & R. Muller (Eds.), *Advances in Parasitology* (Vol. 31, pp. 1-81): Academic Press.

Büning, C., Durmus, T., Molnar, T., de Jong, D. J., Drenth, J. P. H., Fiedler, T., . . . Witt, H. (2007). A study in three European IBD cohorts confirms that the ATG16L1 c.898A > G (p.Thr300Ala) variant is a susceptibility factor for Crohn's disease. *Journal of Crohn's and Colitis, 1*(2), 70-76. doi:10.1016/j.crohns.2007.08.001

Burgoyne, R. D., & Morgan, A. (2003). Secretory Granule Exocytosis. *Physiological Reviews, 83*(2), 581-632. doi:10.1152/physrev.00031.2002

Cadwell, K., Liu, J. Y., Brown, S. L., Miyoshi, H., Loh, J., Lennerz, J. K., . . . Virgin, H. W. t. (2008). A key role for autophagy and the autophagy gene Atg16l1 in mouse and human intestinal Paneth cells. *Nature, 456*(7219), 259-263. doi:10.1038/nature07416

Cadwell, K., Patel, K. K., Maloney, N. S., Liu, T.-C., Ng, A. C. Y., Storer, C. E., . . . Virgin, H. W. (2010). Virus-plus-susceptibility gene interaction determines Crohn's disease gene Atg16L1 phenotypes in intestine. *Cell, 141*(7), 1135-1145. doi:10.1016/j.cell.2010.05.009

Chong, J., Soufan, O., Li, C., Caraus, I., Li, S., Bourque, G., . . . Xia, J. (2018). MetaboAnalyst 4.0: towards more transparent and integrative metabolomics analysis. *Nucleic acids research, 46*(W1), W486-W494. doi:10.1093/nar/gky310

Chong, J., Wishart, D. S., & Xia, J. (2019). Using MetaboAnalyst 4.0 for Comprehensive and Integrative Metabolomics Data Analysis. *Current Protocols in Bioinformatics, 68*(1), e86. doi:10.1002/cpbi.86

Cleynen, I., Boucher, G., Jostins, L., Schumm, L. P., Zeissig, S., Ahmad, T., . . . Lees, C. W. (2016). Inherited determinants of Crohn's disease and ulcerative colitis phenotypes: a genetic association study. *The Lancet, 387*(10014), 156-167. doi:10.1016/S0140-6736(15)00465-1

Cleynen, I., González, J. R., Figueroa, C., Franke, A., McGovern, D., Bortlík, M., . . . Sans, M. (2013). Genetic factors conferring an increased susceptibility to develop Crohn's disease also influence disease phenotype: results from the IBDchip European Project. *Gut, 62*(11), 1556. doi:10.1136/gutjnl-2011-300777

Cohn, Z. A., & Hirsch, J. G. (1960). The isolation and properties of the specific cytoplasmic granules of rabbit polymorphonuclear leucocytes. *The Journal of experimental medicine, 112*(6), 983-1004. doi:10.1084/jem.112.6.983

Conway, K. L., Kuballa, P., Song, J.-H., Patel, K. K., Castoreno, A. B., Yilmaz, O. H., . . . Xavier, R. J. (2013). Atg16l1 is required for autophagy in intestinal epithelial cells and protection of mice from Salmonella infection. *Gastroenterology, 145*(6), 1347-1357. doi:10.1053/j.gastro.2013.08.035

Coornaert, B., Carpentier, I., & Beyaert, R. (2009). A20: central gatekeeper in inflammation and immunity. *The Journal of biological chemistry, 284*(13), 8217-8221. doi:10.1074/jbc.R800032200

Cornish, J. A., Tan, E., Simillis, C., Clark, S. K., Teare, J., & Tekkis, P. P. (2008). The risk of oral contraceptives in the etiology of inflammatory bowel disease: a meta-analysis. *The American journal of gastroenterology, 103*(9), 2394-2400. doi:10.1111/j.1572-0241.2008.02064.x

Croucher, P. J. P., Mascheretti, S., Hampe, J., Huse, K., Frenzel, H., Stoll, M., . . . Schreiber, S. (2003). Haplotype structure and association to Crohn's disease of CARD15 mutations in two ethnically divergent populations. *European Journal of Human Genetics, 11*(1), 6-16. doi:10.1038/sj.ejhg.5200897

de Lange, K. M., Moutsianas, L., Lee, J. C., Lamb, C. A., Luo, Y., Kennedy, N. A., . . . Barrett, J. C. (2017). Genome-wide association study implicates immune activation of multiple integrin genes in inflammatory bowel disease. *Nature genetics, 49*(2), 256-261. doi:10.1038/ng.3760

du Toit, A., Hofmeyr, J.-H. S., Gniadek, T. J., & Loos, B. (2018). Measuring autophagosome flux. *Autophagy, 14*(6), 1060-1071. doi:10.1080/15548627.2018.1469590

Elderman, M., Hugenholtz, F., Belzer, C., Boekschoten, M., van Beek, A., de Haan, B., . . . Faas, M. (2018). Sex and strain dependent differences in mucosal immunology and microbiota composition in mice. *Biology of sex differences, 9*(1), 26-26. doi:10.1186/s13293-018-0186-6

Elson, C. O., Cong, Y., McCracken, V. J., Dimmitt, R. A., Lorenz, R. G., & Weaver, C. T. (2005). Experimental models of inflammatory bowel disease reveal innate, adaptive, and regulatory mechanisms of host dialogue with the microbiota. *Immunological Reviews, 206*(1), 260-276. doi:10.1111/j.0105-2896.2005.00291.x

Ericsson, A. C., Davis, J. W., Spollen, W., Bivens, N., Givan, S., Hagan, C. E., . . . Franklin, C. L. (2015). Effects of Vendor and Genetic Background on the Composition of the Fecal Microbiota of Inbred Mice. *PLOS ONE, 10*(2), e0116704. doi:10.1371/journal.pone.0116704

Fabia, R., Ar'rajab, A., Johansson, M. L., Willén, R., Andersson, R., Molin, G., & Bengmark, S. (1993). The effect of exogenous administration of lactobacillus reuteri r2LC and oat fiber on acetic acid-induced colitis in the rat. *Scandinavian Journal of Gastroenterology, 28*(2), 155-162. doi:10.3109/00365529309096063

Fransen, F., van Beek, A. A., Borghuis, T., Meijer, B., Hugenholtz, F., van der Gaast-de Jongh, C., . . . de Vos, P. (2017). The Impact of Gut Microbiota on Gender-Specific Differences in Immunity. *Frontiers in immunology, 8*, 754-754. doi:10.3389/fimmu.2017.00754

Fujita, N., Itoh, T., Omori, H., Fukuda, M., Noda, T., & Yoshimori, T. (2008). The Atg16L complex specifies the site of LC3 lipidation for membrane biogenesis in autophagy. *Molecular biology of the cell, 19*(5), 2092-2100. doi:10.1091/mbc.e07-12-1257

Fujita, N., Saitoh, T., Kageyama, S., Akira, S., Noda, T., & Yoshimori, T. (2009). Differential Involvement of Atg16L1 in Crohn Disease and Canonical Autophagy: ANALYSIS OF THE ORGANIZATION OF THE Atg16L1 COMPLEX IN FIBROBLASTS. *Journal of Biological Chemistry, 284*(47), 32602-32609. doi:10.1074/jbc.M109.037671

Fukuda, M., & Itoh, T. (2008). Direct link between Atg protein and small GTPase Rab: Atg16L functions as a potential Rab33 effector in mammals. *Autophagy, 4*(6), 824-826. doi:10.4161/auto.6542

Fuss, I. J., Neurath, M., Boirivant, M., Klein, J. S., de la Motte, C., Strong, S. A., . . . Strober, W. (1996). Disparate CD4+ lamina propria (LP) lymphokine secretion profiles in inflammatory bowel disease. Crohn's disease LP cells manifest increased secretion of IFN-gamma, whereas ulcerative colitis LP cells manifest increased secretion of IL-5. *The Journal of Immunology, 157*(3), 1261-1270. Retrieved from https://www.jimmunol.org/content/jimmunol/157/3/1261.full.pdf

Gao, P., Liu, H., Huang, H., Zhang, Q., Strober, W., & Zhang, F. (2017). The Inflammatory Bowel Disease–Associated Autophagy Gene Atg16L1T300A Acts as a Dominant Negative Variant in Mice. *The Journal of Immunology*, 1502652. doi:10.4049/jimmunol.1502652

Garneau, J. E., Dupuis, M.-È., Villion, M., Romero, D. A., Barrangou, R., Boyaval, P., . . . Moineau, S. (2010). The CRISPR/Cas bacterial immune system cleaves bacteriophage and plasmid DNA. *Nature, 468*(7320), 67-71. doi:10.1038/nature09523

Gasiunas, G., Barrangou, R., Horvath, P., & Siksnys, V. (2012). Cas9–crRNA ribonucleoprotein complex mediates specific DNA cleavage for adaptive immunity in bacteria. *Proceedings of the National Academy of Sciences, 109*(39), E2579-E2586. doi:10.1073/pnas.1208507109

Gionchetti, P., Rizzello, F., Helwig, U., Venturi, A., Lammers, K. M., Brigidi, P., . . . Campieri, M. (2003). Prophylaxis of pouchitis onset with probiotic therapy: a double-blind, placebo-controlled trial. *Gastroenterology, 124*(5), 1202-1209. doi:https://doi.org/10.1016/S0016-5085(03)00171-9

Glick, D., Barth, S., & Macleod, K. F. (2010). Autophagy: cellular and molecular mechanisms. *The Journal of pathology, 221*(1), 3-12. doi:10.1002/path.2697

Grossman, C. (1989). Possible underlying mechanisms of sexual dimorphism in the immune response, fact and hypothesis. *Journal of Steroid Biochemistry, 34*(1), 241-251. doi:https://doi.org/10.1016/0022-4731(89)90088-5

Halfvarson, J., Bodin, L., Tysk, C., Lindberg, E., & Järnerot, G. (2003). Inflammatory bowel disease in a Swedish twin cohort: a long-term follow-up of concordance and clinical characteristics. *Gastroenterology, 124*(7), 1767-1773. doi:https://doi.org/10.1016/S0016-5085(03)00385-8

Halme, L., Paavola-Sakki, P., Turunen, U., Lappalainen, M., Farkkila, M., & Kontula, K. (2006). Family and twin studies in inflammatory bowel disease. *World Journal of Gastroenterology, 12*(23), 3668-3672. doi:10.3748/wjg.v12.i23.3668

Hampe, J., Franke, A., Rosenstiel, P., Till, A., Teuber, M., Huse, K., . . . Schreiber, S. (2007). A genome-wide association scan of nonsynonymous SNPs identifies a susceptibility variant for Crohn disease in ATG16L1. *Nature genetics, 39*(2), 207-211. doi:10.1038/ng1954

He, C., & Klionsky, D. J. (2009). Regulation Mechanisms and Signaling Pathways of Autophagy. *Annual Review of Genetics, 43*(1), 67-93. doi:10.1146/annurev-genet-102808-114910

Henke, M. T., Kenny, D. J., Cassilly, C. D., Vlamakis, H., Xavier, R. J., & Clardy, J. (2019). Ruminococcus gnavus, a member of the human gut microbiome associated with Crohn's disease, produces an inflammatory polysaccharide. *Proceedings of the National Academy of Sciences, 116*(26), 12672-12677. doi:10.1073/pnas.1904099116

Hirsch, J. G., & Cohn, Z. A. (1960). Degranulation of polymorphonuclear leucocytes following phagocytosis of microorganisms. *The Journal of experimental medicine, 112*(6), 1005-1014. doi:10.1084/jem.112.6.1005

Hwang, S., Maloney, N. S., Bruinsma, M. W., Goel, G., Duan, E., Zhang, L., . . . Virgin, H. W. (2012). Nondegradative role of Atg5-Atg12/ Atg16L1 autophagy protein complex in antiviral activity of interferon gamma. *Cell Host Microbe, 11*(4), 397-409. doi:10.1016/j.chom.2012.03.002

Ingersoll, M. A. (2017). Sex differences shape the response to infectious diseases. *PLoS Pathog, 13*(12), e1006688. doi:10.1371/journal.ppat.1006688

ISHIKURA, T., KANAI, T., URAUSHIHARA, K., IIYAMA, R., MAKITA, S., TOTSUKA, T., . . . WATANABE, M. (2003). Interleukin-18 overproduction exacerbates the development of colitis with markedly infiltrated macrophages in interleukin-18 transgenic mice. *Journal of Gastroenterology and Hepatology, 18*(8), 960-969. doi:10.1046/j.1440-1746.2003.03097.x

Ishino, Y., Krupovic, M., & Forterre, P. (2018). History of CRISPR-Cas from Encounter with a Mysterious Repeated Sequence to Genome Editing Technology. *Journal of bacteriology, 200*(7), e00580-00517. doi:10.1128/jb.00580-17

Ishino, Y., Shinagawa, H., Makino, K., Amemura, M., & Nakata, A. (1987). Nucleotide sequence of the iap gene, responsible for alkaline phosphatase isozyme conversion in Escherichia coli, and identification of the gene product. *Journal of bacteriology, 169*(12), 5429-5433. doi:10.1128/jb.169.12.5429-5433.1987

Jairath, V., & Feagan, B. G. (2020). Global burden of inflammatory bowel disease. *The Lancet Gastroenterology & Hepatology, 5*(1), 2-3. doi:10.1016/s2468-1253(19)30358-9

Jiang, T., Qin, B., He, J., Lin, S., & Ding, S. (2013). Three isoforms of the Atg16L1 protein contribute different autophagic properties. *Molecular and cellular biochemistry, 378*(1-2), 257-266. doi:10.1007/s11010-013-1616-8

Jinek, M., Chylinski, K., Fonfara, I., Hauer, M., Doudna, J. A., & Charpentier, E. (2012). A programmable dual-RNA-guided DNA endonuclease in adaptive bacterial immunity. *Science (New York, N.Y.), 337*(6096), 816-821. doi:10.1126/science.1225829

Johnson, M., Zaretskaya, I., Raytselis, Y., Merezhuk, Y., McGinnis, S., & Madden, T. L. (2008). NCBI BLAST: a better web interface. *Nucleic acids research, 36*(Web Server issue), W5-W9. doi:10.1093/nar/gkn201

Kamada, N., Hisamatsu, T., Okamoto, S., Chinen, H., Kobayashi, T., Sato, T., . . . Hibi, T. (2008). Unique CD14+ intestinal macrophages contribute to the pathogenesis of Crohn disease via IL-23/IFN-γ axis. *The Journal of clinical investigation, 118*(6), 2269-2280. doi:10.1172/JCI34610

Kaneko, T. (2018). Reproductive technologies for the generation and maintenance of valuable animal strains. *The Journal of reproduction and development, 64*(3), 209-215. doi:10.1262/jrd.2018-035

Kaplan, G. G., Hubbard, J., Korzenik, J., Sands, B. E., Panaccione, R., Ghosh, S., . . . Villeneuve, P. J. (2010). The inflammatory bowel diseases and ambient air pollution: a novel association. *The American journal of gastroenterology, 105*(11), 2412-2419. doi:10.1038/ajg.2010.252

Karginov, F. V., & Hannon, G. J. (2010). The CRISPR system: small RNA-guided defense in bacteria and archaea. *Molecular cell, 37*(1), 7-19. doi:10.1016/j.molcel.2009.12.033

Khor, B., Gardet, A., & Xavier, R. J. (2011). Genetics and pathogenesis of inflammatory bowel disease. *Nature, 474*(7351), 307-317. doi:10.1038/nature10209

Kim, Y. S., Unno, T., Kim, B. Y., & Park, M. S. (2020). Sex Differences in Gut Microbiota. *The world journal of men's health, 38*(1), 48-60. doi:10.5534/wjmh.190009

Klein, A., & Eliakim, R. (2010). Non Steroidal Anti-Inflammatory Drugs and Inflammatory Bowel Disease. *Pharmaceuticals (Basel, Switzerland), 3*(4), 1084-1092. doi:10.3390/ph3041084

Klein, S. L. (2000). The effects of hormones on sex differences in infection: from genes to behavior. *Neuroscience & Biobehavioral Reviews, 24*(6), 627-638. doi:https://doi.org/10.1016/S0149-7634(00)00027-0

Knights, D., Silverberg, M. S., Weersma, R. K., Gevers, D., Dijkstra, G., Huang, H., . . . Xavier, R. J. (2014). Complex host genetics influence the microbiome in inflammatory bowel disease. *Genome Medicine, 6*(12), 107. doi:10.1186/s13073-014-0107-1

Kuballa, P., Huett, A., Rioux, J. D., Daly, M. J., & Xavier, R. J. (2008). Impaired autophagy of an intracellular pathogen induced by a Crohn's disease associated ATG16L1 variant. *PLOS ONE, 3*(10), e3391. doi:10.1371/journal.pone.0003391

Kuczynski, J., Stombaugh, J., Walters, W., González, A., Caporaso, J., & Knight, R. (2011). Using QIIME to analyze 16S rRNA gene sequences from microbial communities. *Current protocols in bioinformatics / editoral board, Andreas D. Baxevanis ... [et al.], Chapter 10,* Unit 10.17. doi:10.1002/0471250953.bi1007s36

Lakatos, P. L., Szamosi, T., & Lakatos, L. (2007). Smoking in inflammatory bowel diseases: good, bad or ugly? *World Journal of Gastroenterology, 13*(46), 6134-6139. doi:10.3748/wjg.v13.i46.6134

Lanas, A., & Chan, F. K. L. (2017). Peptic ulcer disease. *Lancet, 390*(10094), 613-624. doi:10.1016/s0140-6736(16)32404-7

Lassen, K. G., Kuballa, P., Conway, K. L., Patel, K. K., Becker, C. E., Peloquin, J. M., . . . Xavier, R. J. (2014). Atg16L1 T300A variant decreases selective autophagy resulting in altered cytokine signaling and decreased antibacterial defense. *Proceedings of the National Academy of Sciences of the United States of America, 111*(21), 7741-7746. doi:10.1073/pnas.1407001111

Lassen, K. G., & Xavier, R. J. (2014). An alteration in ATG16L1 stability in Crohn disease. *Autophagy, 10*(10), 1858-1860. doi:10.4161/auto.29963

Lavoie, S., Conway, K. L., Lassen, K. G., Jijon, H. B., Pan, H., Chun, E., . . . Xavier, R. J. (2019). The Crohn's disease polymorphism, ATG16L1 T300A, alters the gut microbiota and enhances the local Th1/Th17 response. *Elife, 8*. doi:10.7554/eLife.39982

Levine, B., & Klionsky, D. J. (2004). Development by Self-Digestion: Molecular Mechanisms and Biological Functions of Autophagy. *Developmental Cell, 6*(4), 463-477. doi:https://doi.org/10.1016/S1534-5807(04)00099-1

Levine, B., & Kroemer, G. (2008). Autophagy in the Pathogenesis of Disease. *Cell, 132*(1), 27-42. doi:https://doi.org/10.1016/j.cell.2007.12.018

Li, J., Chen, Z., Stang, M. T., & Gao, W. (2017). Transiently expressed ATG16L1 inhibits autophagosome biogenesis and aberrantly targets RAB11-positive recycling endosomes. *Autophagy, 13*(2), 345-358. doi:10.1080/15548627.2016.1256521

Lino, C. A., Harper, J. C., Carney, J. P., & Timlin, J. A. (2018). Delivering CRISPR: a review of the challenges and approaches. *Drug delivery, 25*(1), 1234-1257. doi:10.1080/10717544.2018.1474964

Liu, C., Wang, H., Shang, Y., Liu, W., Song, Z., Zhao, H., . . . Li, W. (2016). Autophagy is required for ectoplasmic specialization assembly in sertoli cells. *Autophagy, 12*(5), 814-832. doi:10.1080/15548627.2016.1159377

Liu, T.-C., Kern, J. T., VanDussen, K. L., Xiong, S., Kaiko, G. E., Wilen, C. B., . . . Stappenbeck, T. S. (2018). Interaction between smoking and ATG16L1T300A triggers Paneth cell defects in Crohn's disease. *The Journal of clinical investigation, 128*(11), 5110-5122. doi:10.1172/JCI120453

Long, M. D., Kappelman, M. D., Martin, C. F., Chen, W., Anton, K., & Sandler, R. S. (2016). Role of Nonsteroidal Anti-Inflammatory Drugs in Exacerbations of Inflammatory Bowel Disease. *Journal of clinical gastroenterology, 50*(2), 152-156. doi:10.1097/MCG.0000000000000421

Luo, Y., de Lange, K. M., Jostins, L., Moutsianas, L., Randall, J., Kennedy, N. A., . . . Anderson, C. A. (2017). Exploring the genetic architecture of inflammatory bowel disease by whole-genome sequencing identifies association at ADCY7. *Nature genetics, 49*(2), 186-192. doi:10.1038/ng.3761

M. Orholm, V. B. T. I. A. S. L. P. R. K. O. K. (2000). Concordance of Inflammatory Bowel Disease among Danish Twins: Results of a Nationwide Study. *Scandinavian Journal of Gastroenterology, 35*(10), 1075-1081. doi:10.1080/003655200451207

Macleod, M., & Mohan, S. (2019). Reproducibility and Rigor in Animal-Based Research. *ILAR Journal, 60*(1), 17-23. doi:10.1093/ilar/ilz015

Madsen, K. L., Doyle, J. S., Jewell, L. D., Tavernini, M. M., & Fedorak, R. N. (1999). Lactobacillus species prevents colitis in interleukin 10 gene–deficient mice.

Gastroenterology, 116(5), 1107-1114. doi:https://doi.org/10.1016/S0016-5085(99)70013-2

Maeda, S., Hsu, L.-C., Liu, H., Bankston, L. A., Iimura, M., Kagnoff, M. F., . . . Karin, M. (2005). Nod2 Mutation in Crohn's Disease Potentiates NF-κB Activity and IL-1ß Processing. *Science, 307*(5710), 734-738. doi:10.1126/science.1103685

Magoč, T., & Salzberg, S. L. (2011). FLASH: fast length adjustment of short reads to improve genome assemblies. *Bioinformatics (Oxford, England), 27*(21), 2957-2963. doi:10.1093/bioinformatics/btr507

Makarova, K. S., Grishin, N. V., Shabalina, S. A., Wolf, Y. I., & Koonin, E. V. (2006). A putative RNA-interference-based immune system in prokaryotes: computational analysis of the predicted enzymatic machinery, functional analogies with eukaryotic RNAi, and hypothetical mechanisms of action. *Biology direct, 1*, 7-7. doi:10.1186/1745-6150-1-7

Marees, A. T., de Kluiver, H., Stringer, S., Vorspan, F., Curis, E., Marie-Claire, C., & Derks, E. M. (2018). A tutorial on conducting genome-wide association studies: Quality control and statistical analysis. *International journal of methods in psychiatric research, 27*(2), e1608-e1608. doi:10.1002/mpr.1608

Mariño, G., & López-Otín, C. (2004). Autophagy: molecular mechanisms, physiological functions and relevance in human pathology. *Cell Mol Life Sci, 61*(12), 1439-1454. doi:10.1007/s00018-004-4012-4

Markle, J. G., & Fish, E. N. (2014). SeXX matters in immunity. *Trends in immunology, 35*(3), 97-104. doi:10.1016/j.it.2013.10.006

Matsuoka, K., Inoue, N., Sato, T., Okamoto, S., Hisamatsu, T., Kishi, Y., . . . Hibi, T. (2004). T-bet upregulation and subsequent interleukin 12 stimulation are essential for induction of Th1 mediated immunopathology in Crohn's disease. *Gut, 53*(9), 1303-1308. doi:10.1136/gut.2003.024190

Matsuzawa, Y., & Cadwell, K. (2019). Autophagy Protein ATG16L1 prevents necroptosis in the intestinal epithelium. *Gastroenterology*. Retrieved from https://watermark.silverchair.com/izy393.126.pdf?token=AQECAHi208BE49Ooan9kkhW_Ercy7Dm3ZL_9Cf3qfKAc485ysgAAAp4wggKaBgkqhkiG9w0BBwaggKLMIIChwIBADCCAoAGCSqGSIb3DQEHATAeBglghkgBZQMEAS4wEQQMCeIutTPRMJS8k3tsAgEQgIICUc_WO40Ajl9PBfjx61DdliNbvRCYmDeRpQwe9Nxcn0RmVSPWmQAD8eO7P-JaG3C-UO_p92aC94dpKviogmjN7vjHBZWqlb50Ey0_2jwbQSs3WVnh8elM6b_ogxNsHFTfGBCsfnFznvQ_BI25hOL6k7NOTjFElzih_qS7MVVsU5lYKWBR-PzSZ2yeS2O4IAWMwGxOWU020Zw3Xh0nwi7Lekds81mFgeLjp8ph1GrplZmdq05DsNVEleDlr92KPrvhOzktFUigeSlxeVbT5yFAtkOZWSMBCNoj2dNRbXsi-

ZA8mo5n8clR0Pt4kRVW7-nqhzSO-ytqY66tHfa0J8PNic0AbBYd3PSFH0V41Kyz8bLaoIl4zM3NfyG1wKyzXCxnnJJYsk2kWXkVqUzzRFBWvCZYvMENDWIhI2l__JTAG8yqF4_y5uD8L-M_H7cRzq-M82-nZqBlTq4Kui1dB6kCLjFv95IT7KXBQq-qjfFbg9EmnjS1EP6ud04OVDrD57A3TJhLJHhiVZMeEffu-E454vDHQt-uHQnc6J4m9fEL8vpoNNx8VohdMmOMdb3XVCoNqBAPgOKSDNi2b0h_nxxHLFRtX2ZsZE0dD7c8nQapc4ZKPfndsEs-HKBBN05jH7_PQXv02telEuIhrwMpk9mNrK_BkLBL0b-Y52QCJ6kCrW3ck2uOzwsprS5BfZ5vtFkosOQu2M87RSNpiGHJmDwGVMh9oEGOQ0thM6Fxrrgs7M0T7HHK93T7heDUwUpMfnE6vBtNjbVfz-Dy-dcuVtIZNd3e

McGovern, D. P., Kugathasan, S., & Cho, J. H. (2015). Genetics of Inflammatory Bowel Diseases. *Gastroenterology*, *149*(5), 1163-1176 e1162. doi:10.1053/j.gastro.2015.08.001

Messer, J. S., Murphy, S. F., Logsdon, M. F., Lodolce, J. P., Grimm, W. A., Bartulis, S. J., . . . Boone, D. L. (2013). The Crohn's disease: associated ATG16L1 variant and Salmonella invasion. *BMJ Open*, *3*(6), e002790. doi:10.1136/bmjopen-2013-002790

Metwaly, A. (2019). *Functional Characterization of Human Gut Microbiota in Inflammatory Bowel Disease Patients using Gnotobiotic Humanized Mice.* (PhD PhD). Technische Universität München, http://mediatum.ub.tum.de/?id=1488691.

Michielan, A., & D'Incà, R. (2015). Intestinal Permeability in Inflammatory Bowel Disease: Pathogenesis, Clinical Evaluation, and Therapy of Leaky Gut. *Mediators of inflammation, 2015*, 628157-628157. doi:10.1155/2015/628157

Miyoshi, J., Leone, V., Nobutani, K., Musch, M. W., Martinez-Guryn, K., Wang, Y., . . . Chang, E. B. (2018). Minimizing confounders and increasing data quality in murine models for studies of the gut microbiome. *PeerJ*, *6*, e5166-e5166. doi:10.7717/peerj.5166

Miyoshi, K. (1995). Penetration in vitro of naturally ovulated rat eggs and the development of eggs in a chamically defind medium. *J. Mamm Ova Res., 12*, 35-39. Retrieved from https://ci.nii.ac.jp/naid/80008208221/en/

Mizushima, N., Kuma, A., Kobayashi, Y., Yamamoto, A., Matsubae, M., Takao, T., . . . Yoshimori, T. (2003). Mouse Apg16L, a novel WD-repeat protein, targets to the autophagic isolation membrane with the Apg12-Apg5 conjugate. *Journal of Cell Science, 116*(9), 1679-1688. doi:10.1242/jcs.00381

Mojica, F. J. M., Díez-Villaseñor, C. s., García-Martínez, J., & Soria, E. (2005). Intervening Sequences of Regularly Spaced Prokaryotic Repeats Derive from Foreign Genetic Elements. *Journal of Molecular Evolution, 60*(2), 174-182. doi:10.1007/s00239-004-0046-3

Mojica, F. J. M., Juez, G., & Rodriguez-Valera, F. (1993). Transcription at different salinities of Haloferax mediterranei sequences adjacent to partially modified PstI sites. *Molecular Microbiology, 9*(3), 613-621. doi:10.1111/j.1365-2958.1993.tb01721.x

Moller, F. T., Andersen, V., Wohlfahrt, J., & Jess, T. (2015). Familial Risk of Inflammatory Bowel Disease: A Population-Based Cohort Study 1977–2011. *American Journal of Gastroenterology, 110*(4), 564-571. doi:10.1038/ajg.2015.50

Moolenbeek, C., & Ruitenberg, E. J. (1981). The 'Swiss roll': a simple technique for histological studies of the rodent intestine. *Laboratory Animals, 15*(1), 57-60. doi:10.1258/002367781780958577

Murthy, A., Li, Y., Peng, I., Reichelt, M., Katakam, A. K., Noubade, R., . . . van Lookeren Campagne, M. (2014). A Crohn's disease variant in Atg16l1 enhances its degradation by caspase 3. *Nature, 506*(7489), 456-462. doi:10.1038/nature13044

Nagao-Kitamoto, H., Shreiner, A. B., Gillilland, M. G., 3rd, Kitamoto, S., Ishii, C., Hirayama, A., . . . Kamada, N. (2016). Functional Characterization of Inflammatory Bowel Disease-Associated Gut Dysbiosis in Gnotobiotic Mice. *Cellular and molecular gastroenterology and hepatology, 2*(4), 468-481. doi:10.1016/j.jcmgh.2016.02.003

Nagpal, R., Wang, S., Solberg Woods, L. C., Seshie, O., Chung, S. T., Shively, C. A., . . . Yadav, H. (2018). Comparative Microbiome Signatures and Short-Chain Fatty Acids in Mouse, Rat, Non-human Primate, and Human Feces. *Frontiers in Microbiology, 9*(2897). doi:10.3389/fmicb.2018.02897

Nakahira, K., Haspel, J. A., Rathinam, V. A. K., Lee, S.-J., Dolinay, T., Lam, H. C., . . . Choi, A. M. K. (2011). Autophagy proteins regulate innate immune responses by inhibiting the release of mitochondrial DNA mediated by the NALP3 inflammasome. *Nature Immunology, 12*(3), 222-230. doi:10.1038/ni.1980

Ng, S. C., Tang, W., Ching, J. Y., Wong, M., Chow, C. M., Hui, A. J., . . . Chan, F. K. L. (2013). Incidence and Phenotype of Inflammatory Bowel Disease Based on Results From the Asia-Pacific Crohn's and Colitis Epidemiology Study. *Gastroenterology, 145*(1), 158-165.e152. doi:https://doi.org/10.1053/j.gastro.2013.04.007

O. Hammer, D. A.T. Harper, & Ryan, P. D. (2001). PAST: Paleontological Statistics Software Package For Education and Data Analysis. *Palaeontologia Electronia, 4*(1).

Ogata, M., Hino, S.-i., Saito, A., Morikawa, K., Kondo, S., Kanemoto, S., . . . Imaizumi, K. (2006). Autophagy Is Activated for Cell Survival after Endoplasmic Reticulum

Stress. *Molecular and Cellular Biology, 26*(24), 9220-9231. doi:10.1128/mcb.01453-06

Panaccione, R. (2013). Mechanisms of inflammatory bowel disease. *Gastroenterology & hepatology, 9*(8), 529-532. Retrieved from https://pubmed.ncbi.nlm.nih.gov/24719603 https://www.ncbi.nlm.nih.gov/pmc/articles/PMC3980998/

Patel, K. K., & Stappenbeck, T. S. (2013). Autophagy and intestinal homeostasis. *Annual review of physiology, 75*, 241-262. doi:10.1146/annurev-physiol-030212-183658

Peeters, M., Nevens, H., Baert, F., Hiele, M., de Meyer, A. M., Vlietinck, R., & Rutgeerts, P. (1996). Familial aggregation in Crohn's disease: Increased age-adjusted risk and concordance in clinical characteristics. *Gastroenterology, 111*(3), 597-603. doi:https://doi.org/10.1053/gast.1996.v111.pm8780562

Pyo, J. O., Nah, J., & Jung, Y. K. (2012). Molecules and their functions in autophagy. *Experimental & molecular medicine, 44*(2), 73-80. doi:10.3858/emm.2012.44.2.029

Qian, M., Fang, X., & Wang, X. (2017). Autophagy and inflammation. *Clinical and translational medicine, 6*(1), 24-24. doi:10.1186/s40169-017-0154-5

Quast, C., Pruesse, E., Yilmaz, P., Gerken, J., Schweer, T., Yarza, P., . . . Glöckner, F. O. (2013). The SILVA ribosomal RNA gene database project: improved data processing and web-based tools. *Nucleic acids research, 41*(Database issue), D590-D596. doi:10.1093/nar/gks1219

Quezada, S. M., Steinberger, E. K., & Cross, R. K. (2013). Association of age at diagnosis and Crohn's disease phenotype. *Age and ageing, 42*(1), 102-106. doi:10.1093/ageing/afs107

Rebelo Gomes, E., Geraldes, L., Gaspar, Â., Malheiro, D., Cadinha, S., Abreu, C., . . . Faria, E. (2016). Hypersensitivity Reactions to Nonsteroidal Anti-Inflammatory Drugs among Adults: Clinical Features and Risk Factors for Diagnosis Confirmation. *International Archives of Allergy and Immunology, 171*(3-4), 269-275. doi:10.1159/000452627

Riordan, A. M., Ruxton, C. H. S., & Hunter, J. O. (1998). A review of associations between Crohn's disease and consumption of sugars. *European Journal of Clinical Nutrition, 52*(4), 229-238. doi:10.1038/sj.ejcn.1600556

Rioux, J. D., Xavier, R. J., Taylor, K. D., Silverberg, M. S., Goyette, P., Huett, A., . . . Brant, S. R. (2007). Genome-wide association study identifies new susceptibility loci for Crohn disease and implicates autophagy in disease pathogenesis. *Nature genetics, 39*(5), 596-604. doi:10.1038/ng2032

Rogler, G., Hausmann, M., Vogl, D., Aschenbrenner, E., Andus, T., Falk, W., . . . Gross, V. (1998). Isolation and phenotypic characterization of colonic macrophages. *Clinical and experimental immunology, 112*(2), 205-215. doi:10.1046/j.1365-2249.1998.00557.x

Saitoh, T., Fujita, N., Jang, M. H., Uematsu, S., Yang, B.-G., Satoh, T., . . . Akira, S. (2008). Loss of the autophagy protein Atg16L1 enhances endotoxin-induced IL-1β production. *Nature, 456*(7219), 264-268. doi:10.1038/nature07383

Salem, M., Ammitzboell, M., Nys, K., Seidelin, J. B., & Nielsen, O. H. (2015). ATG16L1: A multifunctional susceptibility factor in Crohn disease. *Autophagy, 11*(4), 585-594. doi:10.1080/15548627.2015.1017187

Satsangi, J., Rosenberg, W. M. C., & Jewell, D. P. (1994). The prevalence of inflammatory bowel disease in relatives of patients with Crohn's disease. *European Journal of Gastroenterology & Hepatology, 6*(5), 413-416. Retrieved from https://journals.lww.com/eurojgh/Fulltext/1994/05000/The_prevalence_of_inflammatory_bowel_disease_in.7.aspx

Schultz, M., Veltkamp, C., Dieleman, L. A., Grenther, W. B., Wyrick, P. B., Tonkonogy, S. L., & Balfour Sartor, R. (2002). Lactobacillus plantarum 299V in the treatment and prevention of spontaneous colitis in interleukin-10-deficient mice. *Inflammatory Bowel Diseases, 8*(2), 71-80. doi:10.1097/00054725-200203000-00001

Sengupta, P. (2013). The Laboratory Rat: Relating Its Age With Human's. *International journal of preventive medicine, 4*(6), 624-630. Retrieved from https://pubmed.ncbi.nlm.nih.gov/23930179 https://www.ncbi.nlm.nih.gov/pmc/articles/PMC3733029/

Shi, C.-S., Shenderov, K., Huang, N.-N., Kabat, J., Abu-Asab, M., Fitzgerald, K. A., . . . Kehrl, J. H. (2012). Activation of autophagy by inflammatory signals limits IL-1β production by targeting ubiquitinated inflammasomes for destruction. *Nature Immunology, 13*(3), 255-263. doi:10.1038/ni.2215

Silverberg, M. S., Duerr, R. H., Brant, S. R., Bromfield, G., Datta, L. W., Jani, N., . . . of the, N. I. B. D. G. C. (2007). Refined genomic localization and ethnic differences observed for the IBD5 association with Crohn's disease. *European Journal of Human Genetics, 15*(3), 328-335. doi:10.1038/sj.ejhg.5201756

Slowicka, K., Serramito-Gómez, I., Boada-Romero, E., Martens, A., Sze, M., Petta, I., . . . van Loo, G. (2019). Physical and functional interaction between A20 and ATG16L1-WD40 domain in the control of intestinal homeostasis. *Nature Communications, 10*(1), 1834. doi:10.1038/s41467-019-09667-z

Smythies, L. E., Sellers, M., Clements, R. H., Mosteller-Barnum, M., Meng, G., Benjamin, W. H., . . . Smith, P. D. (2005). Human intestinal macrophages display profound inflammatory anergy despite avid phagocytic and bacteriocidal activity. *The Journal of clinical investigation, 115*(1), 66-75. doi:10.1172/JCI19229

Sutherland, L., Singleton, J., Sessions, J., Hanauer, S., Krawitt, E., Rankin, G., . . . et al. (1991). Double blind, placebo controlled trial of metronidazole in Crohn's disease. *Gut, 32*(9), 1071-1075. doi:10.1136/gut.32.9.1071

Symington, L. S., & Gautier, J. (2011). Double-Strand Break End Resection and Repair Pathway Choice. *Annual Review of Genetics, 45*(1), 247-271. doi:10.1146/annurev-genet-110410-132435

Tanida, I., Ueno, T., & Kominami, E. (2008). LC3 and Autophagy. In V. Deretic (Ed.), *Autophagosome and Phagosome* (pp. 77-88). Totowa, NJ: Humana Press.

Thompson, N. P., Driscoll, R., Pounder, R. E., & Wakefield, A. J. (1996). Genetics versus environment in inflammatory bowel disease: results of a British twin study. *BMJ (Clinical research ed.), 312*(7023), 95-96. doi:10.1136/bmj.312.7023.95

Travassos, L. H., Carneiro, L. A. M., Ramjeet, M., Hussey, S., Kim, Y.-G., Magalhães, J. G., . . . Philpott, D. J. (2010). Nod1 and Nod2 direct autophagy by recruiting ATG16L1 to the plasma membrane at the site of bacterial entry. *Nature Immunology, 11*(1), 55-62. doi:10.1038/ni.1823

Tysk, C., Lindberg, E., Järnerot, G., & Flodérus-Myrhed, B. (1988). Ulcerative colitis and Crohn's disease in an unselected population of monozygotic and dizygotic twins. A study of heritability and the influence of smoking. *Gut, 29*(7), 990-996. doi:10.1136/gut.29.7.990

Vedamurthy, A., & Ananthakrishnan, A. N. (2019). Influence of Environmental Factors in the Development and Outcomes of Inflammatory Bowel Disease. *Gastroenterology & hepatology, 15*(2), 72-82. Retrieved from https://pubmed.ncbi.nlm.nih.gov/31011301 https://www.ncbi.nlm.nih.gov/pmc/articles/PMC6469265/

Venter, J. C., Adams, M. D., Myers, E. W., Li, P. W., Mural, R. J., Sutton, G. G., . . . Zhu, X. (2001). The Sequence of the Human Genome. *Science, 291*(5507), 1304-1351. doi:10.1126/science.1058040

Verstockt, B., Smith, K. G., & Lee, J. C. (2018). Genome-wide association studies in Crohn's disease: Past, present and future. *Clinical & translational immunology, 7*(1), e1001-e1001. doi:10.1002/cti2.1001

Voelkl, B., Altman, N. S., Forsman, A., Forstmeier, W., Gurevitch, J., Jaric, I., . . . Würbel, H. (2020). Reproducibility of animal research in light of biological

variation. *Nature Reviews Neuroscience, 21*(7), 384-393. doi:10.1038/s41583-020-0313-3

vom Steeg, L. G., & Klein, S. L. (2016). SeXX Matters in Infectious Disease Pathogenesis. *PLoS Pathog, 12*(2), e1005374. doi:10.1371/journal.ppat.1005374

Wallace, J. L. (2001). PROSTAGLANDIAN BIOLOGY IN INFLAMMATORY BOWEL DISEASE. *Gastroenterology Clinics of North America, 30*(4), 971-980. doi:https://doi.org/10.1016/S0889-8553(05)70223-5

Wang, A. L., Boulton, M. E., Dunn, W. A., Jr., Rao, H. V., Cai, J., Lukas, T. J., & Neufeld, A. H. (2009). Using LC3 to monitor autophagy flux in the retinal pigment epithelium. *Autophagy, 5*(8), 1190-1193. doi:10.4161/auto.5.8.10087

Wang, C.-W., & Klionsky, D. J. (2003). The molecular mechanism of autophagy. *Molecular medicine (Cambridge, Mass.), 9*(3-4), 65-76. Retrieved from https://pubmed.ncbi.nlm.nih.gov/12865942 https://www.ncbi.nlm.nih.gov/pmc/articles/PMC1430730/

Wild, G. E., Drozdowski, L., Tartaglia, C., Clandinin, M. T., & Thomson, A. B. R. (2007). Nutritional modulation of the inflammatory response in inflammatory bowel disease--from the molecular to the integrative to the clinical. *World Journal of Gastroenterology, 13*(1), 1-7. doi:10.3748/wjg.v13.i1.1

Wildenberg, M. E., Vos, A. C., Wolfkamp, S. C., Duijvestein, M., Verhaar, A. P., Te Velde, A. A., . . . Hommes, D. W. (2012). Autophagy attenuates the adaptive immune response by destabilizing the immunologic synapse. *Gastroenterology, 142*(7), 1493-1503.e1496. doi:10.1053/j.gastro.2012.02.034

Xavier, R. J., & Podolsky, D. K. (2007). Unravelling the pathogenesis of inflammatory bowel disease. *Nature, 448*(7152), 427-434. doi:10.1038/nature06005

Xiong, Q., Li, W., Li, P., Yang, M., Wu, C., & Eichinger, L. (2018). The Role of ATG16 in Autophagy and The Ubiquitin Proteasome System. *Cells, 8*(1), 2. doi:10.3390/cells8010002

Yamazaki, K., McGovern, D., Ragoussis, J., Paolucci, M., Butler, H., Jewell, D., . . . Nakamura, Y. (2005). Single nucleotide polymorphisms in TNFSF15 confer susceptibility to Crohn's disease. *Human Molecular Genetics, 14*(22), 3499-3506. doi:10.1093/hmg/ddi379

Yang, S.-K., Hong, M., Zhao, W., Jung, Y., Baek, J., Tayebi, N., . . . Song, K. (2014). Genome-wide association study of Crohn's disease in Koreans revealed three new susceptibility loci and common attributes of genetic susceptibility across ethnic populations. *Gut, 63*(1), 80-87. doi:10.1136/gutjnl-2013-305193

Yang, S.-K., Ye, B. D., & Song, K. (2015). ATG16L1 contributes to Crohn's disease susceptibility in Koreans: overmuch concern for ethnic difference? *Gut, 64*(4), 687-688. doi:10.1136/gutjnl-2014-308242

Yang, Z., & Klionsky, D. J. (2009). An overview of the molecular mechanism of autophagy. *Current topics in microbiology and immunology, 335*, 1-32. doi:10.1007/978-3-642-00302-8_1

Zuk, M., & McKean, K. A. (1996). Sex differences in parasite infections: Patterns and processes. *International Journal for Parasitology, 26*(10), 1009-1024. doi:https://doi.org/10.1016/S0020-7519(96)80001-4

Vita

Kari Lynn Chesney was born in Downers Grove, Illinois on October 9, 1988 to Robert and Cheri Chesney. Soon after, she was blessed with a baby sister, Kelli, in 1990. During her childhood, she excelled in math and science, though her original answer to "what do you want to be when you grow up' was a lawyer. Her parents always attributed that to her argumentative nature.

After graduating from Downers Grove South High School in 2007, she began undergraduate studies at Illinois State University and graduated *magna cum laude* with her Bachelor of Science with Honors Distinction in Biological Sciences and Psychology, with a minor in chemistry, in 2011. While at Illinois State University, Kari became involved in undergraduate research under the mentorship of Dr. Valerie Farmer-Dougan. It was here she developed a passion for seeking out answers to the toughest scientific questions and completed an honors thesis focused on the "nature verses nurture" question of predatory instincts in prey animals. During this time, Kari was responsible for caring for the rat colonies for the lab, and it was through her care staff duties that she met and worked closely with Dr. Matt Fraker, the contracted veterinarian for research animals at the university. It was this interaction that solidified Kari's decision to pursue veterinary medicine with an emphasis on research as a career.

Upon graduating from Illinois State University, Kari entered the College of Veterinary Medicine at the University of Missouri. During this time, Kari became more confident in her decisions to enter the research field, but a new interest was piqued as well – one in

public policy. Her student leadership roles with the Student American Veterinary Medical Association and the International Veterinary Medical Association exposed Kari to the role of scientists and doctors in advocacy and policymaking. Fortunately, her trajectory coincided well with government relations, since she had planned to pursue a residency in laboratory animal medicine upon graduation.

Kari was accepted to the University of Missouri Comparative Medicine program in 2015 with the intent to stay and complete a PhD. It was here that Kari really honed her skills for vet med and continued to pursue side projects in public policy and advocacy. Soon after entering the program, Kari met Brad Siegler, an extremely ambitious entrepreneur and cofounder of the company EquipmentShare, which at the time of writing this dissertation is valued at $1.4B. He was and continues to be Kari's biggest fan and motivator in life, and they will be married at the end of October 2020.

Kari was also fortunate to join Dr. Elizabeth Bryda's research lab in 2016 as part of the Area Pathobiology PhD program and learn from her guidance and mentorship for many years. Dr. Bryda was the perfect mentor for Kari, both pushing her to be a high-quality researcher while also encouraging her outside interests in policy and advocacy. Due to this support, Kari was able not only complete certification in Science and Public Policy through the University of Missouri Truman School of Public Affairs, but also to take a two-year position as a Legislative Affairs Director for the University of Missouri Graduate Professional Council as well as a position as the South-Central Regional Legislative Director for the National Association of Graduate-Professional Students. These roles were

instrumental in training Kari in policymaking and analysis as well as government relations. It was because of these skills that Kari was confident enough in June 2019 to declare her candidacy for Missouri State Representative of District 50.

Kari's future plans include public service, either as an elected representative or policy analyst. At the time of writing this dissertation, Kari is still campaigning for a state representative seat which will be decided in the November 2020 election. Regardless of the outcome, the future looks bright, and there is no doubt that the skills and knowledge Kari has received over these last many years will take her far.